FINAL TECHNICAL REPORT

STRUCTURAL CHARACTERIZATION AND PILOT PALEOSEISMIC INVESTIGATION OF THE SOUTHERNMOST RODGERS CREEK FAULT, NORTHERN SAN PABLO BAY, CALIFORNIA

Recipient:
Fugro William Lettis & Associates, Inc., 1777 Botelho Dr., Suite 262, Walnut Creek, CA 94596
(925) 256-6070; (925)256-6076 fax; URL www.lettis.com

Principal Investigators:
Robert Givler[1], John Baldwin[1], and Keith Knudsen[2]
Email: r.givler@fugro.com

[1]Fugro William Lettis & Associates, Inc.
[2] URS Corporation
[3]U.S. Geological Survey, Menlo Park, California

Contributors:
Josh Goodman[1], Rufus Catchings[3] and Michael Rymer[3]

Program Elements II

Keywords:
Quaternary geology, neotectonics, paleoseismology, LiDAR, Seismic line, diatom analyses

U. S. Geological Survey
National Earthquake Hazards Reduction Program
Award Number **G09AP00072**

November 2010

This research was supported by the U.S. Geological Survey (USGS), Department of the Interior, under USGS Awards G09AP00072. The views and conclusions contained in this document are those of the authors and should not be interpreted as necessarily representing the official policies, either expressed or implied, of the U.S. Government.

Award G09AP00072

STRUCTURAL CHARACTERIZATION AND PILOT PALEOSEISMIC INVESTIGATION OF THE SOUTHERNMOST RODGERS CREEK FAULT, NORTHERN SAN PABLO BAY, CALIFORNIA

Givler, R.W. [1], Baldwin, J.N.[1], and Knudsen, K.[2]

Principal Investigators:

[1]Fugro William Lettis & Associates, Inc., 1777 Botelho Drive, Suite 262, Walnut Creek, CA 94596
r.givler@fugro.com and j.baldwin@fugro.com; phone: 925-256-6070, fax: 925-256-6076

[2]URS Corporation, 1333 Broadway, Suite 800 Oakland, CA 94612; keith_knudsen@urscorp.com; phone: 510-874-3120

ABSTRACT

The Rodgers Creek fault is thought to be the most likely fault in the San Francisco Bay Region (SFBR) to produce a large earthquake. However, the timing and recurrence of large earthquakes along the Rodgers Creek fault, including fault segmentation with the Hayward fault, are addressed by a limited number of studies that provide only broad constraints on these parameters (Budding et al., 1991; Schwartz et al., 1992; Hecker et al., 2005). Our investigation of the southern Rodgers Creek fault (SRCF) at Tolay marsh was designed to develop additional preliminary earthquake timing and recurrence data for the fault. The pilot feasibility study at Tolay Marsh included (1) detailed mapping of possible late Holocene fault-related geomorphology and Quaternary geology at the site; (2) collecting and interpreting geophysical data across the fault in collaboration with the U.S. Geological Survey; (3) collecting cores of shallow estuarine stratigraphy in transects roughly perpendicular to the fault strike, and (4) evaluating possible stratigraphic and structural evidence for paleoseismic events on the Rodgers Creek fault.

LiDAR-based geomorphic mapping indicates the SRCF cores a northwest-southeast trending bedrock ridge that is cut by multiple Holocene and Quaternary active fault strands that exhibit prominent tectonic geomorphology, including: southwest-and northeast-facing fault scarps, aligned linear channels, closed depressions, aligned springs, and bedrock topographic highs (Hart, 1992; Randolph Loar et al., 2004; RGH Consultants, Inc., 2009).

Preliminary interpretations from a P- and S-wave geophysical survey collected for this study indicate the SRCF forms a broad, approximately 500- to 600-m-wide flower structure that cores the bedrock ridge across the Tolay marsh site. The flower structure consists of three primary fault zones that branch upward toward the ground surface. Some of these faults imaged in the seismic line are coincident with prominent Quaternary and Holocene fault traces from geomorphic mapping and subsurface trench data (RGH Consultants, Inc., 2009). Geologic mapping agrees with a P-wave velocity anomaly along the northwest section of the profile that marks the contact between Sonoma Volcanics and Petaluma Formation. These data indicate the bedrock fault juxtaposing disparate formations has had significant fault slip and may be a primary fault strand.

Shallow coring of estuarine stratigraphy along the northeast and southwest margins of the SRCF pop-up structure provides preliminary evidence for late Holocene rupture history of the fault. Stratigraphic and

paleontologic analyses of gouge and vibracore samples show a sequence of late Pleistocene to Holocene alluvial and late Holocene marsh sediments that include marsh soils (peaty muds), quiet water deposits (mud), and algal mat-rich horizons that overlie Pleistocene (?) coarser-grained overbank alluvium. On the northeastern side of the SRCF along gouge transects #1 and #2, the subsurface marsh stratigraphy defines rises toward the surface defining a northeast-facing subsurface escarpment coincident with present-day topography. Distinct elevation differences between closely spaced borings allow for the interpretation of possible southwest-side up displacement of late Holocene strata (Unit 2d). This interpretation is supported by geophysically imaged subsurface offsets, present-day tectonic geomorphology and trench data to the northwest.

Based on the limited correlations between paleoecological (diatom) data, stratigraphic data, and age-dating coupled with a criteria matrix, we conservatively interpret one paleoseismic event on the SRCF at the Tolay marsh site. Diatom and radiometric analyses of a buried peaty mud horizon (Unit 2d –buried incipient marsh #2) support that a rapid change in paleoecological conditions, possibly coseismic subsidence, occurred after 2150 to 2350 cal yr BP (2σ) and before 1900 to 2300 cal yr BP. Although this marsh study is considered an initial pilot investigation on the capability of Tolay marsh preserving evidence of past surface-fault ruptures on the SRCF, the preliminary age of this event is roughly correlative with events on the both the Northern Hayward fault (HFPG, 1999). Gouge cores and detailed interpretation of vibracores demonstrate that where sampled the Tolay marsh contains weak marsh stratigraphy and limited peaty horizons that can be used to interpret past large magnitude earthquakes. Future marsh studies at this site are not recommended because of limited late Holocene stratigraphy that likely is not adequate for assessing earthquakes within the last 1,000 years.

TABLE OF CONTENTS

ABSTRACT ..... **i**
1.0 INTRODUCTION **1**
2.0 TECTONIC SETTING AND REGIONAL GEOLOGY **2**
2.1 Rodgers Creek Fault 2
2.1.1 Paleoseismic Data: Rodgers Creek Fault 2
2.1.2 Paleoseismic Data: Northern Hayward Fault 3
2.2 Tolay Marsh 3
3.0 APPROACH AND METHODOLOGY **5**
3.1 Geomorphic and Geologic Mapping using LiDAR Data 5
3.2 Geophysical Profile Acquistion and Interpretation 5
3.3 Subsurface Exploration: Gouge Core Transects and Vibracores and Diatom Analyses 7
4.0 RESULTS **10**
4.1 Geomorphic Mapping on LiDAR Data 10
4.2 Geophysical Results 10
4.3 Gouge Core and Vibracore Transect: Stratigraphic, Paleoecologic, and Radiometric Analyses 12
4.3.1 Marsh Stratigraphy and Depositional Environment 12
4.3.2 Paleoecological Environment 16
4.3.3 Radiocarbon Results 19
5.0 DISCUSSION **21**
5.1 Bedrock Structure and Geomorphic Expression of the Southern Rodgers Creek 21
5.2 Origin and Evolution of the Tolay Marsh 21
5.3 Evidence for Coseismic Submergence 22
5.4 Comparison of Preliminary Results with other Paleoseismic Studies 24
6.0 SUMMARY OF FINDINGS **25**
7.0 ACKNOWLEDGEMENTS **26**
8.0 REPORTS/ABSTRACTS PUBLISHED **27**
9.0 REFERENCES **28**

LIST OF TABLES

Table 1	Fault offsets, depth of faulting, fault dip and dip direction from USGS seismic line
Table 2	Description of stratigraphic units within gouge core transect # 1
Table 3	Summary of diatom results for vibracore #2
Table 4	Qualitative overview of diatoms in modern surface samples from marsh/meadow locations in the vicinity of gouge core transect #3
Table 5	Radiocarbon data for the Tolay marsh site, Sonoma County, California
Table 6	Criteria indicative of coseismic subsidence for peaty soils, Tolay marsh site

LIST OF FIGURES

Figure 1	Regional shaded relief map showing the Tolay marsh study site, faults modified from Jennings (1994), and the historical earthquakes of 1969 and 1898.
Figure 2	Southern 25 km of the Rodgers Creek fault showing fault and lineament mapping (Randolph Loar and Caskey, 2001) and previous successful paleoseismic investigations on the fault.
Figure 3	Quaternary geology of the southern Rodgers Creek fault zone (Witter et al., 2006).
Figure 4	Tolay Marsh Study site and fault lineament map.
Figure 5	Slopeshade map of LiDAR data and aerial photography along the southernmost Rodgers Creek fault at the Tolay marsh study area.
Figure 6	P-wave reflection images of the USGS seismic reflection and refraction line across the Rodgers Creek fault at Tolay marsh.
Figure 7	Slopeshade map of LiDAR data and aerial photography of the Tolay marsh site.
Figure 8	Gouge Core Transect #1.
Figure 9	Photomosaic and detailed log of vibracore #2 between 130 cm and 170.5 cm depth.

APPENDICES

Appendix A	Diatom analyses for vibracore #2 Report No. 100702– Eileen Hemphill-Haley Consulting Micropaleontology (July 2010)
Appendix B	C14 data from Beta Analytic and PaleoResearch

1.0 INTRODUCTION

The Rodgers Creek fault has been judged to be the most likely fault in the San Francisco Bay Area to produce a large earthquake. The Working Group on California Earthquake Probabilities (2003) and Uniform California Earthquake Rupture Forecast, Version 2 (WGCEP, 2008) assigned the Hayward-Rodgers Creek fault probabilities of 27% and 31% respectively, of producing an earthquake of magnitude 6.7 or greater in the next 30 years (Figure 1). The age of the most recent event and recurrence information are important parameters for developing rupture scenarios and computing probabilities of future major earthquakes along the Hayward-Rodgers Creek fault (HRCF). Considering the proximity of the southern Rodgers Creek fault (SRCF) to the heavily populated and urbanized North Bay region, the consequences of a large earthquake on the fault are large. The lack of significant seismic moment release on the fault within recorded history suggests that this segment may be primed for a large earthquake. Thus, it is important to regional and local seismic hazard evaluations to understand, as best as possible, the recurrence of large earthquakes on the Rodgers Creek fault, as well as on the HRCF system.

The Rodgers Creek fault includes the central part of an extensive 275-km-long fault system that comprises the Hayward, Rodgers Creek-Healdsburg, and Maacama faults (Figure 1). The Rodgers Creek fault is one fault in a series of right-stepping en echelon faults that include the Hayward fault to the south, and the Healdsburg and Maacama faults to the north (Figures 1 and 2). The surface expression of the Rodgers Creek fault, as mapped by Randolph Loar and Caskey (2001) and Hart (1992) is demarcated by classic fault-related geomorphic features such as offset drainages, side hill benches, tonal lineaments, sag ponds, and springs (Figure 2).

Data used to develop the WGCEP probabilities for the Rodgers Creek fault are based on findings from only two sites along the central part of the Rodgers Creek fault (Budding et al., 1991; Schwartz et al., 1992; Hecker et al., 2005) (Figure 2). Obtaining additional paleoseismic data from the southern part of the fault is important to gain a better understanding of the timing of large paleoearthquakes for the Rodgers Creek fault, hypothesized extensional step-over, and for assessing seismic hazards and calculating probabilities of large earthquakes in the rapidly expanding urban area of the northern San Francisco Bay region.

To better characterize the southern Rodgers Creek fault, we conducted a pilot study at Tolay marsh in Sonoma County to evaluate evidence for late Holocene surface rupture and, if possible, estimate the timing of the most recent event (MRE). The scope of this study includes (1) detailed mapping of possible late Holocene fault-related geomorphology and Quaternary geology at the site; (2) collecting and interpreting geophysical survey data with the U.S. Geological Survey; (3) collecting cores of shallow estuarine stratigraphy in transects roughly perpendicular to the fault strike, and (4) evaluating possible stratigraphic and structural evidence for paleoseismic events on the Rodgers Creek fault.

2.0 TECTONIC SETTING AND REGIONAL GEOLOGY

2.1 Rodgers Creek Fault

The 60-km-long Rodgers Creek fault, located between San Pablo Bay and Santa Rosa, California, strikes approximately N35°W, and is characterized by a late Holocene right-lateral slip rate of 6.4 to 10.4 mm/yr (Budding et al., 1991; Schwartz et al., 1992). The Rodgers Creek fault has been seismically quiescent historically. The only moderate to large earthquakes located near the fault were the 1969 **M** 5.6 and 5.7 earthquakes near Santa Rosa (Cloud et al., 1970; Wong, 1991), and the Mare Island event of 1898 (Figure 3). Based on historical accounts for the region, the 1898 earthquake is interpreted by Toppozada et al. (1992) as a **M**6.2 to **M** 6.7 event that probably occurred along the southernmost section of the Rodgers Creek fault. Ultimately the location of the 1898 event remains uncertain due to the lack of definitive supporting information. A review of contemporary seismicity data along the Rodgers Creek and Hayward faults shows the presence of a seismic gap along the southern Rodgers Creek fault, which encompasses part of our Tolay marsh site. This seismic gap may or may not represent a distinct rupture segment of the HRCF system.

Although active creep has been well documented both south and north of the Rodgers Creek fault, along the Hayward and the Maacama faults, respectively, there is some disagreement whether or not the Rodgers Creek fault creeps. For example, approximately 10 years of theodolite triangulation data document the absence of surface creep observed along the southern Rodgers Creek fault (Wong, 1991; Galehouse, 1992) and more recent measurements appear ambiguous (McFarland et al., 2007). Conversely, recent data from geodetic measurements and from PS-InSAR datasets indicate the fault may be creeping (up to or greater than six mm/yr) near Santa Rosa, California (Floyd et al., 2009) (Funning et al., 2007).

2.1.1 Paleoseismic Data: Rodgers Creek Fault

Paleoseismic investigations at three sites provide information on the late Holocene slip rate and event chronology for the central and southern parts of the Rodgers Creek fault (Budding et. al, 1991; Schwartz et. al, 1992; Hecker et al., 2005; Randolph Loar et al., 2004; Figure 2). Studies along the central Rodgers Creek fault report a geologic slip rate of 6.4 to 10.4 mm/yr, and an average earthquake recurrence interval of 131-370 years (Budding et. al, 1991; Schwartz et. al, 1992; Hecker et al., 2005). At the Triangle G Ranch, Schwartz et al. (1992) identified two events on the central Rodgers Creek fault that predate the most recent event (MRE), including 1) the oldest event occurred shortly before 993 to 1193 AD (962-762 yr BP) and 2) an earlier event occurred after 993-1193 AD (962-762 yr BP) but before 1275-1413 AD (680 to 542 yr BP). Using non-native pollen and review of historical records, Hecker et al. (2005) constrain the timing of the most recent earthquake on the Rodgers Creek fault to after A.D. 1690 and before A.D. 1715 (234 to 315 yr BP) in trenches at the Triangle G Ranch. Hecker et al. (2005) also conclude that a buried channel was right-laterally offset a minimum of 2.2 (+1.2, -0.8) m during the MRE, which is similar to but larger than the 2 (+0.3, -0.2) m estimated at the Beebe Ranch site (Budding et al., 1991). Hecker et al. (2005) also concluded that the MRE produced 0.25 to 0.4 m of vertical deformation along the fault. They go on to compare the MRE on the RCF to the timing of the last prehistoric ruptures on northern and southern sections of the Hayward fault (A.D. 1640-1776; 315-234 yr BP) and suggest that there is a possibility that an earthquake ruptured both the RCF and Hayward fault across the San Pablo Bay step over.

Randolph Loar et al. (2004) conducted a preliminary trench investigation at Martinelli Ranch in Sonoma County (Figure 2) to investigate possible evidence for late Holocene surface rupture along the SRCF. Randolph Loar et al. (2004) hand dug a test-pit and logged two creek banks that exposed an active strand of the fault. Their results indicate that one surface rupturing event occurred along the southern Rodgers Creek fault at the Martinelli Ranch site before 1,050-790 cal yr BP and after 10,730-9,550 cal yr BP.

2.1.2 Paleoseismic Data: Northern Hayward Fault

Timing of paleoearthquakes along the northern Hayward fault at Mira Vista golf course indicate up to nine events occurred between ~ 400 yr BC and 1800 AD (HPEG, 1999). These events (and their corresponding ages constraints) are as follows: 1) E3 (392 yr BC to 54 AD; 2310 to 1901 yr BP), E4 (355 yr BC to 13 yr AD; 2310 to 1942 yr BP), E5 (104 yr BC to 756 yr AD; 2059 to 1199 yr BP), E6 (104 yr BC to 756 yr AD; 2059 to 1199 yr BP), E8 (534 to 968 yr AD; 1421 to 987 yr BP), E9 (718 to 1014 yr AD; 1237 to 941 yr BP), E10 (1027 to 1479 yr AD; 476 to 928 yr BP), and E11 (1640 to 1776 yr AD; 315 to 234 yr BP). The HFPG (1999) report discusses an average recurrence time between 270 yr and 710 yr for a surface rupturing event.

2.2 Tolay Marsh

The Tolay marsh site is located at the intersection between the southern trace of the Rodgers Creek fault and the edge of San Pablo Bay (Figures 1 and 2). This site is located along the original San Pablo Bay shoreline that predates human disturbance and artificial infill since the mid-1800s (Witter et al., 2006; Figures 3 and 4). The site currently is isolated from the Bay by narrow levees rimming slack-water sloughs that meander across the estuary before entering San Pablo Bay. The northwestern limits of the modern bay marsh are partly constrained by a railroad track built on artificial fill overlying Holocene Bay Mud. Northwest of the railroad, the physiographic setting transitions from upper marsh to low-lying Holocene alluvial fan deposits that drape the sides of bedrock highs. This alluvial plain is drained by small intermittent creeks, including Tolay Creek. On the northern side of the SRCF the marsh has been dike and is actively used for hay farming, while the south side is owned by the State of California, managed by the Department of Fish and Game and remains a natural marsh.

The marsh habitat within the active Tolay Marsh (south of the SRCF) includes common salt marsh species such as Pickleweed (*Salicornia*) and Cordgrass (*Spartina*) (mean high water [MHW] to mean high high water [MHHW]), which receive regular tidal saltwater inundations. The habitat surrounding the active marsh includes saltbrush, meadow barley/Mediterranean barley, blue-eyed grass and other grasslands species (MHHW to >MHHW). Mudflats or small depressions within Tolay marsh that are regularly inundated grow algal mat vegetation. Algal mats consist of a layer of thin filamentous algae that form in shallow water where a repeated process of inundation, photosynthesis, and subaerial exposure form thin layers of algal mats. These are commonly found in the subsurface cores expressed as interbedded thin mud laminae.

At the Tolay marsh site, the Southern Rodgers Creek fault (SRCF) cores a northwest-south east-trending bedrock promontory composed of Tertiary Petaluma Formation (on the west) and Sonoma Volcanics (on the east) (Huffman and Armstrong, 1980; Wagner et. al., 2002). Multiple fault strands are mapped subparallel to the bedrock ridge and can be traced up to and across the 1850s bay margin. The Petaluma Formation is faulted against Sonoma Volcanics along the northern margin of the ridge (Wagner et al., 2002). These fault strands are inferred to be either Holocene or Quaternary active based on associated tectonic geomorphology (Hart, 1992; Randolph Loar et al., 2004; Figures 3, 4, and 5).

A Holocene-active trace of the SRCF found in consultant trenches traverses center of the bedrock ridge and projects southwest toward the Tolay marsh site (Hart, 1992; Randolph Loar and Caskey, 2001; Randolph Loar et al., 2004). As part of an Alquist-Priolo fault study, RGH Consultants, Inc. (2009) excavated six exploratory trenches across the bedrock ridge to assess the potential for Holocene faults intersecting a new building footprint (Figure 5). The exploratory trenches encountered northwest-striking, steeply southwest-dipping Petaluma Formation consisting of bedded sandstone, siltstone, and conglomerate. RGH (2009) identified a series of northwest-striking near vertical faults in three of these trenches that align to form a single Holocene fault within the middle of the bedrock ridge (Figure 5). The fault zone consisted of a 2.5 to 5.5 ft wide zone of shearing, indicating primarily strike-slip motion. Upper soils were vertically displaced by only a few inches, consistent with primarily a strike-slip mode of deformation.

3.0 APPROACH AND METHODOLOGY

Our approach to this initial pilot paleoseismic study of the SRCF involved three components: 1) geologic/geomorphic mapping, 2) collection of geophysical data, (3) collecting cores of shallow estuarine stratigraphy in transects, and (4) evaluating possible stratigraphic and structural evidence for paleoseismic events on the Rodgers Creek fault. The first component used geologic and geomorphic mapping along southern Rodgers Creek fault near the Tolay marsh site to identify Holocene active traces of the fault. The second component entailed collection of seismic reflection and refraction survey data to image the SRCF's crustal structure and identify key targets for gouge core transects. The third component consisted of a series of gouge core transects to map the underlying marsh stratigraphy, which included analyses of diatom samples at key stratigraphic horizons to evaluate whether soil horizons experienced rapid (i.e. coseismic submergence) or slow (i.e. normal burial) relative sea-level change.

3.1 Geomorphic and Geologic Mapping using LiDAR Data

We compiled available LiDAR data along the SRCF near Tolay marsh to map active traces of the Rodgers Creek fault (similar to our previous mapping efforts of active faults in the San Francisco Bay region (Randolph Loar et al., 2004; Koehler et al., 2005; Witter et al., 2006). The methodology included office-based and field-based techniques. We first compiled existing data along the fault, including LiDAR data (Figure 5), previously mapped geomorphic features related to active faulting, and then revised the mapping of Randolph Loar et al. (2004) using bare-earth LIDAR data long the fault. Finally, we conducted field reconnaissance to verify and further refine the location of active fault traces.

3.2 Geophysical Profile Acquistion and Interpretation

At the Tolay marsh site, we imaged the main trace(s) of the SRCF by conducting a seismic reflection and refraction survey aligned orthogonal to the SRCF (Figure 5). This work was directed by Mike Rymer and Rufus Catchings of the U.S. Geological Survey on November 18, 2009. The geophysical line traversed the linear southeast-trending ridge and multiple fault lineaments (Figure 5). We collected high resolution shear wave (S-wave) and pressure wave (P-wave) seismic reflection and refraction profiles to obtain geologic data to delineate the location, style and width of deformation associated with the main trace(s) of the southern Rodgers Creek fault, as well as guide the marsh coring program.

With geophones spaced at 5-m intervals, P-wave data were collected over an 800-m-long profile and S-wave data were collected along the northern 600 m of the P-wave profile. P-wave sources were generated by Betsy-Seisgun that sets off a shotgun blank into a shallow (~30 cm deep) hole that is covered with dirt and a metal plate. S-wave sources were generated using multiple sledgehammer impacts on both ends of a weighted wooden block. The data were acquired using three multi-channel seismographs with a total of 165 channels. Data were recorded along the line with three linked 60-channel Geometrics Strataview RX-60 seismographs. The seismographs were coupled to the ground via Mark Products L-40A, single-element, 40-Hz (hertz) geophones. Both Seisgun shots and geophones were spaced at 5-m intervals over the seismic array, with the geophones and shots laterally offset by 1 m. One shot was recorded at each site for 2 s at a 0.5-ms sampling rate without acquisition filters.

Data were acquired in a manner that allows both reflection and refraction images to be produced. First-arrival refractions from each seismogram were inspected and measured. A modified version of the tomographic inversion method described by Hole (1992) was used to develop a P-wave seismic velocity

model from the first-arrival refractions. The data were inverted using a 5-m grid along the profile to the depth of ray coverage. Each shot point and geophone location was surveyed using a differential Global Positioning System (with theoretical accuracies) of a few centimeters.

The seismic reflection data were processed using the interactive seismic reflection processing software package ProMAX ™. The following steps were involved in data processing:

- Geometry Installation: Lateral distances and elevations, described above, were used to define the geometrical set up of the profile.
- Trace Editing: Locally, bad coupling between the geophones and the ground, malfunctioning geophones, or cultural noise close to the seismic sensors resulted in unusually noisy seismic traces. Traces representing those locations were edited. However, such traces were not necessarily unsuitable for all shot gathers; therefore, independent trace editing was employed for individual shot gathers.
- Timing Corrections: Individual hits on the end of the Seisgun source electronically trigger the seismographs; however, there are small (~1–4 ms) delays between the electrical trigger and the actual Seisgun shots. We corrected for the delays by removing from 1 to 4 ms from the start time of each shot gather. We did this to assure each shot initiated at 'zero' time.
- Elevation Statics: Elevation statics were applied to compensate for local changes in elevation. Global Positioning Satellite-determined locations and inversion-determined velocities were used to correct the reflection times to a constant time.
- Muting: Trace muting was used before and after stacking to remove refractions and other arrivals that were not completely removed using filtering techniques. All arrivals before the first-arrival refractions were muted.
- Automatic Gain Control (AGC): A prestack automatic gain control was applied (AGC window, 500 ms).
- Bandpass Filtering: Most of the data of interest for this seismic imaging investigation are between 15 and 200 Hz (pre-stack bandpass, 15-30-400-800; post-stack bandpass, 15-30-200-400). A notch filter of 62 Hz (± 6 Hz) was used. No acquisition filter was used in the field.
- Velocity Analysis: Velocities in the shallow section (~1 m to ~100 m) were calculated using velocity inversion techniques, but velocities in the deeper section were calculated using shot gathers, semblance, and *a priori* data.
- Velocity Inversion: As described above, velocities were measured from the seismic data using a computerized inversion routine.
- Normal Moveout Correction: Due to progressively greater travel times for the seismic waves to reach sensors that were progressively farther from each shot point, there was a delay (moveout) for each seismic arrival on the seismic record. To sum (stack) the data at each common depth point (CDP), a correction was made for the moveout using velocities obtained from the velocity analysis.
- Stacking: To enhance the seismic signal for each CDP, individual reflections were summed together in a process called stacking.

- Depth Conversion: For stacked seismic reflection images that were not migrated, we converted the time sections to depth sections using root mean squared velocities converted from the velocity analysis described above.
- Trace Equalization: A trace equalization filter was applied with a gain of 2-100 Hz.
- Deconvolution: We used a deconvolution (Decon) filter to remove reverberations and spiking.

We developed a tomographic seismic velocity image and stacked and migrated reflection images from the P-wave data (Figure 6). Given the good conditions for seismic imaging at this site (fine-grained, water-saturated sediment in a quiet environment), reflectors at depths greater than 1 km are interpreted. These profiles and interpretative images suggest that the Rodgers Creek fault near San Pablo Bay is much more structurally complex than previously thought. In the shallow subsurface (upper 200 m) we interpret at least three fault zones; two fairly broad (50- to 100-m-wide) zones of disruption and a narrow (5- to 20-m-wide) zone of faulting. All three of these fault zones extend to near the ground surface (Figure 6 and Table 1). See further descriptions in Section 5.2.

3.3 Subsurface Exploration: Gouge Core Transects and Vibracores and Diatom Analyses

After defining the active fault traces using the geomorphic mapping and geophysical data, we completed three gouge core transects across the margins of the SRCF pop-up to characterize marsh stratigraphy and look for evidence of relative sea level change. In February and April of 2010, we used a 2.5-cm diameter hand-operated gouge core to penetrate the marsh sediment to depths of about 2 to 2.5 meters. We completed 29 gouge cores as part of three separate gouge core transects (Figure 5). The gouge cores were logged in the field and used to identify near surface stratigraphy, buried marsh horizons, and fine- to coarse-grained fluvial deposits. This technique was used to provide a relatively quick assessment of laterally continuous marker horizons at depth (Figure 7).

On February 22, 2010, we collected two 7.6-cm diameter cores using a mechanical vibracore device along vibracore transect # 1 (Figures 7, 8 and 9). This transect was chosen for further vibracore samples because near surface stratigraphy preserved several buried peaty muds interpreted as buried incipient marshes. After collecting the vibracore samples #1 and #2, we prepared detailed lithologic descriptions of the core, collected charcoal and plant material for radiocarbon samples, and collected soil samples for diatom analyses. On March 11, 2010, the location of each gouge core and vibracore were surveyed along this transects #1, #2, and #3 using a Topcon total station to determine precise relative elevations between each sample location.

To establish an understanding of stratigraphic age and paleoenvironment, we collected samples for radiocarbon and diatom analyses from gouge cores 21and 23, and vibracore #2 along gouge core transect #1 (Figures 7, 8 and 9). Seven samples consisting of charcoal, bulk peat, and organic-rich mud were submitted to PaleoResearch for plant identification purposes whereas Beta Analytic performed radiocarbon analyses by accelerator mass spectrometry (AMS) method of X samples (Appendix B). Five sediment samples from vibracore #2, were submitted for diatom analysis at the sedimentology lab at Humboldt State University and were processed using methods outlined in Appendix A (Hemphill-Haley, 2010).

Stratigraphic evidence for coseismic land-level change has been reported from numerous estuaries of the Pacific Northwest. Sequences of alternating wetland soils and estuarine mud attest to episodes of rapid sea-level rise and inundation of coastal lowlands, which is consistent with documented coseismic

submergence during subduction zone earthquakes. Contacts between the soils and overlying mud, as observed in outcrop or in cores, are usually sharp, but may appear gradational in less developed or poorly preserved soils, or where remains of herbaceous plants protrude into the overlying mud. Gradational contacts may also indicate nontectonic processes such as eustatic sea-level rise or changes in tidal range within an estuary. Microfossil (e.g. diatom) analyses at closely spaced intervals across stratigraphic contacts can be used to differentiate sudden changes in sea level, as might occur during an earthquake, from slower or smaller changes that may imply nontectonic processes.

Abundant datable materials and preservation of event horizons within the continuous stratigraphy often found in estuaries makes these settings ideal natural paleoseismic laboratories (Knudsen et al., 2002; Koehler et al., 2005). Radiocarbon dating of organic horizons is the principle means of constraining the timing of past earthquakes recorded in marsh stratigraphy. Because bulk peat samples commonly contain roots and recycled organic material, the most reliable age estimates are derived by AMS dating of delicate detrital seeds, sticks, leaves, or bark from trees that perished within decades prior to the time of the event (Kelsey et al., 2002, Witter et al., 2003). We collected plant macrofossils preserved near the upper abrupt contact of each mud over peat couplet for AMS radiocarbon analyses to constrain the age of marsh soils.

It is possible that small coseismic land-level changes or events associated with a frequent recurrence would not be reflected in the estuarine stratigraphy as buried peats. However, these smaller or frequent events may be recorded by (1) changes in vegetative colonies (microfossil and macrofossil), (2) evidence of liquefaction, (3) unconformities, (4) changes in sedimentation rates, and (5) changes in sediment texture. Other possible sources of uncertainty include sea-level rise, interseismic land-level changes and sediment compaction. These processes occur relatively slowly (~1mm/yr rise in sea level) or at rates so slow, if nonzero, that they remain undocumented (e.g. interseismic land-level changes in the Hayward – Rodgers Creek step-over).

Differences in environment and style of deformation associated with earthquakes along the Cascadia margin and along strike slip faults led Knudsen et al. (2002) to modify the Nelson et al. (1996) Cascadia criteria in order to identify coseismic subsidence in small pull-apart basins along the San Andreas fault in northern California. Knudsen et al. (2002) recognized that the magnitude of deformation associated with coseismic subsidence along strike-slip faults is much less widespread than vertical deformation associated with subduction zone events and that tsunami deposits coincident with evidence of marsh submergence may not be a useful criteria for strike-slip faults. Additionally, Knudsen et al. (2002) proposed that rapid fluvial aggradation coincident with stratigraphic sequences indicating relative sea level rise may be a reasonable criterion for identifying coseismic subsidence along strike-slip fault systems. Following Koehler et al., (2005), we interpret that abrupt lower contacts with a change of depositional environment to a lower intertidal level may also be a reasonable criterion, in addition to those proposed by Knudsen et al. (2002).

Stratigraphic sequences in coastal marshes that closely resemble those produced by coseismic subsidence have been attributed to non-tectonic processes (Shennan, 1989; Nelson, 1992a; 1992b; Carver and McCalpin, 1996; Nelson et al., 1996). However, any buried soil formed by non-tectonic processes is unlikely to satisfy more than three of the co-seismic criteria proposed by Nelson et al. (1996) (Carver and McCalpin, 1996, as cited in Knudsen et al., 2002). Therefore, we have evaluated the marsh stratigraphy within Tolay Marsh with respect to the stratigraphic and micropaleontological data obtained in this study and criteria developed by Nelson et al. (1996) and Knudsen et al. (2002) to assess whether environmental changes within Tolay Marsh occurred due to tectonic subsidence or other nontectonic processes. In the discussion section, we compare these data with other Rogers Creek fault sites to the north (Budding et al.,

1991; Schwartz et al., 1992; Randolph Loar et al., 2004; Hecker et al., 2005) and the Mira Vista study on the northern Hayward fault (HFPG, 1999).

4.0 RESULTS

We conducted a multi-disciplinary investigation of the Southern Rodgers Creek fault that included acquisition of a seismic line across the broad fault zone, gouge coring and virbracoring across potential Holocene fault targets, sampling gouge and vibracores for radiocarbon and diatom analyses, and assessing stratigraphic and structural evidence for large coseismic elevation changes across suspected fault targets.

4.1 Geomorphic Mapping on LiDAR Data

The Tolay marsh site is located at the intersection between the southern Rodgers Creek fault and the edge of the 1850s shoreline of the San Pablo Bay (Figures 2, 3, and 4). Here, the SRCF cores a northwest-southeast-trending bedrock promontory composed of Tertiary Petaluma Formation (on the west) and Sonoma Volcanics (on the east) (Huffman and Armstrong, 1980; Wagner et. al., 2002). Multiple fault strands are mapped subparallel to the bedrock ridge and can be traced as projecting across the 1850s bay margin. These fault strands are inferred to be either Holocene or Quaternary active based tectonic geomorphology including: southwest-and northeast-facing fault scarps, aligned linear channels, closed depressions, aligned springs, and bedrock topographic highs (Hart, 1992; Randolph Loar et al., 2004; Figure 5).

As discussed earlier, a Holocene-active strand of the SRCF is located in the center of the bedrock ridge based on trench excavations (RGH Consultants, Inc. 2009) and geomorphic mapping (Hart, 1992; Randolph Loar and Caskey, 2001; Randolph Loar et al., 2004; this study). The central fault strand is coincident with a series of closed depressions within the ridge (southeast of the RGH Consultants trenches) and along strike with a prominent southwest-facing topographic scarp north of Highway 121 (Figure 5). Where this fault strand enters the modern marsh its location becomes obscured as a result of considerable anthropogenic modification from an existing railroad, farming, and flood levee protection.

Two parallel northwest-striking geomorphic lineaments are mapped along the northern margin of a bedrock ridge formed by the SRCF at the Tolay marsh site (Figure 3). The northern most lineaments are formed by the curvilinear northeast-facing margin of the bedrock ridge. To the northwest, these lineaments join to form an ortheast-facing bedrock ridge that aligns with a series of springs north of Highway 121 (Figure 5). Along the northeast margin of the bedrock ridge, these lineaments represents a fault contact between Sonoma Volcanics on the northeast and Petaluma Formation on the southwest.

On the southwestern margin of the bedrock ridge are a series of topographic and tonal lineaments. These lineaments are not along strike with those northwest of Highway 121 suggesting a subtle right-step or widening of the active fault zone. These lineaments include several southwest-facing bedrock scarps, linear marsh/bedrock contacts, and two potentially uplifted bedrock knobs or islands within the modern marsh (Figure 5).

4.2 Geophysical Results

In November 2010, our project team, including researchers with the U.S. Geological Survey, completed a seismic reflection and refraction survey aligned orthogonal to the SRCF (Figures 5 and 6). The geophysical line traversed the linear southeast-trending bedrock and multiple fault lineaments (Figure 5). The high-resolution shear wave (S-wave) and pressure wave (P-wave) seismic reflection and refraction profiles were collected to characterize the location, style and width of deformation, and probable late

Holocene fault traces associated with the southern Rodgers Creek fault. The results of the geophysical study provided fault targets to assess during the marsh coring program.

To date, we have developed a tomographic seismic velocity image and stacked and migrated reflection images from the P-wave data (Figure 6). Analyses of S-wave data are pending. Given the good conditions for seismic imaging at this site (fine-grained, water-saturated sediment in a quiet environment), we observe reflectors at depths greater than 1 km. Figure 6 illustrates three seismic lines including: a) uninterpreted P-wave seismic line, b) interpreted P-wave seismic line, and c) P-wave velocity superimposed on the interpreted P-wave seismic line.

Preliminary interpretations of the P-wave data suggest that the Rodgers Creek fault at the Tolay marsh site is structurally complex and appears to form an approximately 500-to 600-m-wide transpressional flower structure. In the shallow subsurface (upper 200 m), we interpret at least 11 fault strands comprising three distinct fault zones: two fairly broad (50- to 100-m-wide) zones of disruption and a narrow (5- to 20-m-wide) zone of faulting. Table 1 lists the location of each interpreted fault strand, reflector offset, depth of inferred shallowest faulting, fault dip, and dip direction. Figure 6 illustrates shallow faults in the seismic line extending from >400 m depth to the ground surface. Apparent vertical displacements range between 15 m to less than 5 m in the upper 100 m. However, the dominate sense of slip on the SRCF is dextral strike-slip so the actual true fault displacements likely are much larger than 15 to 5 meters.

Preliminary interpretations of P-wave velocity data and stacked/migrated reflection images illustrate a correlation with bedrock geologic mapping (Wagner et al., 2002). For example, a high to low velocity boundary coincides with Sonoma Volcanics (P-wave velocity high) and Petaluma Formation (P-wave velocity low; Figure 6). If true, this correlation suggests that faults 6 and 7 (Table 1) have potentially accommodated greater fault slip than the other strands that lack the inferred bedrock juxtaposition. This distinct change in velocity across a narrow zone is used to infer the primary zone of fault at the Tolay marsh site, and is consistent with bedrock mapping northwest of the marsh.

Table 1. Fault offsets, depth of faulting, fault dip and dip direction from USGS seismic line

Fault	Station Along Seismic line (meters)	Approximate Depth of Shallowest Faulting (meters)	Approximate Offset (meters)	Fault Dip	Dip Direction
1	45	40	10	53°	N
2	112	15	10	65°	N
3	237	0	5-10	90°	-
4	360	15	5 at 90 m depth	90°	-
5	400	40	15 at 85 m depth	75°	N
6	495	<5	≤5	90°	-
7	543	30	<5 m at 90 m depth	90°	-
8	600	<10	7	90°	-
9	685	<12	10	75°	N
10	720	<20	10	85°	S
11	775	<30	?	83-90°	S

4.3 Gouge Core and Vibracore Transect: Stratigraphic, Paleoecologic, and Radiometric Analyses

In describing the stratigraphy at the Tolay marsh site, we present lithologic, paleontologic, and radiometric data and use this information to characterize the depositional environment. From these data, we interpret the history of relative sea level and environmental changes that affected Tolay marsh. The implications of the stratigraphic record to a potential earthquake chronology are presented in the Discussion section below.

Our gouge core exploration program included three gouge core transects. Gouge core transects #1 and #2 were located across the northeast-side of the SRCF zone on reclaimed land ;and transect #3 was located on the southwest side of the SRCF zone within the modern Tolay marsh. Gouge core transect #3 was a reconnaissance transect aimed at gaining a preliminary understanding of the modern marsh stratigraphy absent of most reclaimed land cultural modifications. Along transect #3, coarse alluvium (Unit 0 discussed below), was relatively shallow and no prominent paleo-marsh deposits were preserved in the deeper stratigraphy. Thus, our gouge core and vibracore efforts were focused on the northeast-side of the fault where multiple marsh-like deposits were encountered. Below is a description of the stratigraphy interpreted in gouge core transect #1.

4.3.1 Marsh Stratigraphy and Depositional Environment

The stratigraphy observed in gouge cores and vibracore samples along gouge core transect #1 reveals several alluvial and shallow estuarine stratigraphic packages capped by incipient marshes (peaty muds) and laminated algal mat-rich horizons (Figure 8; Table 2). The marsh stratigraphy presented here

represents the combined description of twelve gouge cores and two vibracores along gouge core transect #1 (Table 2). The depth of exploration along this transect ranged from 1.5 to 2.8 m.

Table 2. Description of stratigraphic units within gouge core transect # 1

Unit	Sub Unit	Description
Unit 5	Unit 5	Light brown to light gray silty CLAY to CLAY – upper 20 cm very soft with porous open soil structure (AP horizon), becomes stiffer with depth, abundant rootlets, generally massive with laminations, pinhole porosity [**Bay Mud with modern soil**]
Unit 4	Unit 4b	Gray to gray brown silty CLAY – moist, moderately stiff, 2 to 4 cm thick horizons with black laminations, black laminations appear to be charcoal 1-2 mm thick, 1-2mm diameter, FeO stains, fine rootlets common, upper contact sharp to clear [**Bay Mud with algal mat laminations**]
	Unit 4a	Very dark gray brown silty CLAY – massive, moist, stiff, very weak orange brown mottles <1 mm thick, appears bioturbated near base [**BAY Mud**]
Unit 3	Unit 3d	Black to gray CLAY – moist, moderately stiff, 1-2 mm thick laminations of charcoal or MnO horizons, upper contact sharp to clear [**Bay Mud with algal mat laminations**]
	Unit 3c	Gray to very dark gray silty CLAY – massive, moist, FeO mottles surrounding root casts, clay along root casts, marbleized appearance with no texture change throughout, appears bioturbated towards base of unit, very small black flecks = charcoal or MnO horizons [**Bay Mud**]
	Unit 3b	Light gray to gray to black silty CLAY– moist, soft, fine rootlets, 3-5 mm thick laminations of black to dark gray charcoal mats, also contains reddish brown vegetal mats, Upper contact sharp to gradual [**Bay Mud with algal mat laminations**]
	Unit 3ab	Black silty CLAY, massive, moderately stiff to stiff, 5-1 cm long FeO stains to granular nodules, with trace yellowish brown stains, random mottles with marbleized appearance, sparse to no distinct plant material, where vegetal matter is present forms weak horizontal parting, otherwise generally massive with weak subangular blocky soil structure, [**possible Buried Incipient Marsh**]
	Unit 3a	Gray to very dark gray silty CLAY – massive, moist, FeO mottles surrounding root casts, clay along root casts, marbleized appearance with no texture change throughout, appears bioturbated towards base of unit, very small black flecks = charcoal or MnO horizons [**Bay Mud**]
Unit 2	Unit 2e	Very dark gray brown to greenish gray to black CLAY – moist, soft, silky, generally massive with 2-3 cm thick horizons with black charcoal-rich laminations and minor reddish brown plant-rich horizons (less prominent than Unit 2d), root casts resemble pickle weed stems(?), Upper contact clear [**Bay Mud with algal mat laminations**]
	Unit 2d	Very dark gray brown to dark brown to black CLAY – moist, soft, silky, 2-4 cm thick horizons with black charcoal-rich laminations and reddish brown vegetal-rich horizons, root casts (pickle weed stems?), upper contact generally sharp in places clear [**Peaty Bay Mud – Buried Incipient Marsh #2**]
	Unit 2c	Light to dark gray sandy CLAY to SAND with clay, trace pea gravel, subrounded chert clasts [**Overbank Alluvium**].
	Unit 2b	Light gray CLAY – moist, soft, weak to prominent laminations of black plant material, grassy vegetal matter parallel to laminations [**Bay Mud with algal mat laminations**]
	Unit 2a	Black to very dark gray CLAY – massive, very soft, very little plant material no algal mat laminations [**Bay Mud**]
Unit 1	Unit 1c	Olive gray silty CLAY, massive with no charcoal laminations, minor plant debris and MnO_2 specs throughout, oxide mottles throughout [**Bay Mud**]
	Unit 1b	Black to very dark gray CLAY – very soft, moist, 1 to 2 cm thick alternating vegetal-rich horizons, upper 1 cm marked by black charcoal rich horizon, reddish brown plant material forms horizontal root mats, plant material = leafy grass (Cord Grass?), odoriferous, Upper contact sharp to clear [**Peaty Bay Mud – Buried Incipient Marsh #1**]
	Unit 1a	Light to dark gray sandy CLAY to SAND with clay, trace pea gravel, subrounded chert clasts [**Overbank Alluvium**].
Unit 0	Unit 0	Light bluish gray to gray clayey SILT to silty CLAY with trace sand and gravel. Massive with no visible laminations or bedding. Fining-upward sequence, pea gravel, subangular to subrounded chert nodules, 0.5 to 1 cm thick vertical anastamosing root casts with orange brown weathering rinds [**Overbank Alluvium**]

The stratigraphy within gouge core transect #1 consists of six different stratigraphic packages from basal sandy Quaternary alluvium (Unit 0) to the modern Bay mud (Units 1 to 4) with modern soil (Unit 5). Units were grouped based on similar stratigraphic/textural characteristics and the presence/absence of vegetal-rich horizons (e.g. Unit 4b). We identify six different stratigraphic packages within the buried marsh stratigraphy in gouge core transects 1 and 2 that represent either incipient marshes (peaty mud – Unit 1b and 2d) or Bay mud with agal matt laminations (Units 2b, 3b, 3d, and 4d). Each of these vegetal-rich horizons appear to cap an underlying massive or weakly laminated Bay mud. A detailed description of each unit and sub unit is provided on Table 2. Generally the units have the following characteristics (listed from oldest to youngest):

- Unit 0 – Overbank Alluvium – massive clayey silt to silty clay with trace sand and gravel. This unit is moderately stiff to stiff with a generally fining upward sequence. Seen throughout all the gouge core transects this unit is interpreted as a basal sandy alluvium that underlies the marsh stratigraphy of Tolay Marsh.

- Unit 1 – Massive soft clay (Bay mud) overlain by peaty mud (buried incipient marsh #1). The base of this unit is marked by a thin sandy unit (Unit 1a) above Unit 0. Upper contact sharp to clear.

- Unit 2 – Massive soft clay (Bay mud) with vegetal-rich laminations and vegetal-poor horizons. This unit is capped by peaty mud (buried incipient marsh #2, Unit 2d). Upper contact generally sharp in places clear

- Unit 3 – Massive soft clay (Bay mud) with a bioturbated base. A laterally discontinuous horizon with agal mat laminations preserved within Unit 3 and appears to onlap Unit 2 in the southern part of the section. Unit 3 is capped by a thin but laterally continuous laminated algal mat-rich horizon (Unit 3d). Upper contact is sharp to clear.

- Unit 4 – Massive soft clay (Bay mud) appears bioturbated near the base of the unit and is capped by a 15 to 40 cm thick horizon of thin agal mat laminations (2 to 4 cm thick) separated by massive clay. Upper contact is sharp to clear.

- Unit 5 – Silty clay to clay that is generally massive with no agal mat laminations or buried peaty mud. The upper 20 cm are very soft with a porous open soil structure interpreted as modern AP horizon.

Gouge core transects #1 (shown on Figure 7 and 8) and #2 (not shown) demonstrate that the marsh stratigraphy rises toward the surface in a westerly direction and defines a northeast-facing subsurface slope over which the deposits thin (Figure 8). The deeper stratigraphy (Units 1, 2, and 3) overlies Pleistocene stratigraphy (Unit 0) and appears to pinch out against the buried subsurface slope. We identify distinct elevation differences between closely spaced gouge cores 29 and 20 that allow for the interpretation of possible southwest-side-up faulting of Unit 2d (see Section 5.3 for further details). Another distinct elevation difference between gouge cores 17 and 30 is inferred that allows for the interpretation of possible northeast-side up faulting of Unit 1c. However, the interpretation of faulting between gouge cores 17 and 30 is very weak because it is based on primarily on gouge core 17 (identifying the deep section of Unit 1c) and not confirmed in multiple gouge cores.

4.3.2 Paleoecological Environment

We collected five paleoecological samples from vibracore #2 between a depth of 130 to 170 cm to characterize the depositional environment and biostratigraphic characteristics of the marshes in gouge transect #1. The stratigraphic, lithologic and biostratigraphic characteristics of the deposits are described below and summarized in Tables 3 and 4, Figures 7, 8 and 9, and Appendix A.

4.3.2.1 Vibracore Diatom Samples

Diatoms were present in all vibracore samples with a total of about 95 different diatom taxa identified in the five core samples (Appendix A). Of these diatom taxa, 31 exceeded 2% of the assemblage in at least 1 sample (See Appendix A Figure 1). The results of these analyses are summarized in Table 3 and described in more detail in Appendix A. Below is a description of the results of these analyses starting with the deepest (oldest) to the shallowest samples (youngest).

Sample DS1 at 166 cm in vibracore #2 was assumed to have accumulated in a marsh or meadow setting based on its lithology (red-brown organic-rich mud; Unit 2d) (Figures 8 and 9). The diatom data indicate the setting was probably a brackish-marine intertidal marsh. Diatoms are abundant and well preserved in this sample, dominated by *Fragilaria subsalina*, which is commonly found in coastal salt marshes (Jensen, 1985; Witkowski et al., 2000). Other prominent benthic diatoms include *Navicula peregrina*, *Achnanthes brevipes*, and *Bacilaria paradoxa*. In combination with *F. subsalina*, this assemblage shows that this was a wet, brackish-marine setting, and not a fresh or relatively dry setting as would be expected above MHHW. Planktonic diatoms, which are usually a significant component of lower intertidal samples, are absent from DS1. This shows that the site was protected from regular flooding from San Pablo Bay.

A paleoecological shift (relative sea-level rise) is indicated by a change from a "salt marsh assemblage" in sample DS1 at 166 cm, to a "lower intertidal/shallow subtidal assemblage" in sample DS3 at 155 cm (Figure 9). Unlike the diatom assemblage in DS1, which consists of a low-diversity, well-preserved assemblage (Figure 9; Appendix A), DS3 contains a diverse, mixed assemblage of well-preserved benthic and planktonic diatoms and abundant diatom fragments. The lithology for DS3, mud with plant laminae, may be indicative of a lower intertidal algal mat zone, which would be consistent with an interpretation of a lower intertidal/shallow subtidal diatom assemblage. Further, diatom preservation is qualitatively better in DS3 than in massive mud at DS-4a (153.5 cm), with more frequent occurrences of delicate elongate taxa. It is possible that the diatoms in DS3 are better preserved because of less sediment reworking by currents and infauna in an algal mat zone.

Lower intertidal to shallow subtidal environments are indicated for samples DS3, DS-4a, DS3a, and DS-5 based on dominant diatom taxa (Figures 9; Table 3). Estuarine-marine planktonic diatoms are particularly prominent in DS3, but present in the remaining samples as well, indicating an open exchange with the San Francisco Bay estuary. Mixed assemblages of benthic diatoms, including well-preserved *Tryblionella granulata*, *T. navicularis*, and *Diploneis stroemii*, all support deposition on tidal flats, sloughs, or shallow subtidal areas.

Table 3. Summary of diatom results for vibracore #2

Core sample	Lithology[a]	Paleoenvironment based on diatoms	Diatom evidence
DS5 (148 cm)	Base of very dark greenish gray CLAY, massive with weak clay laminations	Lower intertidal or shallow subtidal zone	Well-preserved benthic diatoms commonly found in lower intertidal /shallow subtidal zone (esp. *Diploneis stroemii*), with less frequent but well-preserved coastal planktonic species. Abundant diatom fragments typical of coastal/tidal flat deposits.
DS3a (151 cm)	Black to dark gray clay with weak charcoal laminations	Lower intertidal or shallow subtidal zone	Well-preserved benthic diatoms commonly found in lower intertidal /shallow subtidal zone (esp. *Tryblionella granulata*), with less frequent but well-preserved coastal planktonic species. Abundant diatom fragments typical of coastal/tidal flat deposits.
DS4a (153.5 cm)	Very dark greenish gray CLAY, massive with weak clay laminations	Lower intertidal or shallow subtidal zone	Mix of well-preserved coastal planktonic diatoms and benthic taxa typical of tidal flats. Abundant diatom fragments typical of coastal/tidal flat deposits.
DS3 (155 cm)	Top of very dark brown CLAY, plant material forming mats	Lower intertidal or shallow subtidal zone (algal mat/tidal flat area?)	Mix of well-preserved coastal planktonic diatoms and benthic taxa typical of tidal flats. Abundant diatom fragments typical of coastal/tidal flat deposits. Greater frequency of unbroken elongate valves than in DS3, possibly suggesting less sediment reworking.
DS1 (166 cm)	Reddish brown CLAY, organic-rich mud (buried peaty mud)	Salt marsh (likely protected from regular flooding of San Pablo Bay)	Abundant well-preserved benthic diatoms commonly found on salt marshes; very rare planktonic diatoms (< 1.5% of assemblage).

Evidence for relative sea-level rise (submergence) is indicated by a shift in diatom assemblages between samples DS1 and DS3 (Figures 1, 2; Table 1). Well-preserved benthic diatoms in DS1 (organic-rich peaty mud) are commonly found on salt marshes (Jensen, 1985; Witkowski et al., 2000), and the absence of coastal planktonic diatoms suggests the site was protected from regular inundation from the San Pablo Bay. Diatoms in DS3 (mud with plant material forming mats) consist of a mix of coastal planktonic and brackish-marine benthic diatoms consistent with lower intertidal or shallow subtidal areas. Therefore, the diatom data suggest that a previously protected marsh at the core site (sample DS1) was converted to a tidal flat, slough, or shallow subtidal area open to San Pablo Bay (sample DS3). Although speculative at this point, it is possible that the lithology for DS3 is the result of sediment accumulation related to rapid sea level rise and deposition of intertidal algal mats. The diatom assemblage in DS3 would be consistent – though not definitive – of accumulation in an algal mat zone.

The three additional core samples (DS4a, 153.5 cm; DS3a, 151 cm; and DS5, 148 cm) also contain diatom assemblages consistent with accumulation in the lower intertidal or shallow subtidal zone. Comparable to DS3, these samples show: (1) a mix of lower intertidal benthic taxa and varying amounts of well-preserved coastal planktonic species; (2) relatively high species richness (> 0.2) as compared to the marsh sample (0.06), which is typical for lower intertidal as compared to high intertidal or supratidal settings; and (3) fewer well-preserved taxa but abundant diatom fragments, indicative of sediment reworking by currents or infauna. Planktonic diatoms are slightly less prominent in the uppermost 2 samples (DS5, DS3a), possibly suggesting some shoaling and less influx from San Pablo Bay, but this is speculative and the data may also be recording relatively greater production or preservation of benthic taxa rather than reductions in accumulation of planktonic species.

4.3.2.2 Modern diatoms from marsh/meadow surfaces near the core site

In order to possibly identify modern analogs to the vibracore diatom samples, diatoms were evaluated in 7 samples collected from marsh/meadow surfaces in the modern Tolay marsh near gouge core transect #3 (Table 4; Figure 5). Although there were some species in common between the modern (Tolay marsh) samples #3-7 and the vibracore samples, there were no obvious similarities between overall assemblages. The modern assemblages from the grassy high marsh or supratidal settings (Tolay marsh samples #1 and #2) did not compare to any vibracore samples, as all of the vibracore samples contained species indicative of wet salt marsh or lower intertidal/shallow subtidal settings. None of the modern samples contained high numbers of Fragilaria subsalina, which is the dominant species in vibracore samples DS1 (Appendix A Figure 1). Planktonic diatoms are absent in the modern samples. Planktonic diatoms are also not found in DS1, but are prominent in the remaining core samples.

Therefore, none of the modern marsh samples collected for the study are strong analogs or share distinctive similarities to the marsh samples selected for analysis from vibracores #2. The environment that supported the assemblage dominated by *F. subsalina* in DS1 is not represented by any of the marsh settings sampled on the modern surface near the core location. Further, the modern analog settings for the remaining core samples (DS3, 4a, 3a, and 5) would more likely be tidal flats or shallow channels since prominent taxa in those samples include benthic taxa (e.g., *Tryblionella granulata*, *Diploneis stroemii*) commonly found in lower intertidal/shallow subtidal areas, as well as large coastal planktonic diatoms (*Cyclotella striata*, *Coscinodiscus radiatus*).

Table 4. Qualitative overview of diatoms in modern surface samples from marsh/meadow locations in the vicinity of gouge core transect #3

Sample	Sample description	Diatom summary
Tolay Marsh #1	> MHHW (grasslands above marsh); blue-eyed grass + unidentified plant	Diatoms represented by only a few valves of P innularia borealis, Hantzschia amphioxys: consistent with fresh, dry grassy environment. Highly comparable to sample #2.
Tolay Marsh #2	~MHHW high marsh; Australian saltbrush (?), Meadow Barley/ Mediterranean Barley	Diatoms represented by only a few valves of P innularia borealis, Hantzschia amphioxys: consistent with fresh, dry grassy environment. Highly comparable to sample #1.
Tolay Marsh#3	MHW-MHHW; *Salicornia*	Diatoms frequent but not abundant; most common taxa are Navicula atwateri, N. salinarum; less frequent Nitzschia faciculata. Probably represents drier conditions than indicated by diatoms (particularly M. nummuloides) in salt marsh sample #4.
Tolay Marsh#4	MHW-MHHW; *Salicornia, Spartina*	Diatoms common, indicative of wet low marsh environment: Melosira nummuloides, Tryblionella navicularis, Nitzschia fasciculata, Caloneis westii, Nitzschia s capelliformis; Navicula peregrina present but rare; no planktonic diatoms.
Tolay Marsh #5	MHW-MHHW; *Salicornia, Spartina*	Diatoms rare overall for unknown reason. Nitzschia fasciculata and Tryblionella navicularis present but rare.
Sears Point #6	MHW-MHHW; *Salicornia, Jaumea*	Common benthic diatoms, esp. Nitzschia fasciculata, Tryblionella navicularis, Nitzschia sigma, Luticola muticoides. Very rare, possibly planktonic, taxa represented by Thalassiosira spp.
Sears Point #7	MHW-MHHW; *Salicornia, Spartina*	Common benthic diatoms; no planktonic diatoms. Prominent taxa = Nitzschia fasciculata, Gyrosigma eximium, Tryblionella acuminata. Trybionella navicularis present but rare.

Note: Salicornia = "pickleweed;" *Spartina* = "cordgrass."

[1] Planktonic diatoms are absent in the modern samples with the possible exception of a few rare valves of the genus *Thalassiosira* in sample #6.

4.3.3 Radiocarbon Results

A total of seven radiocarbon samples were collected from the cores and dated to assess the sedimentation rate in the marsh, and age of the marsh and key peat deposits. The radiocarbon results are presented in Table 5.

In general, the radiocarbon ages for the buried soils are consistent with the stratigraphic position of each sample with some anomalous ages. The radiocarbon samples were chosen because they were preserved within distinct, laterally continuous horizons with sharp upper contacts. Three samples were selected from Unit 2d and two from Unit 2e. In general, the dates overlap and indicate that Unit 2d peaty mud was deposited between 1990 and 2350 cal yr BP (2-sigma error). The lone exception is sample GC-23-RC4 from gouge core 23 and Unit 2d which yielded a considerably older age ranging from 2735 to 2765 cal yr BP. This sample is located considerably southwest from gouge core #21 and vibracore #2 and abuts the buried topographic slope, thus it may be receiving reworked material from the adjacent slope face. Radiocarbon samples from the base and top of Unit 3 indicate this unit was deposited after 2120 to 1900 cal yr BP and before 1690 to 1540 cal yr BP (Figure 8; Table 5). Radiocarbon samples VC2-RC8 and VC2-RC9 cap the end of deposition for Unit 2e (and the maximum age of deposition for Unit 3) between

2160 to 2260 and 1900 to 2120 cal by BP, respectively. The radiocarbon age for VC2-RC8 is measured as older than the deeper VC2-RC9 and thus appears out of sequence. We believe the radiocarbon age for VC2-RC8 is incorrect because this radiocarbon sample was run as a bulk sample of organic-rich soil (the sample lacked enough plant material for a conventional date). Radiocarbon sample GC-21RC1 indicates deposition of Unit 3d likely ended around 1690 to 1660 cal yr BP (Figure 8; Table 5).

Table 5. Radiocarbon data for the Tolay marsh site, Sonoma County, California

Core No.	Laboratory Sample No.	Sample Material	Sample Depth (cm)[b]	Stratigraphic Unit	$\delta^{13}C$	Lab-Reported Age (14C yr BP at 1σ)[c]	Calibrated Age (Cal yr BP at 2 σ)[d]
GC-21-RC1	PRI-10-37-RC1	Plant material	83 to 89	Unit 3d	-21.4	1690±15	1690 to 1660 1630 to 1540
GC-21 RC-3	PRI-10-37-RC3	Plant material – wood debris	157	Unit 2d	-23.1	2250±20	2340 to 2290 2260 to 2150
GC-23-RC4	PRI-10-37-RC4	Plant material – wood debris	119	Unit 2d	-27.1	2615±15	2765 to 2735
VC2 RC-8[a]	Beta – 279299	Bulk sample – organic-sediment	143	Unit 2e	-20.3	2240±40	2350 to 2300 2260 to 2160
VC2 RC-9[a]	Beta – 2793000	Plant material	150.5	Unit 2e	NA[e]	2040±40	2120 to 1900
VC RC-10[a]	Beta – 279301	Plant material	155	Unit 2d	-14.5	2120±40	2300 to 2260 2160 to 1990
VCR2 RC-11[a]	Beta – 279302	Charcoal	160	Unit 2d	NA[e]	2260±40	2350 to 2290 2280 to 2150

a Standard pretreatment of samples performed by Beta Analytic.
b Sample interval measured as depth below marsh surface.
c Conventional ages reported by radiocarbon laboratory based on the Libby half life (5570) for ^{14}C.
d Calibrated age ranges before AD 1950 reported to the nearest decade, calibrated by Beta Analytic using methods outlined in Stuiver and Reimer (1993) and Stuiver et al. (1998).
e The original sample was too small to provide a 13C/12C ratio on the original material. However, a ratio including both natural and laboratory effects was measured during the 14c detection to calculate the true Conventional Radiocarbon age.

5.0 DISCUSSION

5.1 Bedrock Structure and Geomorphic Expression of the Southern Rodgers Creek

Our data compilation, geomorphic mapping, and the USGS seismic line images indicate that the SCRF is structurally complex at the Tolay marsh site and has geologic/geomorphic evidence of Holocene surface fault rupture (Figures 5 and 6). Prominent tectonic geomorphology, along with trench data, help to identify recently active SRCF fault strands. Preliminary interpretations of the P-wave data suggest that the fault strands form an approximately 500-to 600-m-wide flower structure coincident with a bedrock ridge traversing the center of the site. In the subsurface (upper 200 m), as many as 11 fault strands define three distinct fault zones of variable width: two that are fairly broad (50- to 100-m-wide) and one that is narrow (5- to 20-m-wide) (Table 1). The faults extend from >400 m at depth and up to the ground surface (in some cases) with apparent vertical displacements ranging from 15 m to less than 5 m. Several of these faults are also roughly coincident with mapped geomorphic lineaments and Holocene active faults. For example, faults 1, 2, 3, 4, 5, 6, and 7 are coincident with topographic lineaments on the southwest and northeast margin of the bedrock ridge (Figures 5 and 7).

The findings from the geologic and geomorphic mapping, and geophysical data, indicate faults #6 and #7 (Figures 5, 6, and 7) represent an active fault strands of the SRCF that have accommodated considerable strike-slip deformation. Fault #7 is coincident with the northeastern margin of the bedrock ridge that bisects the site and intersects gouge core Transects #1 and #2 (Figure 5). Fault #6splays from fault #7 and extends to within5 meters of the ground surface (Figure 6) and is along strike with a prominent Holocene fault mapped along the northeastern ridge crest northwest of Highway 121. These geomorphic lineaments are coincident with bedrock faults mapped by Wagner et al. (2002) that separate Sonoma Volcanics and Petaluma Formation. In addition, faults #6 and #7 also coincide with a velocity anomaly within the geophysical profile we interpret to represent the contact between Sonoma Volcanics on the northeast and Petaluma Formation on the southwest. These data indicate the bedrock fault represented by faults #6 and #7 has accommodated a significant component of lateral slip to juxtapose dissimilar rock types.

5.2 Origin and Evolution of the Tolay Marsh

Tolay marsh is located northwest of the Tolay Creek sloughs and is split by the bedrock promontory cored by the SRCF fault (Figure 5). Based on the location of Tolay marsh at the northern margin of the San Francisco Bay, we infer that Tolay Marsh began forming as a result of Holocene sea level rise and aggregation of bay mud over sandy alluvium (Unit 0).

We infer the following history of sediment accumulation and environmental change within Tolay Marsh based on sedimentologic characteristics of the buried peaty muds, distributions of algal mats, and their associated fossil diatom assemblages. The stratigraphy within gouge core transect #1 indicates four periods of relative landscape stability where incipient "marsh deposits" were able to develop (either weakly developed marshes or algal mat-rich horizons). Each of these weakly organic deposits cap a massive clay (or bay mud) that was deposited through submergence, either sea-level rise or land subsidence. Early mudflat deposition in an intertidal setting began before ~2700 to 2300 yr BP when sea level rose high enough to preserve Units 1b (Buried incipient marsh #1). This early marsh was then buried by clay interspersed with algal mat laminations (Units 2b). The next period of landscape stability is marked by Unit 2d (buried incipient marsh #2) which formed around 1900 to 2350 cal yr BP. Unit 3 was deposited subsequently and capped by a laterally continuous algal mat-rich horizon that formed

between 1660 and 1690 yr BP. Overlying Units 4b and 5 represent the latest periods of stability, but their ages remain unconstrained.

5.3 Evidence for Coseismic Submergence

Evidence for co-seismic submergence within the Tolay marsh study area is generally weak with possibly one recorded earthquake between 2350 and 1990 yr BP. Evidence for co-seismic submergence and recent faulting with transect #1 includes: 1) paleoecologic data that suggests a change in diatoms within the Unit 2d peaty mud, and 2) potentially 10 to 15 cm of vertical offset of Unit 2d in the southern portion of the transect. Interpretation of additional event stratigraphy is plausible, but driven by the structural geologic conditions and existing diatom assemblage information, we refrain from speculating on other event scenarios.
To evaluate whether the buried Tolay marsh soils (i.e., peats) were buried by rapid sea level rise controlled by either tectonic subsidence or alternative non-tectonic processes, we used coseismic criteria modified from Nelson et al. (1996) and Knudsen et al. (2002). These criteria are shown in Table 6, and include: (1) presence of an abrupt upper lithologic contact; (2) diatom evidence for relative sea level change; (3) evidence for sustained submergence and/or rapid aggradation; (4) wide lateral extent of submergence; (5) synchroneity with other paleoseismic events; and (6) located near an active fault. Buried peaty soils that satisfy more than three coseismic criteria are considered more likely to have a coseismic subsidence origin than a non-tectonic origin (Carver and McCalpin, 1996 as summarized by Knudsen et al., 2002). Therefore, we sum the number of criteria satisfied for each buried peat soil (Table 6), and present evidence supporting possibly one event (buried incipient marsh #2) caused by rapid relative sea level rise.

Unit 2d (buried incipient marsh #2) satisfies five of the six criteria proposed to distinguish coseismic from non-tectonic sea level change (Table 6). Diatom assemblages from Unit 2d (diatom samples DS1 and DS3) indicate that the depositional environment changed from a salt marsh (isolated from regular San Pablo Bay flooding) to a tidal flat (lower intertidal or shallow subtidal zone). The diatom data suggest that a previously protected marsh at the site (sample DS1) was converted to a tidal flat, slough, or shallow subtidal area open to San Pablo Bay (sample DS3). Although speculative at this point, it is possible that the lithology for DS3 is the result of sediment accumulation and deposition of intertidal algal mats. The lateral continuity and sharp upper contact (2 mm) of buried marsh within Unit 2d (sample DS1) suggest this change could be consistent with rapid coseismic submergence for a sustained period long enough to develop a new base level and create aggradation at the inter tidal level. However, the well-preserved peaty mud within Unit 2d is overlain by 4 to 6 cm of algal mat-rich mud. This change suggests that some type of rapid change in depositional environment occurred (subsidence or sea level rise), but was not large enough to totally submerge the area and prevent algal mats from forming. Finally, the lateral continuity of the buried incipient marsh within Unit 2d across the width of the paleo-marsh (50 m – between two transects) indicates that relative sea level change (subsidence) occurred across a large area of the paleo-marsh surface near the SRCF.

Based on the stratigraphic and paleoecologic evidence for rapid submergence of Unit 2d, we speculate that it is possible that an earthquake on the SRCF caused coseismic land-level change within Tolay marsh around 2350 to 1990 cal yr BP. The interpretation of coseismic subsidence of Unit 2d is supported by the possible faulting and uplift of the unit between gouge cores 29 and 20. Here, we map elevated Quaternary overbank alluvium that is overlain by a thin sandy unit (Unit 2c – GC23 and VC#1) followed by the buried marsh of Unit 2d. The base of Unit 2d was measured 10 to 15 cm higher in GC29 than GC20 located directly to the east, which we speculate could represent fault offset. This fault offset would be consistent with reverse faulting (up on the southwest) along the margin of the SRCF flower structure.

The upper contacts of Units 3d and 4d satisfy three of the five coseismic criteria (Table 6. At the upper contacts a coseismic subsidence interpretation is supported by lateral continuity, contact abruptness, and proximity to an active fault. Both Units 3 and 4 have thick sections of massive mud (> 50 cm) capped by agal mat-rich soil horizons that are laterally continuous over the entire section (Figure 8), which suggest a change in base level causing aggradation of mud lacking algal mats. However, these units all formed in a tidal flat environment requiring only a small change in base level to aggrade massive mud or preserve algal mats. No diatom samples from the upper contacts of Unit 3d and 4d were sampled as part of this limited pilot study and thus the paleoecologic environment of these units remains uncertain. Using diatom samples DS3 to DS5 collected from Units 2d and 2e and their similar sedimentologic characteristics, we infer that the paleoecologic environment of Units 3d and 4d closely resemble that of Units 2d and 2e. However, lacking the diatom data, we are unable to substantiate if the preservation of Units 3d and 4d was the result of coseismic submergence or non-tectonic aggradation.

The upper contact of Unit 1b satisfies two of the possible five coseismic criteria (Table 6). The basal contact of Unit 2a is sharp, but this unit was limited to the northeastern portion of the transects and is not laterally continuous based on the limited data (Figure 8). We believe it is likely that these deposits are preserved further to the northeast, but their extent remains poorly constrained. The peaty mud of Unit 1b contained abundant plant material (cord grass?) and represents one of the most well-preserved buried marsh deposits encountered at the site. Unit 1a is interpreted as being conformable with the east-facing slope of Quaternary alluvium (Unit 0). This stratigraphic relation is consistent with either basin infilling or a subsiding basin coincident with a change in sea-level elevation.

Table 6. Criteria indicative of coseismic subsidence for peaty soils, Tolay marsh site

Stratigraphic Horizon	Abrupt Lithologic Contact	Diatom Evidence for Relative Sea Level Change	Evidence for Sustained Submergence and/or Rapid Aggradation	Wide lateral Extent of Submergence	Synchronous with other Paleoseismic Events	Located Near an Active Fault	Number of Criteria Satisfied	Caused by Co-Seismic Subsidence
Unit 1b	Yes	NA*	No	No	?	Yes	2	Possible
Unit 2d	Yes	Yes	Yes	Yes	Yes (on the NHF)	Yes	4	Yes (?)
Unit 3d	Yes	NA*	Yes	Yes	Yes (on the NHF)	Yes	4	No
Unit 4d	Yes (sharp t o clear)	NA*	Yes	Yes	?	Yes	4	No

*NA – not available

5.4 Comparison of Preliminary Results with other Paleoseismic Studies

The single prehistoric paleoseismic event interpreted from this limited pilot study is tentatively correlative with event(s) identified at other sites along the northern Hayward fault and the central Rodgers Creek fault. The age of the Tolay marsh event (i.e. subsidence of Unit 2d) is interpreted as occurring after 2150 to 2350 yr BP (2σ) but before 1900 to 2300 yr BP. Under these timing constraints, the Tolay marsh event is roughly contemporaneous with two poorly constrained events (E3 and E4) on the northern Hayward fault (HFPG, 1999). For instance, events E3 and E4 occurred between 392 yr BC and 54 yr AD (2347 to 1902 yr BP); and 355 yr BC to 13 yr AD (2310 and 1942 yr BP). Interestingly, Randolph Loar et al. (2004) identified a broadly constrained event that occurred before 1,050-790 cal yr BP and after 10,730-9,550 cal yr BP that could be correlative with the submergence event of Unit 2d. However, this event is so poorly constrained it adds little to the understanding of the late Holocene paleoseismic history of the SRCF. Schwartz et al. (1992) does not report any paleoseismic events on the central Rodgers Creek fault older than 1,000 yr BP thus a more robust correlation is not possible at this time.

6.0 SUMMARY OF FINDINGS

Our pilot investigation of Tolay marsh straddling the SRCF provides evidence of coseismic submergence in the late Holocene. The pilot feasibility study consisted of: (1) mapping Holocene fault-related geomorphology and Quaternary geology at the site; (2) collecting and interpreting geophysical data across the SRCF; and (3) evaluating possible stratigraphic and structural evidence for coseismic submergence related to large earthquakes on the SRCF.

Preliminary interpretation of a P- and S-wave seismic line collected for this study indicate faults identified from the mapping and nearby consultant trenches form a broad approximately 500-to 600-m-wide transpressional structure that coincides with a northwest-trending bedrock ridge that projects into Tolay marsh (Figure 6). Three fault zones align with the bedrock high and consist of multiple upward branching fault strands that closely approach the ground surface. Several of the fault strands seismically imaged coincide with mapped Quaternary and Holocene fault traces (Figure 5). Faults along the northeastern margin of the bedrock ridge imaged in the geophysical survey are defined by a P-wave velocity anomaly that demarcates the juxtaposition of Sonoma Volcanics and Petaluma Formation, and thus is inferred as a primary strand intersecting the marsh site.

Coring of marsh sediment along the northeast and southwest margins of the fault-controlled bedrock ridge provides evidence for coseismic elevation changes across the SRCF. Stratigraphic and paleontologic analyses of gouge and vibracore samples is used to interpret "older" (late Pleistocene (?) to Holocene) alluvium overlain by multiple sequences of buried late Holocene marsh sediments (poorly to well developed),subtidal (mud), and algal mat deposits. Compilation of subsurface coring data along transects #1 and #2 that intersect the SRCF indicate a thinning of deposits across a buried east-facing ridge and thickening of deposits east of the ridge. Distinct elevation differences across the base of marsh and mud strata near this subsurface inflection allow for the interpretation of possible southwest-side-up vertical displacement of Unit 2d. The location of these stratigraphic and structural anomalies is roughly coincident with geophysically-imaged subsurface offsets. The style and pattern of deformation inferred from transects is consistent with the expected style of coseismic deformation on the northeast margin of the SRCF transpressional structure.

Based on the paleoecological data, stratigraphic data, and a criteria matrix, we tentatively interpret one paleoseismic event on the SRCF at the Tolay marsh site. Diatom and radiometric analyses on a buried peaty mud horizon (Unit 2d –buried incipient marsh #2) suggest that a rapid change in paleoecological environment, possibly subsidence, occurred after 2150 to 2350 yr BP (2σ) and before 1900 to 2300 yr BP. The evidence for this submergence event remains poorly constrained and further work is required to confirm the existence of this event. Additional event horizons are speculated and discussed in this pilot study; however only this late Holocene event defined by Unit 2d satisfies the majority of the criteria for coseismic subsidence (Table 6) allowing for the interpretation of a tectonically-controlled submergence event at the Tolay marsh site (Carver and McCalpin, 1996; Nelson et al., 1996; Knudsen et al., 2002; Koehler et al., 2005).

Further paleoseismic investigations at the Tolay marsh site are not recommended at this time because (1) the fault zone architecture of the SRCF is a complex flower structure that may not produce distinct coseismic relative elevation changes large enough to be identified directly through traditional marsh paleoseismic studies; and (2) the weak marsh stratigraphy encountered within the upper horizons (<1 m or approximately last 1,500 yrs) generally does not contain well-preserved incipient marsh deposits suitable for further study.

7.0 ACKNOWLEDGEMENTS

This research was supported by the U.S. Geological Survey's National Earthquake Hazard Reduction Program, under Award No. G09AP00072. The views and conclusions contained in this document are those of the Principal Investigators and should not be interpreted as necessarily representing the official policies, either expressed or implied, of the U.S. Government. We give many thanks to the California Department of Fish and Game, and Mr. Justin Faggioli for allowing FWLA and the USGS access and approval to conduct this study. Thanks to Suzanne Hecker of the U.S. Geological Survey for providing detailed aerial photos of the Tolay marsh site. The acquisition of the seismic line was supported by several very hard working U.S. Geological Survey staff (Coyn Criley, Mark Goodman, and Robert Sickler) and devoted USGS volunteers (Joe Catchings and Coe Criley), which made this experiment possible. Cary Gott of Vineyard & Winery Estates kindly shared the RGH Consultants, Inc (2009) study at Roche Winery.

8.0 REPORTS/ABSTRACTS PUBLISHED

Although we plan to present the results of this research at a regional Geological Society of America meeting or Seismological Society of America soon, no research abstracts or report have been presented to discuss the initial findings of the study.

9.0 REFERENCES

Argus, D.F., and Gordon, R.G., 2001, Present tectonic motion across the Coast Ranges and San Andreas fault system in central California: Geological Society of America Bulletin, v. 113, p. 1580-1592.

Aydin, A., 1982, The East Bay Hills, a compressional domain resulting from interaction between the Calaveras and Hayward-Rodgers Creek faults: California Division of Mines and Geology Special Publication 62, p.11-22.

Budding, K.E., Schwartz, D.P., and Oppenheimer, D.H., 1991, Slip rate, earthquake recurrence, and seismogenic potential of the Rodgers Creek fault zone, northern California: Initial Results: Geophysical Research Letters, v. 18, no. 3, p. 447-450.

Carver, G.A., and McCalpin, J.P., 1996, Paleoseismology of Compressional Tectonic Environments, In: McCalpin, J.P. (Ed.), 1996, Paleoseismology, Chapter 5, International Geophysics Series, Vol. 60, Academic Press.

Cloud, W.K., Hill, D.M., Huffman, M.E., Jennings, T.V., McEvily, T.V., Nason, R.D., Steinbrugge, K.V., Tocher, D., Unger, J.D., Youd, T.L., 1970, The Santa Rosa Earthquakes of October, 1969, in Mineral Information Service, California Division of Mines and Geology, v. 23, no. 3, p. 43-63.

Floyd, M.A., Funning, G.J., Lipovsky, B., 2998, Geodetic evidence for creep along the Rodgers Creek and Maacama fault zones, northern California, American Geophysical Union Fall Meeting, abstract #G23B-0692

Funning, G.J., Burgmann, R., Ferretti, A., Novali, F., Fumagalli, A., 2007, Creep on the Rodgers Creek fault, northern San Francisco Area from a 10 year PS-InSAR dataset, Geophysical Research Letters, V. 34, L19306, doi:10.1029/2007GL030836

Galehouse, J.S., 1992, Creep rates and creep characteristics of Eastern San Francisco Bay Area faults: 1979-1992, in Borchardt, Glenn and others, eds., Proceedings of the Second Conference on Earthquake hazards in the Eastern San Francisco Bay Area: California Department of Conservation, Division of Mines and Geology Special Publication 113, p. 45-53.

Harris, R.A., and Simpson, R.W., 1998, Suppression of large earthquakes by stress shadows: a comparison of Coulomb and rate-and-state failure: Journal of Geophysical Research, v. 103, p. 24,439.

Hart, E.W., 1992, Recently active traces of the Rodgers Creek fault, Sonoma County, California: California Department of Conservation, Division of Mines and Geology Open-File Report 92-7, 14 p.

Hayward fault Paleoearthquake Group, 1999, Timing of Paleoearthquakes on the Northern Hayward fault Preliminary Evidence in El Cerrito, California, U.S. Geological Survey Open-File Report 99-318. 35 p.

Hecker, S., Pantosti, D.P., Schwartz, D.P., Hamilton, J.C., Reidy, L.M., Powers, T.J. 2005. The most recent large Earthquake on the Rodgers Creek Fault, San Francisco Bay Area. Bulletin of the Seismological Society of America. Vol. 95, No. 3. pp. 844-860, June 2005.

Herd, D.G. 1978. Map of Quaternary faulting along the southern Rodgers Creek fault zone, Glen Ellen, Petaluma River, and Sears Point 7.5 m quadrangles, California, USGS Open File Report. 78-306, map scale 1:24,000

Huffman M.E., and Armstrong, C.F., 1980, Geology for planning in Sonoma County: California Division of Mines and Geology Special Report 120, 29 p., plus plates.

Jennings, C.W. 1994. Fault activity map of California and adjacent areas. California Division of Mines and Geology. California Geologic Data Map Series, Map No. 6. 1:750,000 scale.

Jensen, N.G., 1985, Friedrich Hustedt: The Pennate Diatoms. A translation of Hustedt's "Die Kieselalgen, 2 Teil." Koeltz, Koenigstein, 918 pp.

Kelsey, H.M., R.C. Witter, and E. Hemphill-Haley, 2002, Plate-boundary earthquakes and tsunamis of the past 5500 yr, Sixes River estuary, southern Oregon: Geological Society of America Bulletin, 114, 3, 298-314.

Koehler, R.D. Witter, R.C., Simpson, G.D., Hemphill-Haley, E., Lettis, W.R. 2005. Paleoseismic Investigation of the Northern San Gregorio Fault, Half Moon Bay, California. U.S. Geological Survey National Earthquake Hazards Reduction Program. Award No. 04HQGR0045. 2005

Koehler, R.D. Witter, R.C., Simpson, G.D., Hemphill-Haley, E., Lettis, W.R., 2004, Paleoseismic Investigation of the Northern San Gregorio Fault at Pillar Point Marsh near Half Moon Bay, California U.S. Geological Survey National Earthquake Hazards Reduction Program Award Number 02HQGR0071

Knudsen, K. L., R. C. Witter, C. E. Garrison-Laney, J. N. Baldwin, G. A. Carver, L. B. Grant, and W. R. Lettis (2002). Past earthquake-induced rapid subsidence along the northern San Andreas fault: a paleoseismological method for investigating strike-slip faults, Bull. Seismol. Soc. Am. 92, 2612–2636.

McFarland, F.S., Lienkaemper, J.J., Caskey, S.J., Grove, K., 2007, Data from Theodolite Measurements of Creep Rates on the San Francisco Bay Region Faults, California: 1979-2007, U.S.Geological Survey Open-file report 2007-1367, 14 p.

Nelson, A.R., 1992a, Discordant 14C ages from buried tidal-marsh soils in the Cascadia subduction zone, southern Oregon coast, Quaternary Research, 38, 74-90.

Nelson, A.R., 1992b, Holocene tidal-marsh stratigraphy in south-central Oregon coast-Evidence for localized sudden submergence in the Cascadia subduction zone, *In:* Quaternary Coasts of the United States-Marine and Lacustrine Systems, C.P. Fletcher and J.F. Wehmiller (Editors), Special Publication Society Economic Paleontol. Mineral., 48, 287-301.

Nelson, A.R., Shennan, I., and Long, A.J., 1996, Identifying coseismic subsidence in tidal-wetland stratigraphic sequences at the Cascadia subduction zone of western North America, Journal of Geophysical Research, 101, No. B3, 6115-6135.

Prescott, W.H., Savage, J.C., Svarc, J.L., and Manaker, David, 2001, Deformation across the Pacific-North America plate boundary near San Francisco, California: Journal of Geophysical Research, B, Solid Earth and Planets, v. 106, no. 4, p. 6673-6682.

RGH Consultants, Inc., 2009, Alquist-Priolo Fault Hazard Study: New Carneros Winery 27665 Arnold Drive Sonoma California, prepared for O'Neil Vintners and Distillers, dated April 15, 2009.

Randolph Loar, C.E., and Caskey, S.J., 2001 Neotectonics of the southern Rodgers Creek fault, Sonoma County, CA [abs]: EOS Transactions, Annual American Geological Union Meeting, v. 82, no. 47, p. F935.

Randolph Loar, L., 2002, Neotectonics of the Southern Rodgers Creek Fault, Sonoma County, California: Masters Thesis, San Francisco State University, 154 p.

Randolph Loar, L. C. E., Witter, R. C., and Lettis, W. R., 2004, Paleoseismic investigation of the southern Rodgers Creek fault, Martinelli Ranch, Sonoma County, CA, Final Technical Report for the U.S. Geological National Earthquake Hazards Program, 14 p.

Schwartz, D.P., Pantosti, D., Hecker, S., Okumura, K., Budding, K.E., and Powers, T., 1992, Late Holocene behavior and seismogenic potential of the Rodgers Creek fault zone, Sonoma County, California, Borchardt, G., et al., eds. Proceedings of the Second Conference on Earthquake Hazards in the Eastern San Francisco Bay Area: California Division of Mines and Geology Special Publication 113, p. 393-398.

Schwartz, D.P., Seitz, G., Lienkaemper, J., Dawson, T., Hecker, S., Lettis, W., and Kelson, K., 2001, The Bay Area Earthquake Cycle: A paleoseismic perspective: Eos (American Geophysical Union, Transactions), v. 82 (47), p. Abstract S12F-07.

Shennan, I., 1989, Holocene crustal movements and sea-level changes in Great Britain, Journal of Quaternary Science, 4, 77-90. Simpson, R.W., and Reasenberg, P.A., 1994, Earthquake-induced static-stress changes on Central California faults: Simpson, Robert W. (editor), The Loma Prieta, California, earthquake of October 17, 1989; tectonic processes and models, P 1550-F, p. F 55-F89, illus. incl. 2 tables, sketch map, 87 refs.

Toppozada, T.R., Bennett, J.H., Hallstrom, C.L., and Youngs, L.G., 1992. 1898 "Mare Island" earthquake at the southern end of the Rodgers Creek fault, m Borchardt, G., and others, eds., Proceedings of the Second Conference on Earthquake Hazards in the Eastern San Francisco Bay Area: California Division of Mines and Geology Special Publication 113, p. 385-392.

Wagner, D.L., Rice, S.J., Bezore, S.P., Randolph-Loar, C.E., Allen, J.R. and Witter, R.C., 2002, Geologic map of the Petaluma River 7.5' Quadrangle, Marin and Sonoma counties, California: A digital database: California Geological Survey website, http://www.conservation.ca.gov/-cgs/rghm/rgm/preliminary_geologic_maps.htm

Witkowski, A., Lange-Bertalot, H., and Metzeltin, D., 2000, Diatom Flora of Marine Coasts I. In Lange-Bertalot, H. (ed.), Iconographia Diatomologica, vol. 7. A.R.G. Gantner Verlag.

Witter, R.C., H.M. Kelsey, and E. Hemphill-Haley, 2003, Great Cascadia earthquakes and tsunamis of the past 6,700 years, Coquille River estuary, southern coastal Oregon, Geological Society of America Bulletin, Geological Society of America Bulletin, 115, 10, 1289-1306.

Witter, R.C., Knudsen, K.L, Sowers, J.M., Wentworth, C.M., Koehler, R.D., and Randolph Loar, C. E., 2006, Maps of Quaternary Deposits and Liquefaction Susceptibility in the Central San Francisco Bay Region, California: U.S. Geological Survey Open-File Report 2006-1037, scale 1:24,000 (http://pubs.usgs.gov/of/2006/1037/).

Wong, I.G., 1991, Contemporary seismicity, active faulting and seismic hazards of the Coast Ranges between San Francisco Bay and Healdsburg, California: Journal of Geophysical Research, v. 96, no. B12, p.19,891-19,904.

WGCEP (Working Group on California Earthquake Probabilities), 2003, Earthquake probabilities in the San Francisco Bay region: 2002-2031, a summary of findings: United States Geological Survey Open File Report 03-214. http://geopubs.wr.usgs.gov/open-file/of03-214.

Working Group on California Earthquake Probabilities, 2008, The Uniform California Earthquake Rupture Forecast, Version 2 (UCERF 2). 2007. U.S. Geological Survey Open-File Report 2007-1437 and California Geological Survey Special Report 203 [http://pubs.usgs.gov/of/2007/1437/]

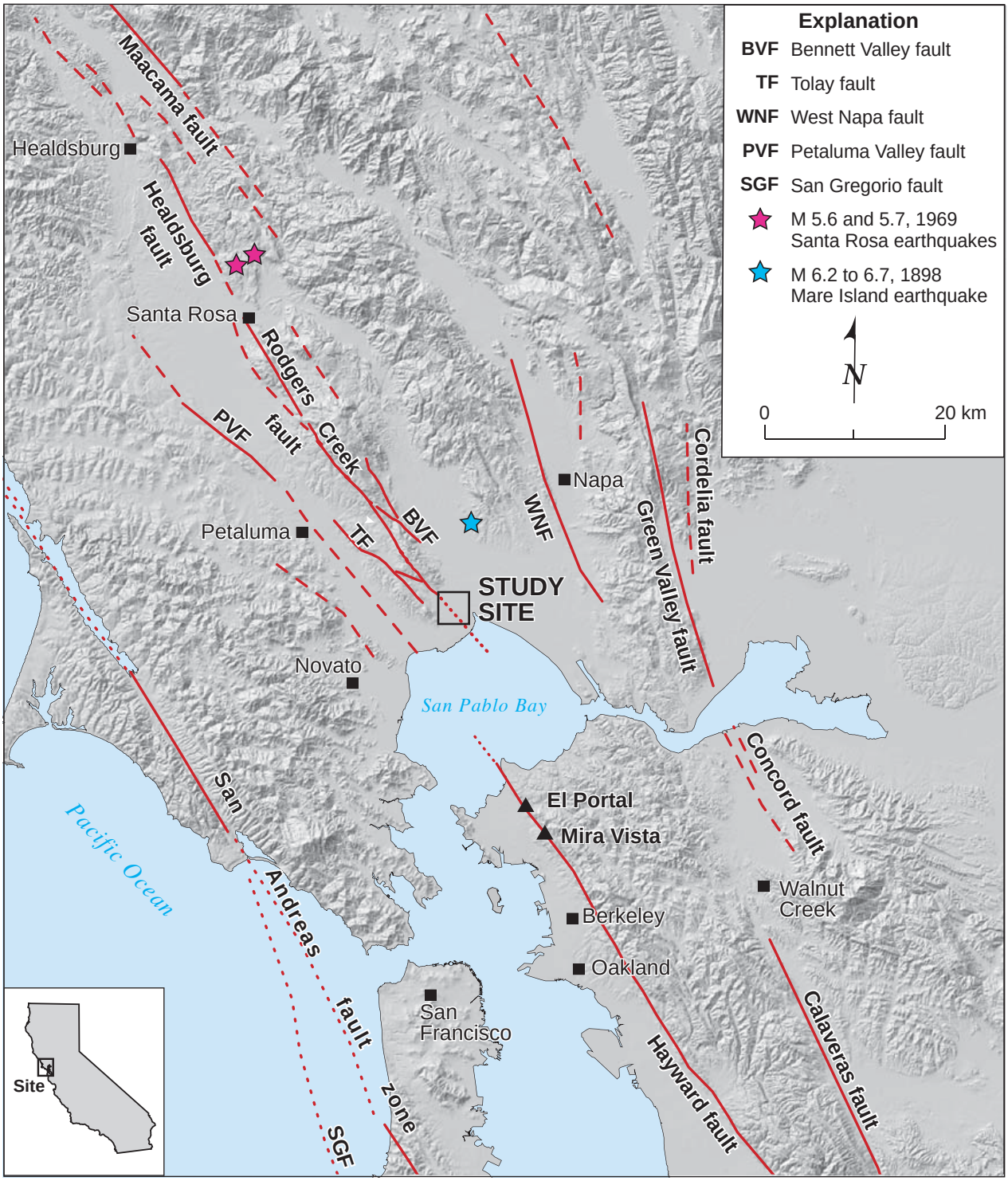

Figure 1. Regional shaded relief map showing the Tolay marsh study site, faults modified from Jennings (1994), and the historical earthquakes of 1969 and 1898.

Graphics/Projects, 2067 Rodgers Creek Marsh Study/ F1 Regional fault map.ai Friday, November 12 2010 13:46:35

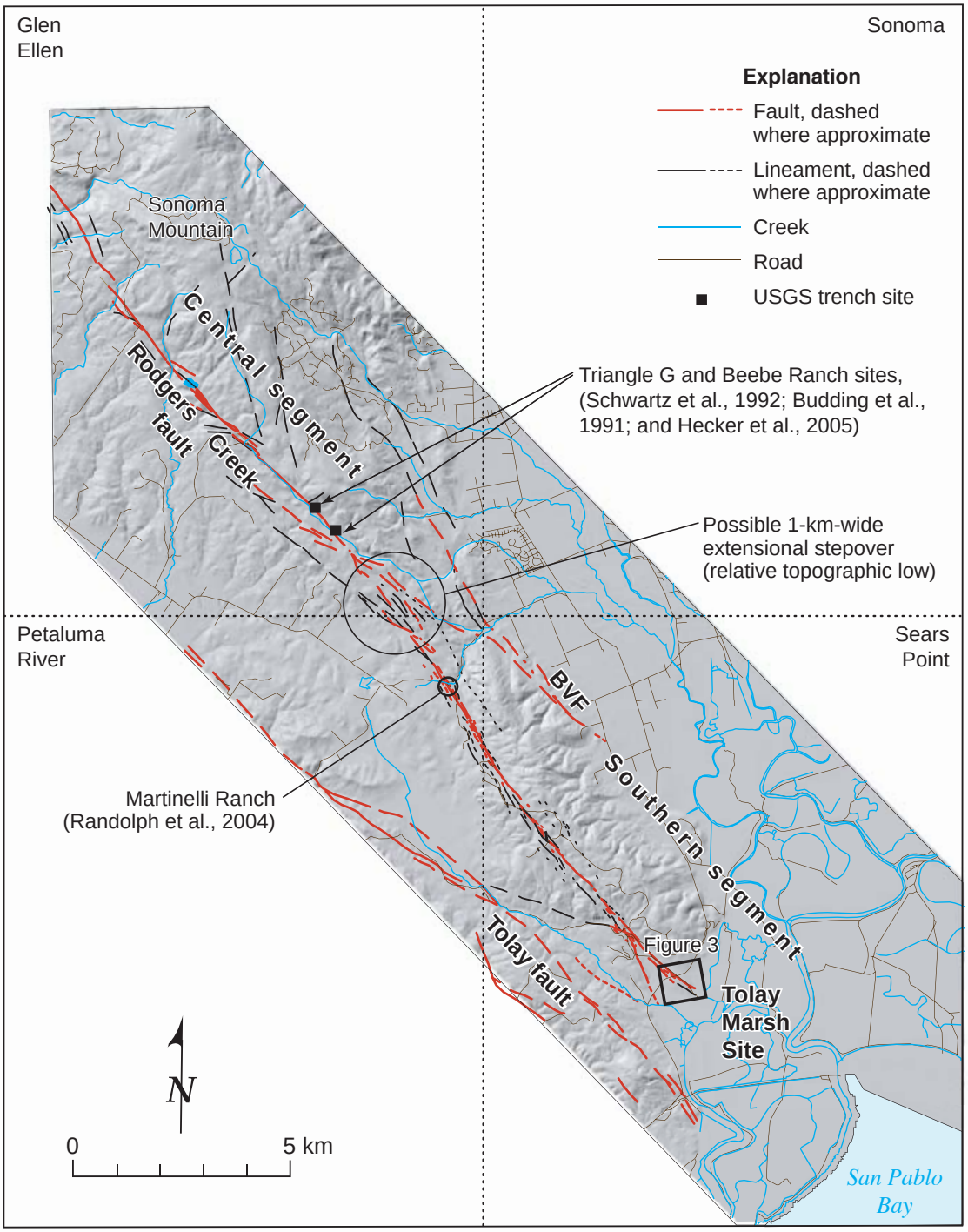

Figure 2. Southern 25 km of the Rodgers Creek fault showing fault and lineament mapping (Randolph and Caskey, 2001) and previous paleoseismic investigations on the fault. USGS 7.5-minute Quadrangle boundaries shown by dotted line. BVF-Bennett Valley fault.

Graphics, Projects, 2067 Rodgers Creek Marsh Study/ F2 Study area DEM.ai Friday, November 12 2010 13:48:58

Graphics/Projects/2067 Rodgers Creek Marsh Study/ F3 and F4 Regional_Geology Map L.ai Friday, November 12 2010 13:51:57

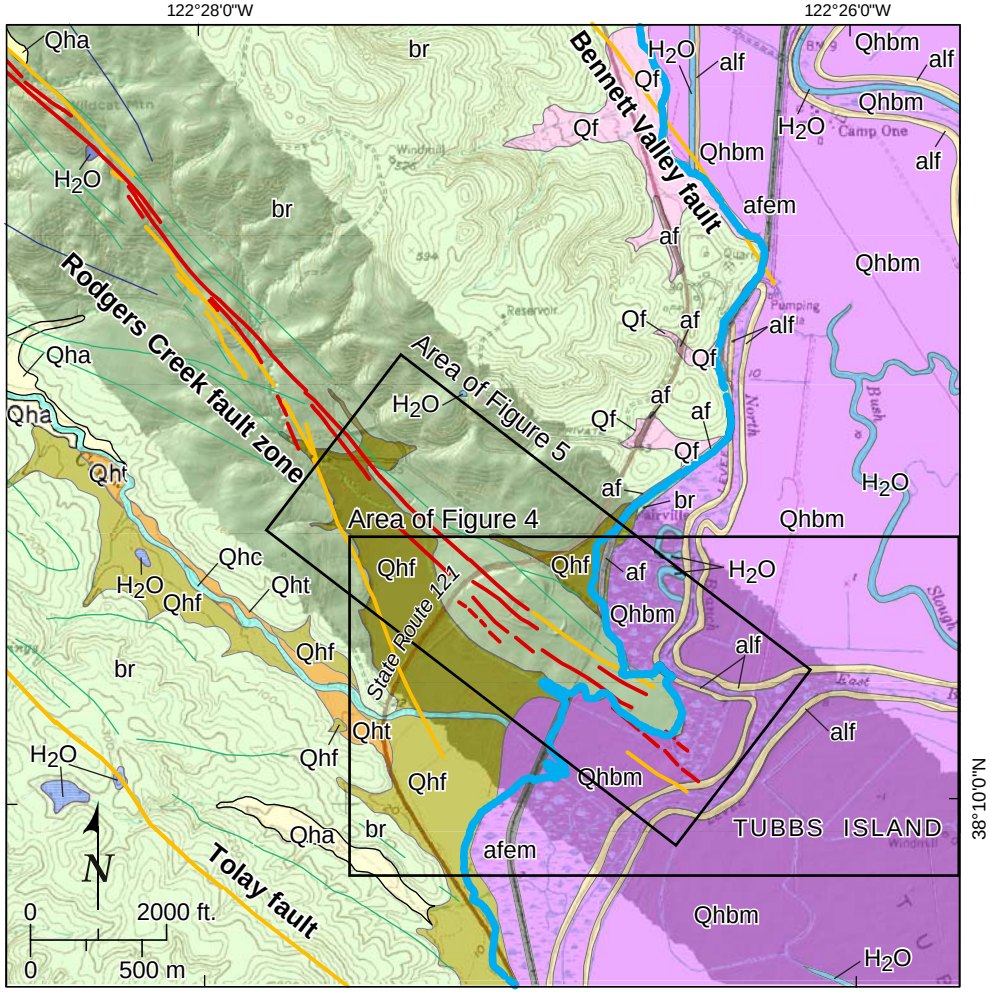

For explanation see Figure 4

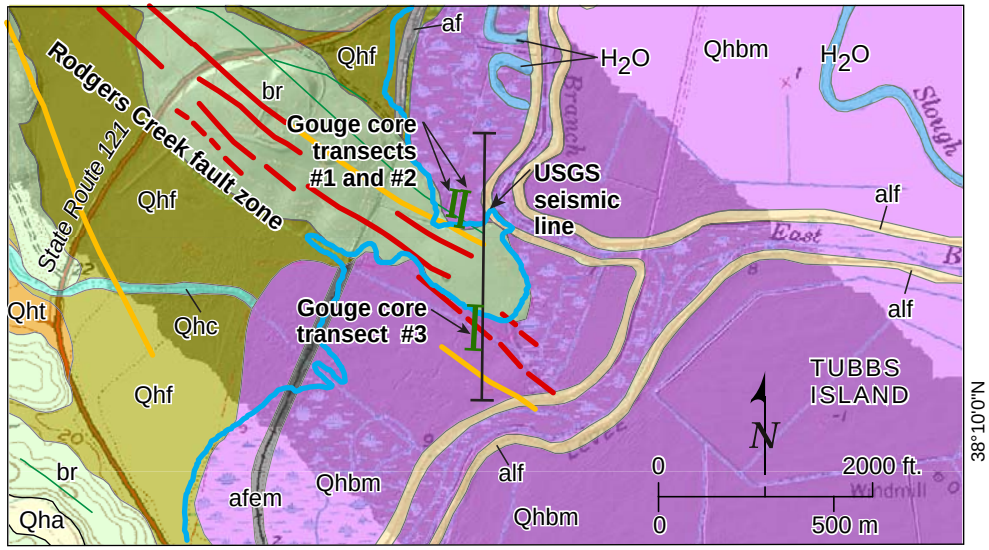

Explanation

Historical marsh boundary (circa 1850)

USGS seismic line

Gouge core transect

Faults (from Randolph et al., 2004)

Holocene

Potentially Holocene

Quaternary

Potentially Quaternary

Geologic Units (from Witter et al., 2006)

Qf	Latest Pleistocene to Holocene alluvial fan deposits	Qht	Holocene stream terrace deposits
Qha	Holocene alluvium, undifferentiated	af	Artificial fill (historical)
Qhbm	Holocene San Francisco Bay Mud	afem	Artificial fill over estuarine mud (historical)
Qhc	Modern stream channel deposits	alf	Artificial levee fill (historical)
Qhf	Holocene alluvial fan deposits	br	Pre-Quaternary deposits and bedrock

Figure 3. Quaternary geology of the southern Rodgers Creek fault zone (Witter et al., 2006).

Figure 4. Tolay marsh study site and fault lineament map.

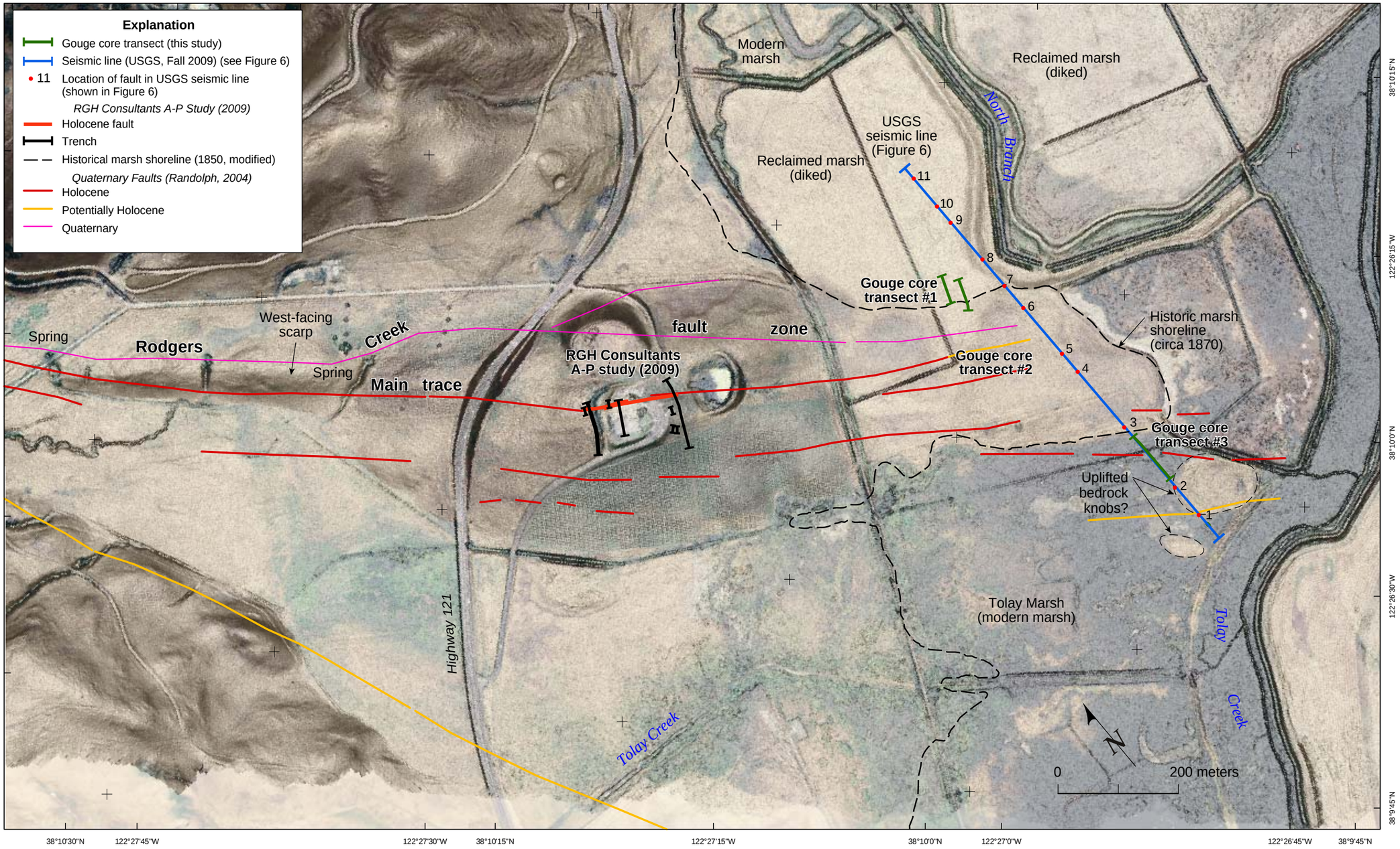

Figure 5. Slopeshade map of LiDAR data and aerial photography along the southernmost Rodgers Creek fault at the Tolay marsh study area.

Graphics, Projects, 2067, Rodgers Creek Marsh Study, 10.28.10

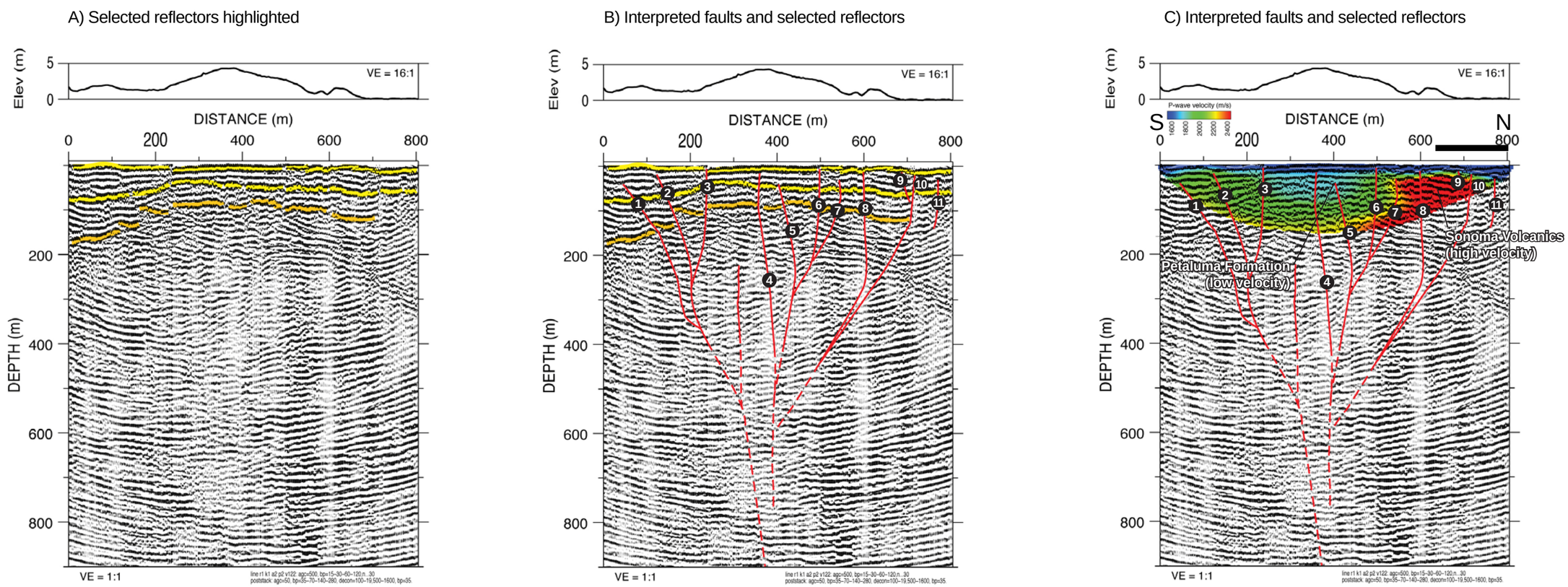

Note: For a description of interpreted fault locations, depths of shallow faulting, fault dip and dip direction, see Table 1.

Figure 6. P-wave reflection images of the USGS seismic reflection and refraction line across the Rodgers Creek fault at Tolay Marsh.

Graphics, Projects, 2067, Rodgers Creek Marsh Study, 10.28.10

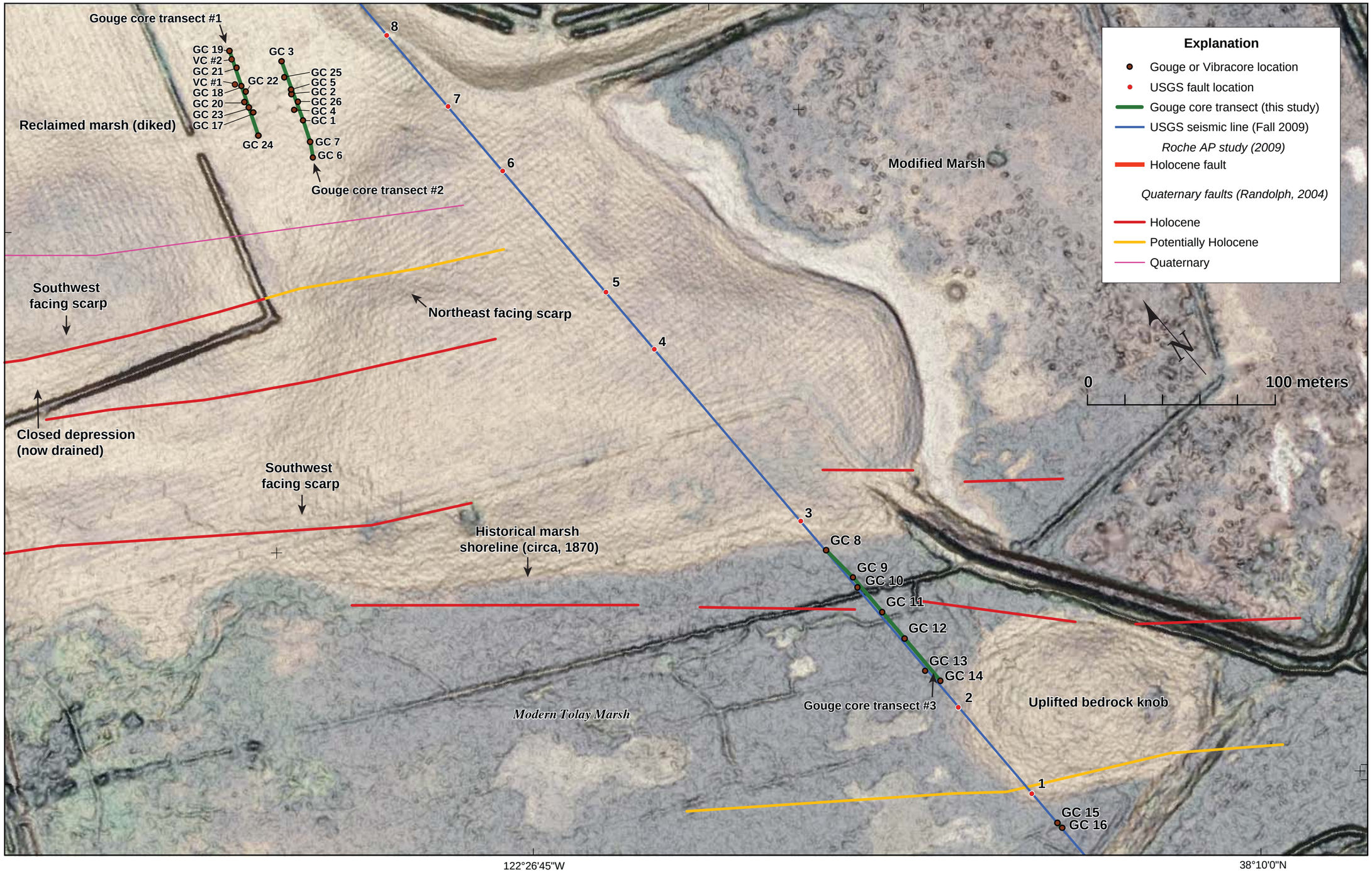

GRAPHICS/2067 Rodgers Creek Marsh Study/ Figure 7 Boring map detail.ai Friday, November 12 2010 13:08:14

Figure 7. Slopeshade map of LiDAR data and aerial photography of the Tolay marsh site.

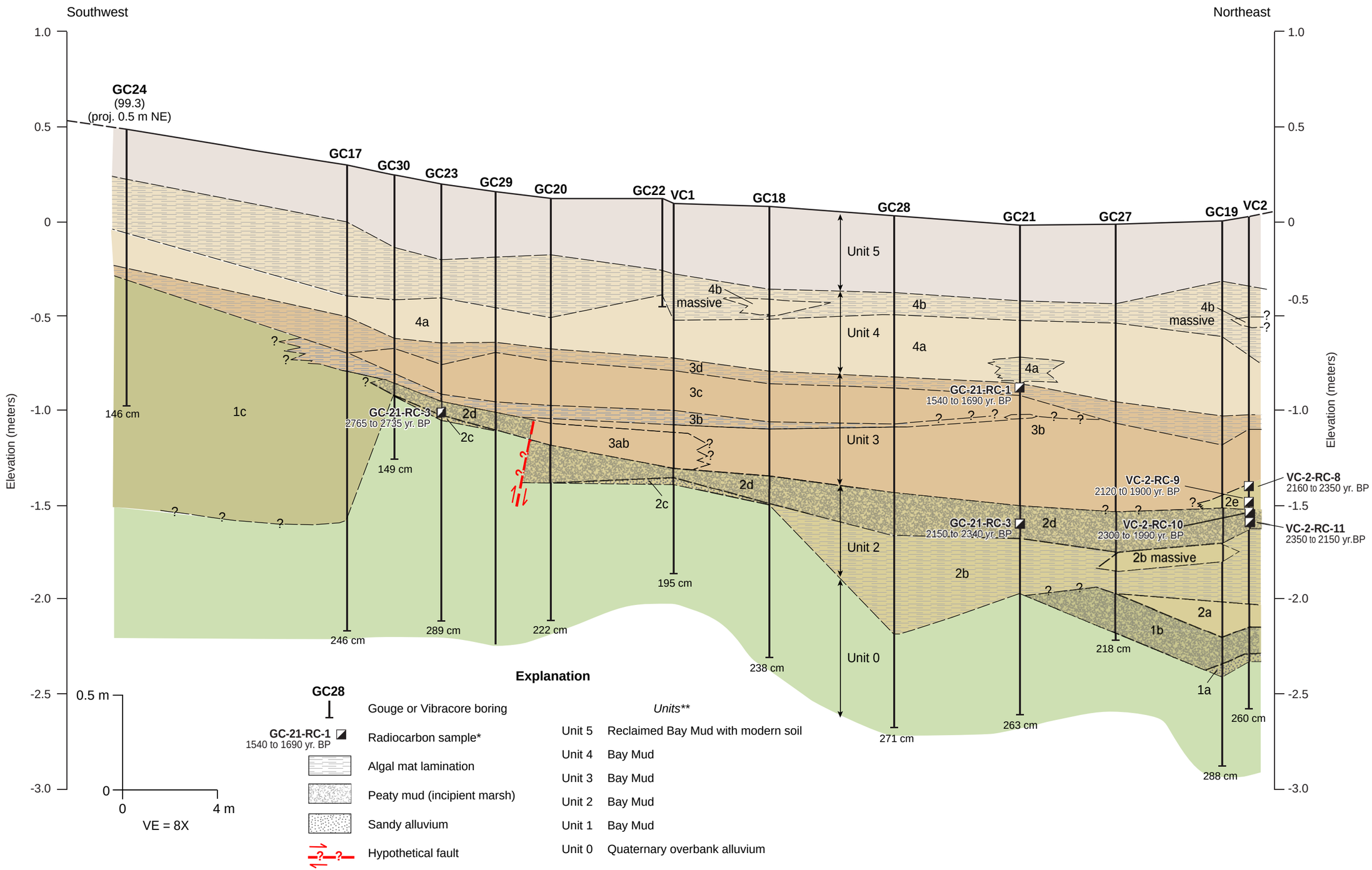

* Ages reported in Cal yr. BP at 2σ (for details, see Table 5).
**For a detailed description of stratigraphic units, see Table 2.

Figure 8. Gouge core transect #1.

Graphics, Active Projects, 2067, Rodgers Creek Marsh Study, 10.28.10

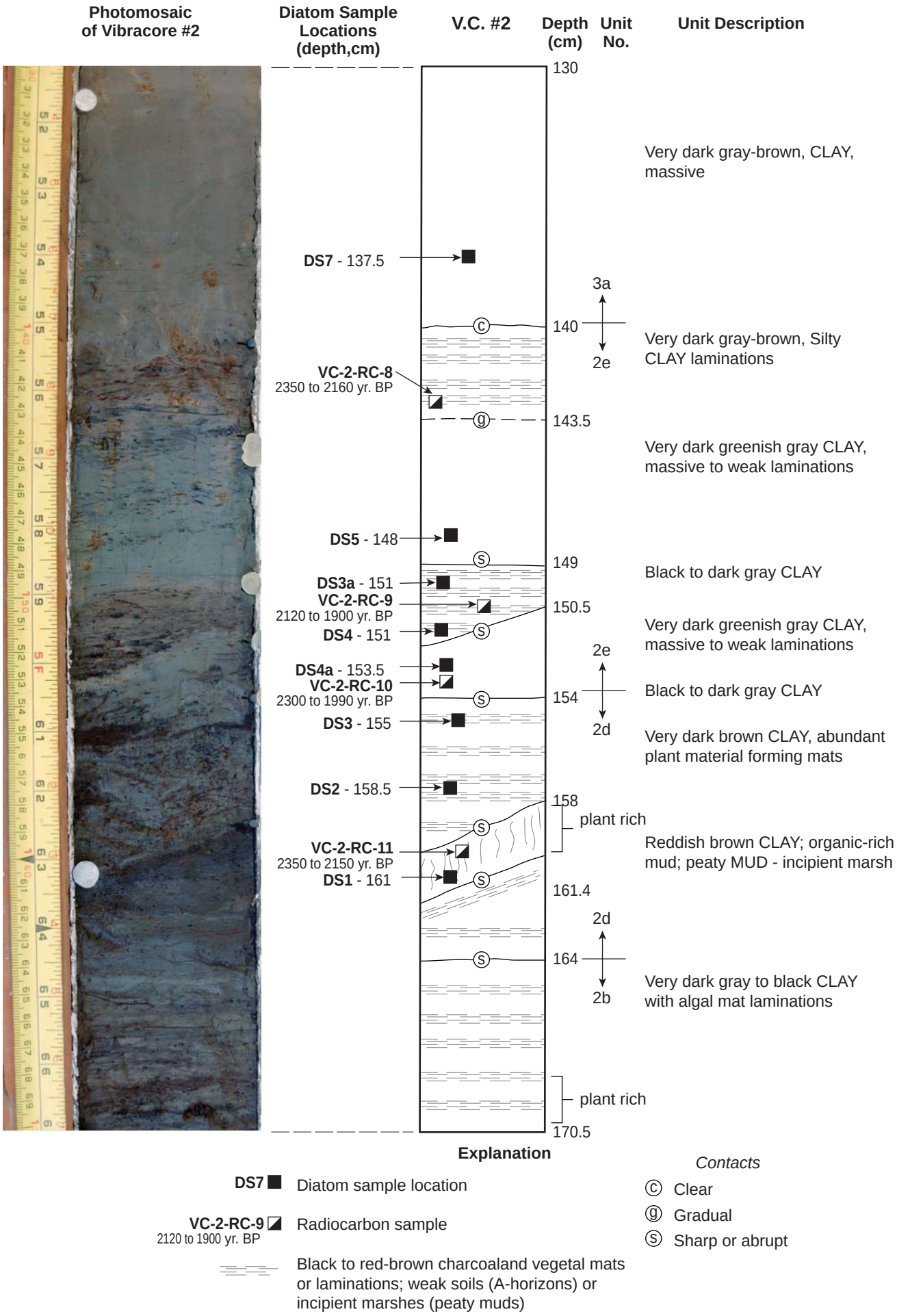

Graphics/Projects/2067 Rodgers Creek Marsh Study/ F9 Column VC2.ai Friday, November 12 2010 13:13:12

Figure 9. Photomosaic and detailed log of Vibracore boring #2 between 130 cm and 170.5 cm depth.

Appendix A:

Diatom analyses for vibracore #2 Report No. 100702–
Eileen Hemphill-Haley Consulting Micropaleontology (July 2010)

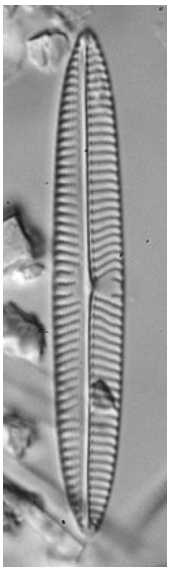

Diatom analyses for Vibracore #2
FWLA Project #2067

Eileen Hemphill-Haley Consulting Micropaleontology
1871 Pickett Road, McKinleyville, CA 95519
707-834-7404 / ehh@ehhmusic.com

Report No. 100702
July 2010

Contents

1 RESULTS 1
2 METHODS (SAMPLE PROCESSING, TAXA IDENTIFICATION, AND DATA COMPILATION) 4
3 OBSERVATIONS / BASIS FOR CONCLUSIONS 6
4 SUMMARIES FOR INDIVIDUAL CORE SAMPLES 9
5 REFERENCES 11

Tables

Table 1. Results of diatom analyses for Vibracore #2.
Table 2. Qualitative overview of diatoms in modern surface samples in the vicinity of Vibracore #2.

Figures

Figure 1. Relative percent of dominant estuarine and marine diatom taxa in Vibracore #2.
Figure 2. Summary of diatom data for Vibracore #2.
Figure 3. Species richness for diatom samples in Vibracore #2.

1 RESULTS

Diatoms were analyzed in 5 subsamples from Vibracore #2, collected near the Rogers Creek fault for Fulgro William Lettis and Associates (FWLA) project #2067. The purpose of the analysis was to: (1) estimate the depositional setting for different lithologies in the core based on entrained diatom assemblages, and (2) determine if there was evidence for significant paleoenvironmental changes at the core site over time. In particular, the goal was to determine if there was evidence, based on diatoms, for changes in relative sea level that might be attributed to land-level changes caused by offset of the Rogers Creek fault. The samples analyzed for this report are:
DS-5 (148 cm): Massive dark greenish gray clay with weak clay laminations.
DS-3a (151 cm): Black to dark gray clay with weak coal laminations.
DS-4a (153.5 cm): Massive greenish gray clay with weak clay laminations.
DS-3 (155 cm): Dark brown clay with plant material forming mats.
DS-1 (166 cm): Reddish brown clay (organic-rich mud / buried peaty mud).

Evidence for relative sea-level rise (submergence) at the core site is indicated by a shift in diatom assemblages between samples DS-1 and DS-3 (Figures 1, 2; Table 1). Well-preserved benthic diatoms in DS-1 (organic-rich or peaty mud) are commonly found on salt marshes (Jensen, 1980; Witkowski et al., 2000), and the absence of coastal planktonic diatoms suggests the site was protected from regular inundation from the San Pablo Bay. Diatoms in DS-3 (mud with plant material forming mats) consist of a mix of coastal planktonic and brackish-marine benthic diatoms consistent with lower intertidal or shallow subtidal areas. Therefore, the diatom data suggest that a previously protected marsh at the core site (sample DS-1) was converted to a tidal flat, slough, or shallow subtidal area open to San Pablo Bay (sample DS-3). Although speculative at this point, it is possible that the lithology for DS-3 is the result of sediment accumulation and deposition of intertidal algal mats. The diatom assemblage in DS-3 would be consistent – though not definitive – of accumulation in an algal mat zone. The 3 additional core samples (DS-4a, 153.5 cm; DS-3a, 151 cm; and DS-5, 148 cm) also contain diatom assemblages consistent with accumulation in the lower intertidal or shallow subtidal zone. Comparable to DS-3, these sample show: (1) a mix of lower intertidal benthic taxa and varying amounts of well-preserved coastal planktonic species; (2) relatively high species richness (> 0.2) as compared to the marsh sample (0.06), which is typical for lower intertidal as compared to high intertidal or supratidal settings; and (3) fewer well-preserved taxa but abundant diatom fragments, indicative of sediment reworking by currents or infauna. Planktonic diatoms are slightly less prominent in the uppermost 2 samples (DS-5, DS-3a), possibly suggesting some shoaling and less influx from San Pablo Bay, but this is speculative and the data may also be recording relatively greater production or preservation of benthic taxa rather than reductions in accumulation of planktonic species.

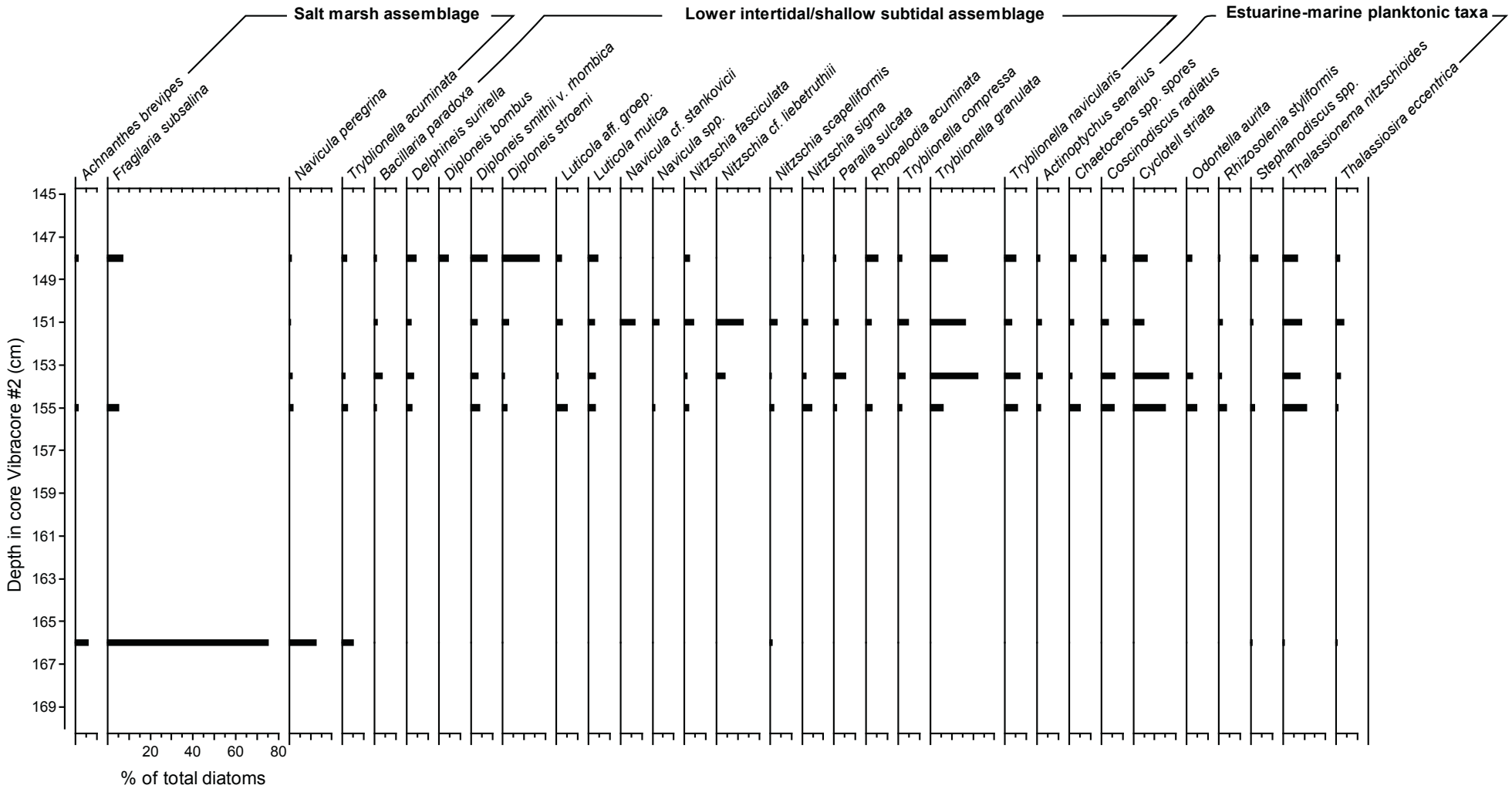

Figure 1. FWLA Project #2067: Relative percent of dominant estuarine and marine diatom taxa in Vibracore #2.

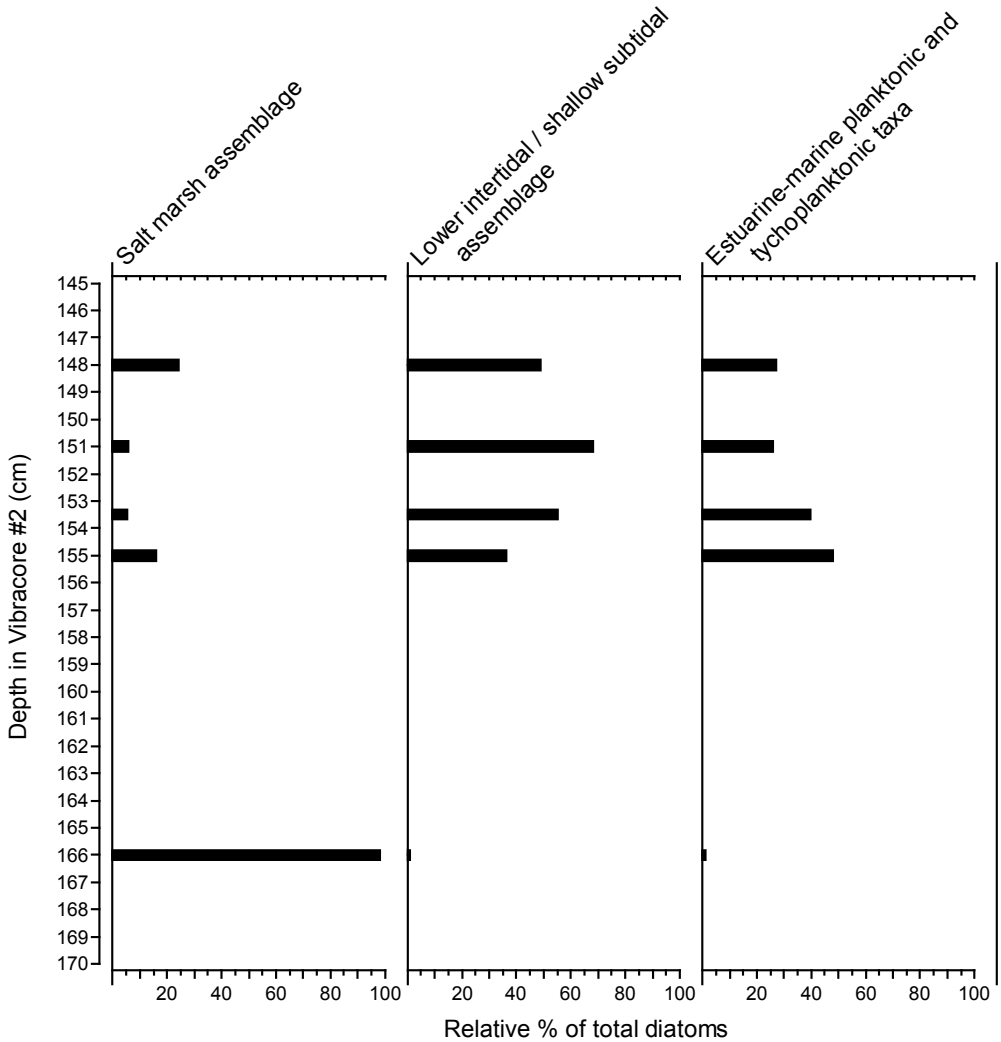

Figure 2. FWLA Project #2067: Summary of diatom data for Vibracore #2. Evidence for relative sea-level rise (salt marsh replaced by lower intertidal or shallow subtidal environment) is indicated by a shift in diatom assemblages between 166 cm and 155 cm.

Table 1. Summary of diatom results for Vibracore #2 (FWLA Project #2067).

Core sample	Lithology[a]	Paleoenvironment based on diatoms	Diatom evidence
DS-5 (148 cm)	Base of very dark greenish gray CLAY, massive with weak clay laminations	Lower intertidal or shallow subtidal zone	Well-preserved benthic diatoms commonly found in lower intertidal /shallow subtidal zone (esp. *Diploneis stroemii*), with less frequent but well-preserved coastal planktonic species. Abundant diatom fragments typical of coastal/tidal flat deposits.
DS-3a (151 cm)	Black to dark gray clay with weak charcoal laminations	Lower intertidal or shallow subtidal zone	Well-preserved benthic diatoms commonly found in lower intertidal /shallow subtidal zone (esp. *Tryblionella granulata*), with less frequent but well-preserved coastal planktonic species. Abundant diatom fragments typical of coastal/tidal flat deposits.
DS-4a (153.5 cm)	Very dark greenish gray CLAY, massive with weak clay laminations	Lower intertidal or shallow subtidal zone	Mix of well-preserved coastal planktonic diatoms and benthic taxa typical of tidal flats. Abundant diatom fragments typical of coastal/tidal flat deposits.
DS-3 (155 cm)	Top of very dark brown CLAY, plant material forming mats	Lower intertidal or shallow subtidal zone (algal mat/tidal flat area?)	Mix of well-preserved coastal planktonic diatoms and benthic taxa typical of tidal flats. Abundant diatom fragments typical of coastal/tidal flat deposits. Greater frequency of unbroken elongate valves than in DS-3, possibly suggesting less sediment reworking.
DS-1 (166 cm)	Reddish brown CLAY, organic-rich mud (buried peaty mud)	Salt marsh (likely protected from regular flooding San Pablo Bay)	Abundant well-preserved benthic diatoms commonly found on salt marshes; very rare planktonic diatoms (< 1.5% of assemblage).

[a]From core description by Robert Givler (FWLA project manager)

2 METHODS (SAMPLE PROCESSING, TAXA IDENTIFICATION, AND DATA COMPILATION)

A total of 5 core subsamples and 7 modern (surface) deposits were analyzed for the project.[1] The 5 samples from Vibracore #2 were collected from different lithological units between 151 cm and 166 cm (Table 1). The 7 surface samples were collected from modern marsh or meadow surfaces in the general vicinity of the core site (Table 2).

[1] The samples were submitted by Robert Givler, FWLA Project Manager.

To examine diatoms in the core subsamples and surface sediment, the material was first chemically pretreated with 30% H_2O_2 to remove organic material, and then rinsed several times with distilled H2O. An aliquot of the cleaned sample was then transferred to a glass coverslip and allowed to dry. The cover slip was then permanently mounted on glass slides using Zrax mounting medium. I counted at least 300 diatom valves per sample at high magnification (1250x) in order to compile a statistically sound representation of the ecologically pertinent taxa in each sample. Diatom taxa in the samples ranged in size from <10 µm to ~ 300 µm, with most taxa ranging between 10 and 60 µm (diameter for centric valves; longest axis for pennate valves).

Diatoms were identified to species level whenever possible. I relied on a number of well-established references for species identification, particularly floras by Krammer and Lange-Bertalot (1986-1991); Witkowski et al. (2000), Baltic Marine Biologists Publications edited by Snoeijs et al. (1993-1998), and the Jensen (1980) translation of earlier works by Hustedt.

I used Microsoft Excel to compile and organize the counts data, which allowed for basic analysis and easy comparison of assemblages among different samples. The software packages Tilia 2.0 and TGView 1.3.1[2] were used to further organize and graph the data. In addition to compiling the counts data, I also made note of the relative preservation of different species as an additional qualitative tool to aid in the evaluation. Identifying which diatom species are well preserved (and which are not) can be informative because estuarine/littoral environments are highly productive areas for diatoms, and also areas of intense reworking and redeposition. In benthic deposits that show a range in the preservation of diatom valves (from dissolved or fragmented to all or mostly intact), the best-preserved taxa likely provide the most reliable evidence for the final depositional environment.

For this project, relative percentages are based on total diatoms excluding *Aulacoseira granulata* and *Cyclotella meneghiniana*. These are small freshwater taxa with resilient valves, and widely distributed as reworked particles in the San Francisco Bay area. These taxa were excluded in the final analysis to emphasize ecologically significant taxa, and reduce "noise" from possibly reworked material.

[2] Written by Dr. Eric Grimm, Illinois State Museum: http://www.ncdc.noaa.gov/paleo/tiliafaq.html

3 OBSERVATIONS / BASIS FOR CONCLUSIONS

Modern diatoms from marsh/meadow surfaces near the core site

In order to possibly identify modern analogs to the core lithologies, diatoms were evaluated in 7 samples collected from marsh/meadow surfaces in the vicinity of Vibracore #2 (Table 2). Although there were some species in common between the modern (Sears Point) samples #3-7 and the downcore samples, there were no obvious similarities between overall assemblages. The modern assemblages from the grassy high marsh or supratidal settings (Sears Point samples #1 and #2) did not compare to any downcore samples, as all of the downcore samples contained species indicative of wet salt marsh or lower intertidal/shallow subtidal settings. None of the modern samples contained high numbers of Fragilaria subsalina, which is the dominant species in downcore samples DS-1 (Figure 1). Planktonic diatoms are absent in the modern samples.[3] Planktonic diatoms are also not found in DS-1, but are prominent in the remaining core samples.

Table 2. Qualitative overview of diatoms in modern surface samples from marsh/meadow locations in the vicinity of Vibracore #2 (FWLA Project #2067).

Sample	Sample description	Diatom summary
Sears Point #1	> MHHW (grasslands above marsh); blue-eyed grass + unidentified plant	Diatoms represented by only a few valves of Pinnularia borealis, Hantzschia amphioxys: consistent with fresh, dry grassy environment. Highly comparable to sample #2.
Sears Point #2	~MHHW high marsh; Australian saltbrush (?), Meadow Barley/ Mediterranean Barley	Diatoms represented by only a few valves of Pinnularia borealis, Hantzschia amphioxys: consistent with fresh, dry grassy environment. Highly comparable to sample #1.
Sears Point #3	MHW-MHHW; *Salicornia*	Diatoms frequent but not abundant; most common taxa are Navicula atwateri, N. salinarum; less frequent Nitzschia faciculata. Probably represents drier conditions than indicated by diatoms (particularly M. nummuloides) in salt marsh sample #4.
Sears Point #4	MHW-MHHW; *Salicornia, Spartina*	Diatoms common, indicative of wet low marsh environment: Melosira nummuloides, Tryblionella navicularis, Nitzschia fasciculata, Caloneis westii, Nitzschia scapelliformis; Navicula peregrina present but rare; no planktonic diatoms.
Sears Point #5	MHW-MHHW; *Salicornia, Spartina*	Diatoms rare overall for unknown reason. Nitzschia fasciculata and Tryblionella navicularis present but rare.
Sears Point #6	MHW-MHHW; *Salicornia, Jaumea*	Common benthic diatoms, esp. Nitzschia fasciculata, Tryblionella navicularis, Nitzschia sigma, Luticola muticoides. Very rare, possibly planktonic, taxa represented by Thalassiosira spp.
Sears Point #7	MHW-MHHW; *Salicornia, Spartina*	Common benthic diatoms; no planktonic diatoms. Prominent taxa = Nitzschia fasciculata , Gyrosigma eximium, Tryblionella acuminata. Trybionella navicularis present but rare.

Note: Salicornia = "pickleweed;" *Spartina* = "cordgrass."

[3] Planktonic diatoms are absent in the modern samples with the possible exception of a few rare valves of the genus *Thalassiosira* in sample #6.

Therefore, none of the modern samples collected for the study are strong analogs for any of the downcore samples. The environment that supported the assemblage dominated by *F. subsalina* in DS-1 is not represented by any of the marsh settings sampled on the modern surface near the core location. Further, the modern analog settings for the remaining core samples (DS-3, 4a, 3a, and 5) would more likely be tidal flats or shallow channels since prominent taxa in those samples include benthic taxa (e.g., *Tryblionella granulata*, *Diploneis stroemii*) commonly found in lower intertidal/shallow subtidal areas, as well as large coastal planktonic diatoms (*Cyclotella striata*, *Coscinodiscus radiatus*).

Downcore samples

Diatoms were present in all downcore samples, and most abundant and well preserved in sample DS-1. A total of about 95 different diatom taxa were identified in the 5 core samples (Appendix A), of which 31 exceeded 2% of the assemblage in at least 1 sample (Figure 1).

Sample DS-1 at 166 cm was assumed to have accumulated in a marsh or meadow setting based on its lithology (red-brown organic-rich mud). The diatom data indicate the setting was probably a brackish-marine intertidal marsh. Diatoms are abundant and well preserved in this sample, dominated by *Fragilaria subsalina*, which is commonly found in coastal salt marshes (Jensen, 1980; Witkowski et al., 2000). Other prominent benthic diatoms include *Navicula peregrina*, *Achnanthes brevipes*, and *Bacilaria paradoxa*. In combination with *F. subsalina*, this assemblage shows that this was a wet, brackish-marine setting, and not a fresh or relatively dry setting as would be expected above MHHW. Planktonic diatoms, which are usually a significant component of lower intertidal samples, are absent from DS-1. This shows that the site was protected from regular flooding from San Pablo Bay.

A paleoecological shift (relative sea-level rise) at the core site is indicated by a change from a "salt marsh assemblage" in sample DS-1 at 166 cm, to a "lower intertidal/shallow subtidal assemblage" in sample DS-3 at 155 cm (Figures 1, 2). Unlike the diatom assemblage in DS-1, which consists of a low-diversity, well-preserved assemblage (Figures 1, 3; Appendix 1), DS-3 contains a diverse, mixed assemblage of well-preserved benthic and planktonic diatoms and abundant diatom fragments. The lithology for DS-3, mud with plant laminae, may be indicative of a lower intertidal algal mat zone, which would be consistent with an interpretation of a lower intertidal/shallow subtidal diatom assemblage. Further, diatom preservation is qualitatively better in DS-3 than in massive mud at DS-4a (153.5 cm), with more frequent occurrences of delicate elongate taxa. It is possible that the diatoms in DS-3 are better preserved because of less sediment reworking by currents and infauna in an algal mat zone.

Lower intertidal to shallow subtidal environments are indicated for samples DS-3, DS-4a, DS-3a, and DS-5 based on dominant diatom taxa (Figures 1-3; Table 1; Appendix A). Estuarine-marine planktonic diatoms are particularly prominent in DS-3, but present in the remaining samples as well, indicating an open exchange with the San Francisco Bay estuary. Mixed assemblages of benthic diatoms, including well-preserved *Tryblionella granulata*, *T. navicularis*, and *Diploneis stroemii*, all support deposition on tidal flats, sloughs, or shallow subtidal areas.

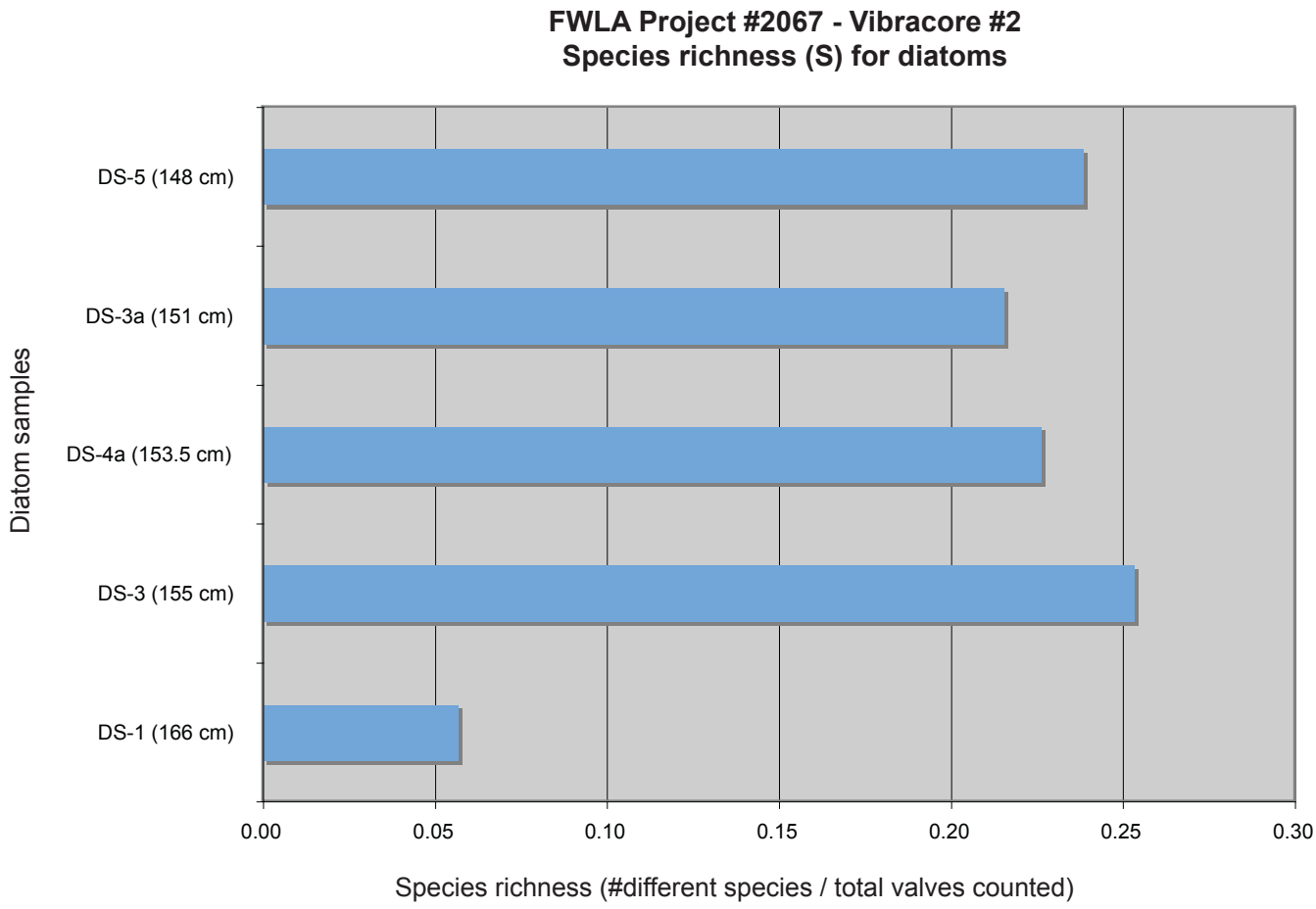

Figure 3. FWLA Project #2067: Species richness for diatom assemblages in Vibracore #2. The lower value for species richness in DS-1 is consistent with accumulation in a protected marsh environment.

4 SUMMARIES FOR INDIVIDUAL CORE SAMPLES

The following are observations for 5 subsamples from Vibracore #2.

DS-5 (148 cm)
Lithology: Massive dark greenish gray clay with weak clay laminations.
Diatom summary: Diatoms present and diverse, dominated by estuarine/marine taxa. The sample is silty with abundant diatom fragments. Well-preserved diatom taxa are relatively infrequent compared to the number of broken valves. The overall assemblage is diverse with > 50 different species (species richness = 0.24), indicative of mixing and input from different environments. Benthic diatoms dominate the assemblage (benthic/planktonic ratio = 3.1), but some well-preserved coastal taxa are present. Benthic taxa dominated by prominent well-preserved valves of *Diploneis stroemii*, and less frequent *D. smithii* var. *rhombica*, and *Tryblionella granulata*. These taxa are commonly found in lower intertidal or shallow subtidal areas; *D. stroemii* often found on sandier substrate.
Prominent diatoms:
Benthic
Diploneis stroemii (14%)
Tryblionella granulata (6%)
D. smithii var. *rhombica* (6%)
Planktonic
Thalassionema nitzschioides (5%)
Cyclotella striata (5%)
Inferred paleoenvironment: Lower intertidal or shallow subtidal zone.

DS-3a (151 cm):
Lithology: Black to dark gray clay with weak coal laminations.
Diatom summary: Diatoms present and diverse, dominated by estuarine/marine taxa. The assemblage is a mix of infrequent well-preserved valves against a background of sediment and abundant diatom fragments. The overall assemblage is diverse with > 50 different species (species richness = 0.22), although most are not well preserved. Benthic diatoms dominate the assemblage (benthic/planktonic ratio = 3.3), but there are a few very well preserved planktonic specimens with intact frustules (i.e., the 2 diatoms valves still attached – an indication of good preservation). Benthic taxa dominated by *Tryblionella granulata*, a common lower intertidal species.
Prominent diatoms:
Benthic
Tryblionella granulata (13%)
Nitzschia cf. *liebetruthii* (10%)
Tryblionella compressa (4%)
Planktonic
Thalassionema nitzschioides (7%)
Cyclotella striata (4%)
Inferred paleoenvironment: Lower intertidal or shallow subtidal zone.

DS-4a (153.5 cm)
Lithology: Massive greenish gray clay with weak clay laminations.
Diatom summary: Diatoms present and diverse, dominated by estuarine/marine taxa. Assemblage a mix of infrequent well-preserved valves and abundant valve fragments ("background" material). The overall assemblage is diverse with > 50 different species (species richness = 0.23), although most are not well preserved. Planktonic diatoms are prominent (benthic/planktonic ratio = 1.8), with a number of intact frustules that stand out in contrast to the dominantly fragmented material. The most common benthic species are *Tryblionella granulata* and *T. navicularis*, which are common lower intertidal taxa. These species have thick valves resistant to dissolution and breakage, so their occurrences in this sample (and others in the core) could be in part indicative of preferential preservation as well as paleoenvironment.
Prominent diatoms:
Benthic
Tryblionella granulata (18%)
Tryblionella navicularis (6%)
Nitzschia cf. *liebetruthii* (4%)
Planktonic
Cyclotella striata (14%)
Thalassionema nitzschioides (7%)
Coscinodiscus radiatus (5%)
Inferred paleoenvironment: Lower intertidal or shallow subtidal zone.

DS-3 (155 cm)
Lithology: Dark brown clay with plant material forming mats.
Diatom summary: Diatoms are present and dominated by marine/estuarine taxa. The assemblage consists of infrequent, well-preserved planktonic and benthic taxa that stand out in contrast to "background" material of mineral grains and abundant fragments of diatom valves. The assemblage is diverse with > 50 different species (species richness = 0.25), although most are not well preserved. Coastal planktonic diatoms are prominent (benthic/planktonic ratio = 1.4), indicating connection with San Pablo Bay: the combination of these and the various benthic taxa is consistent with deposition in a lower intertidal or possibly subtidal environment. The lithology (mud with plant laminae) possibly suggests a zone of benthic algal mats. Qualitatively, diatom preservation in this sample is slightly better than that in the overlying massive mud sample (DS-4a), with more frequent occurrences of easily broken elongate taxa. This relatively better preservation may be the result of less sediment reworking by currents and infauna because of the presence of algal mats.
Prominent diatoms:
Benthic
Tryblionella granulata (5%)
Tryblionella navicularis (4%)
Fragilaria subsalina (4%)
Planktonic

Cyclotella striata (12%)
Thalassionema nitzschioides (9%)
Coscinodiscus radiatus (5%)
Chaetoceros spp. spores (4%)
Odontella aurita (3%)

Inferred paleoenvironment: Lower intertidal (algal mat?) or shallow subtidal zone.

DS-1 (166 cm)

Lithology: Reddish brown clay (organic-rich mud / buried peaty mud).

Diatom summary: Diatoms abundant and well preserved, dominated by large pennate (benthic) taxa. Planktonic diatoms are very rare (~1% of the assemblage), and low species richness (0.06) indicates a limited number of taxa, which is consistent with an *in situ* marsh assemblage with minimal mixing or influx from other environments.

Prominent diatoms (all benthic):
Fragilaria subsalina (70%)
Navicula peregrina (12%)
Achnanthes brevipes (5%)
Tryblionella acuminata (5%)

Inferred paleoenvironment: Salt marsh: wet environment conducive to benthic diatom growth, but protected from regular inundation and deposition of taxa from other environments (e.g., coastal planktonic, lower intertidal, fluvial).

5 REFERENCES

Baltic Marine Biologists Publication No. 16a, 1993, Intercalibration and distribution of diatom species in the Baltic Sea, vol. 1. Snoeijs, P.J.M. (ed.), Opulus Press, Uppsala, 129 pp.

Baltic Marine Biologists Publication No. 16b, 1994, Intercalibration and distribution of diatom species in the Baltic Sea, vol. 2. Snoeijs, P.J.M. and Vilbaste, S. (eds.), Opulus Press, Uppsala, 125 pp.

Baltic Marine Biologists Publication No. 16c, 1995, Intercalibration and distribution of diatom species in the Baltic Sea, vol. 3. Snoeijs, P.M.J., and Potapova, M. (eds.), Opulus Press, Uppsala, 126 pp.

Baltic Marine Biologists Publication No. 16d, 1996, Intercalibration and distribution of diatom species in the Baltic Sea, vol. 4. Snoeijs, P.J.M., and Kasperoviciene, J., (eds.), Opulus Press, Uppsala, 126 pp.

Baltic Marine Biologists Publication No. 16e, 1998, Intercalibration and distribution of diatom species in the Baltic Sea, vol. 5. Snoeijs, P.J.M., and Balashova, N. (eds.), Opulus Press, Uppsala, 144 pp.

Hendey, N.I., 1964, An Introductory Account of the Smaller Algae of British Coastal Waters. Part V: Bacillariophyceae (Diatoms), 317 pp. London.

Jensen, N.G., 1985, Friedrich Hustedt: The Pennate Diatoms. A translaton of Hustedt's "Die Kieselalgen, 2 Teil." Koeltz, Koenigstein, 918 pp.

Krammer, K., and Lange-Bertalot, H., 1986, Bacillariophyceae 1, Naviculaceae. In Ettl, H., Gerloff, J., Heynig, H., and Mollenhauer, D., (eds), Süsswasserflora von Mitteleuropa, vol. 2, no. 1. Fischer, Stuttgart.

Krammer, K., and Lange-Bertalot, H., 1988, Bacillariophyceae 2, Epithemiaceae, Bacillariaceae, Surirellaceae. In Ettl, H., Gerloff, J., Heynig, H., and Mollenhauer, D., (eds), Süsswasserflora von Mitteleuropa, vol. 2, no. 2. Fischer, Stuttgart.

Krammer, K., and Lange-Bertalot, H., 1991a, Bacillariophyceae 3, Centrales, Fragilariaceae, Eunotiaceae. In Ettl, H., Gerloff, J., Heynig, H., and Mollenhauer, D., (eds), Süsswasserflora von Mitteleuropa, vol. 2, no. 3. Fischer, Stuttgart.

Krammer, K., and Lange-Bertalot, H., 1991b, Bacillariophyceae 4, Achnanthaceae. In Ettl, H., Gerloff, J., Heynig, H., and Mollenhauer, D., (eds), Süsswasserflora von Mitteleuropa, vol. 2, no. 4. Fischer, Stuttgart.

Witkowski, A., Lange-Bertalot, H., and Metzeltin, D., 2000, Diatom Flora of Marine Coasts I. In Lange-Bertalot, H. (ed.), Iconographia Diatomologica, vol. 7. A.R.G. Gantner Verlag.

Sample	**DS-5**	**DS-5 (%)**	**DS-3a**	**DS-3a (%)**	**DS-4a**	**DS-4a (%)**
depth in core (cm)	**148**		**151**		**153.5**	
traverses	135 / 8		140/3		140 / 2.5	
Total counts	300		301		300	
Total used for % (excludes possible reworked diatoms)	235		260		230	
Well preserved large planktonic species	VR		R		R	
BENTHIC BRAKCKISH-MARINE SPECIES						
Achnanthes brevipes	2	0.9%		0.0%		0.0%
Amphora holsatica		0.0%	1	0.4%		0.0%
Amphora libyca		0.0%		0.0%		0.0%
Bacillaria paxillifer	1	0.4%	2	0.8%	6	2.6%
Caloneis amphisbaena fo. Subsalina		0.0%		0.0%		0.0%
Caloneis bacillum		0.0%	2	0.8%		0.0%
Caloneis westii	1	0.4%	2	0.8%	2	0.9%
Catenula adhaerens		0.0%		0.0%	2	0.9%
Cocconeis distans		0.0%	2	0.8%	1	0.4%
Cocconeis placentula	5	2.1%		0.0%	1	0.4%
Cocconeis scutellum		0.0%		0.0%	1	0.4%
Cosmioneis pusilla	1	0.4%	2	0.8%		0.0%
Delphineis surirella	8	3.4%	4	1.5%	6	2.6%
Denticula subtilis	1	0.4%		0.0%		0.0%
Dimeregramma minor		0.0%		0.0%		0.0%
Diploneis bombus	8	3.4%		0.0%		0.0%
Diploneis littoralis		0.0%	3	1.2%		0.0%
Diploneis pseudovalis	2	0.9%		0.0%	1	0.4%
Diploneis smithii v. rhombica	14	6.0%	6	2.3%	6	2.6%
Diploneis stroemii	32	13.6%	5	1.9%	1	0.4%
Epithemia turgida		0.0%	2	0.8%	1	0.4%
Fragilaria subsalina	13	5.5%		0.0%		0.0%
Frustulia vulgaris	2	0.9%		0.0%	2	0.9%
Gomphonema olivaceum v. staurophorum		0.0%	1	0.4%		0.0%
Gyrosigma eximium	2	0.9%	5	1.9%		0.0%
Gyrosigma nodiferum		0.0%		0.0%	3	1.3%
Hyalodiscus scoticus	2	0.9%		0.0%		0.0%
Luticola cf. groep.	4	1.7%	6	2.3%	1	0.4%
Luticola mutica	8	3.4%	6	2.3%	6	2.6%
Mastogloia exigua	1	0.4%	2	0.8%		0.0%
Melosira moniliformis	1	0.4%		0.0%		0.0%
Navicula aff. "Saline Salzkotten" of Witkowski et al., 2000		0.0%		0.0%	4	1.7%
Navicula arenaria		0.0%		0.0%	2	0.9%
Navicula cf. stankovicii		0.0%	14	5.4%		0.0%
Navicula elegans		0.0%		0.0%		0.0%
Navicula menisculus	3	1.3%		0.0%		0.0%
Navicula peregrina	2	0.9%	1	0.4%	2	0.9%
Navicula phyllepta		0.0%	1	0.4%		0.0%
Navicula spp.		0.0%	6	2.3%		0.0%

Sample	**DS-5**	**DS-5 (%)**	**DS-3a**	**DS-3a (%)**	**DS-4a**	**DS-4a (%)**
depth in core (cm)	**148**		**151**		**153.5**	
Nitzschia angustata		0.0%	2	0.8%	1	0.4%
Nitzschia brevissima	2	0.9%	2	0.8%		0.0%
Nitzschia denticula		0.0%		0.0%	3	1.3%
Nitzschia dissipata	3	1.3%	1	0.4%		0.0%
Nitzschia dubiiformis		0.0%		0.0%		0.0%
Nitzschia fasciculata	4	1.7%	9	3.5%	2	0.9%
Nitzschia lanceola	1	0.4%		0.0%		0.0%
Nitzschia cf. liebetruthii		0.0%	26	10.0%	7	3.0%
Nitzschia scapelliformis		0.0%	7	2.7%	1	0.4%
Nitzschia sigma	1	0.4%	5	1.9%	3	1.3%
Nitzschia spp.		0.0%		0.0%		0.0%
Nizschia commutata	4	1.7%		0.0%		0.0%
Opephora marina		0.0%	1	0.4%		0.0%
Paralia sulcata	1	0.4%	4	1.5%	10	4.3%
Planothidium delicatula		0.0%	2	0.8%		0.0%
Rhaphoneis amphiceros	2	0.9%		0.0%		0.0%
Rhoicosphenia abbreviata	3	1.3%		0.0%		0.0%
Rhopalodia acuminata	10	4.3%	5	1.9%		0.0%
Scolioneis tumida		0.0%		0.0%	2	0.9%
Sieminskia wohlenbergii		0.0%		0.0%	2	0.9%
Stauroneis phoenicenteron		0.0%	1	0.4%		0.0%
Surirella striatula		0.0%		0.0%	1	0.4%
Triceratium reticulum		0.0%	1	0.4%		0.0%
Tryblionella acuminata	3	1.3%		0.0%	2	0.9%
Tryblionella compressa	3	1.3%	10	3.8%	6	2.6%
Tryblionella debilis		0.0%		0.0%	1	0.4%
Tryblionella granulata	15	6.4%	34	13.1%	41	17.8%
Tryblionella lanceola		0.0%	4	1.5%		0.0%
Tryblionella levidensis	2	0.9%	1	0.4%	2	0.9%
Tryblionella littoralis	1	0.4%	2	0.8%	1	0.4%
Tryblionella navicularis	9	3.8%	6	2.3%	13	5.7%
Tryblionella salinarum		0.0%	2	0.8%		0.0%
Tryblionella vexans	1	0.4%	2	0.8%	3	1.3%
PLANKTONIC BRAKCKISH-MARINE SPECIES						
Actinoptychus senarius	2	0.9%	4	1.5%	4	1.7%
Actinoptychus splendens		0.0%	1	0.4%		0.0%
Chaetoceros spp. spore	6	2.6%	4	1.5%	2	0.9%
Coscinodiscus radiatus	4	1.7%	7	2.7%	12	5.2%
Coscinodiscus spp.	1	0.4%	2	0.8%		0.0%
Cyclotella elgeri	1	0.4%		0.0%	1	0.4%
Cyclotella sp.	1	0.4%	1	0.4%	3	1.3%
Cyclotella striata	12	5.1%	10	3.8%	31	13.5%
Odontella aurita	4	1.7%		0.0%	5	2.2%
Rhizosolenia styliformis	1	0.4%	3	1.2%	2	0.9%
Stephanodiscus sp.	6	2.6%	2	0.8%		0.0%
Thalassionema nitzschioides	13	5.5%	18	6.9%	15	6.5%
Thalassiosira eccentrica	3	1.3%	7	2.7%	3	1.3%

Sample	**DS-5**	**DS-5 (%)**	**DS-3a**	**DS-3a (%)**	**DS-4a**	**DS-4a (%)**
depth in core (cm)	**148**		**151**		**153.5**	
Thalassiosira lacustris		0.0%	1	0.4%	2	0.9%
Thalassiosira leptopus	2	0.9%		0.0%		0.0%
Thalassiosira pacifica		0.0%		0.0%		0.0%
Thalassiosira spp.	1	0.4%		0.0%	1	0.4%
POSSIBLE REWORKED FW/ESTUARINE TAXA						
Aulcacosira granulata	53		23		56	
Cyclotela meneghiniana	9		17		14	
EXTRA OBSERVATIONS						
FRESHWATER DIATOMS						
Meridion circulare			1			
Eunotia bidens	1					
Gomphonema grovei	1					
Pinnularia similis	1					
unidentified pennate diatoms	3		30		35	
unidentified centric diatoms	5		1			
Silicoflagellate					1	
chrysophyte cysts						
Total (all identified diatoms)	300		301		300	
Total (excluding AULGRN, CYCMEN, FW spp)	235		260		230	
brackish-marine benthic	178		200		149	
brackish marine planktonic	57		60		81	
% benthic diatoms	75.7%		76.9%		64.8%	
% planktonic diatoms	24.3%		23.1%		35.2%	
benthic/planktonic ratio	3.12		3.33		1.84	
Species richness	0.19		0.19		0.17	
Species richness (excluding FW taxa)	0.24		0.22		0.23	

Sample	**DS-3**	**DS-3 (%)**	**DS-1**	**DS-1 (%)**
depth in core (cm)	**155**		**166**	
traverses	140 / 5.5		130 / .3	
Total counts	301		302	
Total used for % (excludes possible reworked diatoms)	233		300	
Well preserved large planktonic species	R		n/a	
BENTHIC BRAKCKISH-MARINE SPECIES				
Achnanthes brevipes	2	0.9%	16	5.3%
Amphora holsatica		0.0%		0.0%
Amphora libyca	4	1.7%		0.0%
Bacillaria paxillifer	1	0.4%		0.0%
Caloneis amphisbaena fo. Subsalina		0.0%	1	0.3%
Caloneis bacillum	2	0.9%		0.0%
Caloneis westii	4	1.7%		0.0%
Catenula adhaerens		0.0%		0.0%
Cocconeis distans	2	0.9%	1	0.3%
Cocconeis placentula	3	1.3%		0.0%
Cocconeis scutellum	1	0.4%		0.0%
Cosmioneis pusilla	1	0.4%		0.0%
Delphineis surirella	4	1.7%		0.0%
Denticula subtilis		0.0%	1	0.3%
Dimeregramma minor	1	0.4%		0.0%
Diploneis bombus		0.0%		0.0%
Diploneis littoralis		0.0%		0.0%
Diploneis pseudovalis		0.0%		0.0%
Diploneis smithii v. rhombica	7	3.0%		0.0%
Diploneis stroemii	3	1.3%		0.0%
Epithemia turgida	1	0.4%	2	0.7%
Fragilaria subsalina	9	3.9%	210	70.0%
Frustulia vulgaris		0.0%		0.0%
Gomphonema olivaceum v. staurophorum	1	0.4%		0.0%
Gyrosigma eximium	2	0.9%		0.0%
Gyrosigma nodiferum	4	1.7%		0.0%
Hyalodiscus scoticus		0.0%		0.0%
Luticola cf. groep.	9	3.9%		0.0%
Luticola mutica	6	2.6%		0.0%
Mastogloia exigua	1	0.4%		0.0%
Melosira moniliformis		0.0%		0.0%
Navicula aff. "Saline Salzkotten" of Witkowski et al., 2000		0.0%		0.0%
Navicula arenaria		0.0%		0.0%
Navicula cf. stankovicii		0.0%		0.0%
Navicula elegans	1	0.4%		0.0%
Navicula menisculus		0.0%	9	3.0%
Navicula peregrina	3	1.3%	35	11.7%
Navicula phyllepta		0.0%		0.0%
Navicula spp.	2	0.9%		0.0%

Sample	**DS-3**	**DS-3 (%)**	**DS-1**	**DS-1 (%)**
depth in core (cm)	**155**		**166**	
Nitzschia angustata		0.0%		0.0%
Nitzschia brevissima	1	0.4%		0.0%
Nitzschia denticula		0.0%		0.0%
Nitzschia dissipata		0.0%	2	0.7%
Nitzschia dubiiformis	3	1.3%	2	0.7%
Nitzschia fasciculata	3	1.3%		0.0%
Nitzschia lanceola		0.0%		0.0%
Nitzschia cf. liebetruthii		0.0%		0.0%
Nitzschia scapelliformis	3	1.3%	2	0.7%
Nitzschia sigma	8	3.4%		0.0%
Nitzschia spp.	2	0.9%		0.0%
Nizschia commutata		0.0%		0.0%
Opephora marina		0.0%		0.0%
Paralia sulcata	2	0.9%		0.0%
Planothidium delicatula		0.0%		0.0%
Rhaphoneis amphiceros		0.0%		0.0%
Rhoicosphenia abbreviata		0.0%		0.0%
Rhopalodia acuminata	5	2.1%		0.0%
Scolioneis tumida		0.0%		0.0%
Sieminskia wohlenbergii		0.0%		0.0%
Stauroneis phoenicenteron		0.0%		0.0%
Surirella striatula		0.0%		0.0%
Triceratium reticulum	1	0.4%		0.0%
Tryblionella acuminata	4	1.7%	14	4.7%
Tryblionella compressa	3	1.3%		0.0%
Tryblionella debilis		0.0%		0.0%
Tryblionella granulata	11	4.7%		0.0%
Tryblionella lanceola		0.0%		0.0%
Tryblionella levidensis	3	1.3%		0.0%
Tryblionella littoralis	3	1.3%	1	0.3%
Tryblionella navicularis	10	4.3%		0.0%
Tryblionella salinarum		0.0%		0.0%
Tryblionella vexans	1	0.4%		0.0%
PLANKTONIC BRAKCKISH-MARINE SPECIES				
Actinoptychus senarius	3	1.3%		0.0%
Actinoptychus splendens		0.0%		0.0%
Chaetoceros spp. spore	9	3.9%		0.0%
Coscinodiscus radiatus	11	4.7%		0.0%
Coscinodiscus spp.		0.0%		0.0%
Cyclotella elgeri		0.0%	1	0.3%
Cyclotella sp.	2	0.9%		0.0%
Cyclotella striata	27	11.6%		0.0%
Odontella aurita	8	3.4%		0.0%
Rhizosolenia styliformis	6	2.6%		0.0%
Stephanodiscus sp.	3	1.3%	1	0.3%
Thalassionema nitzschioides	20	8.6%		0.0%
Thalassiosira eccentrica	1	0.4%		0.0%

Sample	**DS-3**	**DS-3 (%)**	**DS-1**	**DS-1 (%)**
depth in core (cm)	**155**		**166**	
Thalassiosira lacustris	1	0.4%		0.0%
Thalassiosira leptopus	1	0.4%		0.0%
Thalassiosira pacifica	1	0.4%		0.0%
Thalassiosira spp.	3	1.3%	2	0.7%
POSSIBLE REWORKED FW/ESTUARINE TAXA				
Aulcacosira granulata	57		2	
Cyclotela meneghiniana	10			
EXTRA OBSERVATIONS				
FRESHWATER DIATOMS				
Meridion circulare	1			
Eunotia bidens				
Gomphonema grovei				
Pinnularia similis				
unidentified pennate diatoms	26		8	
unidentified centric diatoms	3			
Silicoflagellate				
chrysophyte cysts			10	
Total (all identified diatoms)	301		302	
Total (excluding AULGRN, CYCMEN, FW spp)	233		300	
brackish-marine benthic	137		296	
brackish marine planktonic	96		4	
% benthic diatoms	58.8%		98.7%	
% planktonic diatoms	41.2%		1.3%	
benthic/planktonic ratio	1.43		74.00	
Species richness	0.20		0.06	
Species richness (excluding FW taxa)	0.25		0.06	

Appendix B:

C^{14} data from Beta Analytic and PaleoResearch

RADIOCARBON DATES FOR MARSH DEPOSITS FROM GC 21 AND GC 23, TOLAY CREEK, CALIFORNIA

By

Linda Scott Cummings

With Assistance from
R. A. Varney
and
Peter Kovácik

PaleoResearch Institute
Golden, Colorado

PaleoResearch Institute Technical Report 10-37

Prepared For

William Lettis and Associates
Walnut Creek, California

April 2010

INTRODUCTION

Three samples from cores in a marshy area adjacent to Tolay Creek, California, were submitted for radiocarbon dating. Botanic components of the peat and marsh deposits were separated, then submitted for AMS dating. Three radiocarbon dates were obtained.

METHODS

Recovery of datable material involved slightly different methods for these samples. Samples RC3 and RC4 contained sufficient organic material in the peat to allow separation of these fragments and dating of individual fibrous elements of the peat. These fibrous pieces could not be identified further. Sample RC1 was a mixture of fibrous pieces within a clay matrix. This sample was screened to recover the fibrous pieces for dating. Again, none of these organic pieces could be identified.

Radiocarbon Dating

The organic pieces removed from the peat were weighed prior to selecting subsamples for pre-treatment. The remainder of each sample was permanently curated at PaleoResearch. The subsample selected for pre-treatment was first subjected to hot (at least 110 ˚C), 6N hydrochloric acid (HCl), with rinses to neutral between each HCl treatment, until the supernatant is clear. This removes iron compounds and calcium carbonates that would hamper removal of humate compounds later. Next the samples were subjected to 5% potassium hydroxide (KOH) to remove humates. Once again, the samples were rinsed to neutral and re-acidified with pH 2 HCl between each KOH step. This step was repeated until the supernatant is clear, signaling removal of all humates. After humate removal, each sample was made slightly acidic and left that way for the next step.

Each submitted sample was then freeze-dried using a vacuum system, freezing out all moisture at -98 ˚C. Each individual sample was combined with cupric oxide (CuO) and elemental silver (Ag^o) in a quartz tube, then flame sealed under vacuum.

Standards and laboratory background samples also are treated in the same manner as the organic samples of unknown age. A radiocarbon “dead” EUA wood blank from Alaska that is more than 70,000 years old (currently beyond the detection capabilities of AMS) was treated using the same chemical processing as the samples of unknown age in order to calibrate the laboratory correction factor. Standards of known age, such as Two Creeks wood that dates to 11,400 RCYBP and others from the Third International Radiocarbon Intercomparison (TIRI), were also processed simultaneously to establish the laboratory correction factor. Each wood standard was run in a quantity similar to the submitted samples of unknown age and sealed in a quartz tube after the requisite pre-treatment. Once all the wood standards, blanks, and submitted samples of unknown age were prepared and sealed in their individual quartz tubes, they were combusted at 820 ˚C, soaked for an extended period of time at that temperature, and then slowly allowed to cool to enable the chemical reaction that extracts carbon dioxide ($C0_2$) gas.

Following this last step, all samples of unknown age, the wood standards, and the laboratory backgrounds were sent to the Keck Carbon Cycle AMS Facility at the University of California, Irvine, where the $C0_2$ gas was processed into graphite. The graphite in these samples was then placed in the target and run through the accelerator, which produces the numbers that are converted into the radiocarbon date presented in the data section. Dates are presented as conventional radiocarbon ages, as well as calibrated ages using Intcalc04 curves on Oxcal v.3.10.

DISCUSSION AND CONCLUSIONS

Samples of fibrous organic matter (peat) were obtained from gouge cores placed in a marshy area adjacent to Tolay Creek, California, which borders San Francisco Bay to the north. The organic components were separated for AMS radiocarbon dating. Samples RC1 and RC3 are from gouge core 21 (Table 1). A radiocarbon date of 1690 ± 15 RCYBP (PRI-10-37-RC1) was returned for the fibrous organic material in sample RC1 from a depth of 83-89 cm below the present ground surface (cmbpgs). This date calibrates to an age range of 1690-1660 and 1630-1540 CAL yr. BP at the two-sigma level (Table 2, Figure 1). The fibrous organic material in sample RC3 from a depth of 157 cmbpgs yielded a radiocarbon date of 2250 ± 20 RCYBP (PRI-10-37-RC3) and a two-sigma calibrated age range of 2340-2290 and 2260-2150 CAL yr. BP (Figure 2). Sample RC4 was taken from gouge core 23 at a depth of 119 cmbpgs. The fibrous organic material in sample RC4 yielded a radiocarbon date of 2615 ± 15 RCYBP (PRI-10-37-RC4), which calibrates to an age range of 2765-2735 CAL yr. BP at the two-sigma level (Figure 3).

TABLE 1
PROVENIENCE DATA FOR SAMPLES FROM CORES AT TOLAY CREEK, CALIFORNIA

Sample No.	Gouge Core	Depth (cmbpgs)	Sample Provenience/ Description	Analysis
RC1	CG-21	83-89	Incipient marsh; rootlets, charcoal mats, seeds	Botanic ID/Peat AMS ^{14}C Date
RC3	GC-21	157	Buried marsh; rootlets, wood debris	Botanic ID/Peat AMS ^{14}C Date
RC4	GC-23	119	Buried soil; rootlets, grass, wood debris	Botanic ID/Peat AMS ^{14}C Date

TABLE 2
RADIOCARBON RESULTS FOR SAMPLES FROM CORES AT TOLAY CREEK, CALIFORNIA

Sample No.	Sample Identification	AMS ^{14}C Date*	1-sigma Calibrated Date (68.2%)	2-sigma Calibrated Date (95.4%)	$\delta^{13}C$** ($^{o}/_{oo}$)
PRI-10-37-RC1	Peat (fibrous organic material)	1690 ± 15 RCYBP	1615-1555 CAL yr. BP	1690-1660 1630-1540 CAL yr. BP	-21.4
PRI-10-37-RC3	Peat (fibrous organic material)	2250 ± 20 RCYBP	2340-2300 2240-2180 CAL yr. BP	2340-2290 2260-2150 CAL yr. BP	-23.1
PRI-10-37-RC4	Peat (fibrous organic material)	2615 ± 15 RCYBP	2755-2740 CAL yr. BP	2765-2735 CAL yr. BP	-27.1

* Reported in radiocarbon years at 1 standard deviation measurement precision (68.2%), corrected for $\delta^{13}C$

** $\delta^{13}C$ values are measured by AMS during the ^{14}C measurement for use during the ^{14}C calculation and should not be used for dietary or paleoenvironmental interpretations.

FIGURE 1. PRI RADIOCARBON AGE CALIBRATION

Laboratory Number: PRI-10-37-RC1
Sample Identification: Peat (Fibrous organic material)
Conventional AMS ^{14}C Date: 1690 ± 15 RCYBP
1-sigma Calibrated Date (68.2%): 1615-1555 CAL yr. BP
2-sigma Calibrated Date (95.4%): 1690-1660; 1630-1540 CAL yr. BP
$\delta^{13}C$ ($^{o}/_{oo}$): -21.4 (Measured for ^{14}C calculation, not valid for dietary or paleoenvironmental interpretations)

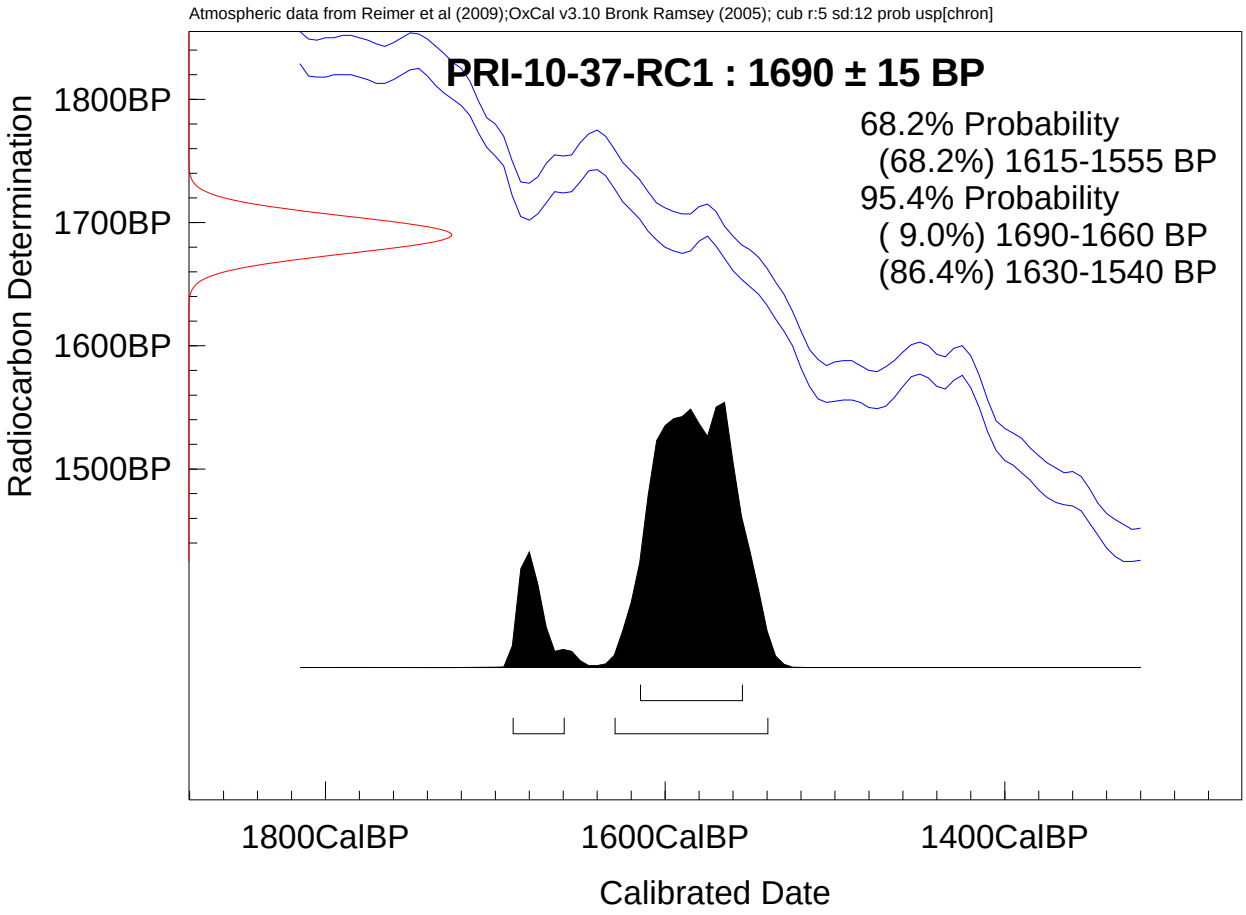

Intercept Statement. PaleoResearch Institute utilizes OxCal3.10 (Bronk Ramsey, 2005) for radiocarbon calibration, which is a probability-based method for determining conventional ages. We prefer this method over the intercept-based alternative because it provides our clients with a calibrated date that reflects the probability of its occurrence within a given distribution (reflected by the amplitude (height) of the curve), as opposed to individual point estimates (Telford, et al. 2004). As a result, the probability-based method offers more stability to the calibrated values than those derived from intercept-based methods that are subject to adjustments in the calibration curve (Telford, et al. 2004).

References

Telford, R. J., E. Heegaard, and H. J. B. Birks, 2004, *The Holocene* 14(2), pp. 296-298.

FIGURE 2. PRI RADIOCARBON AGE CALIBRATION

Laboratory Number: PRI-10-37-RC3
Sample Identification: Peat (Fibrous organic material)
Conventional AMS ^{14}C Date: 2250 ± 20 RCYBP
1-sigma Calibrated Date (68.2%): 2340-2300; 2240-2180 CAL yr. BP
2-sigma Calibrated Date (95.4%): 2340-2290; 2260-2150 CAL yr. BP
$\delta^{13}C$ ($^{o}/_{oo}$): -23.1 (Measured for ^{14}C calculation, not valid for dietary or paleoenvironmental interpretations)

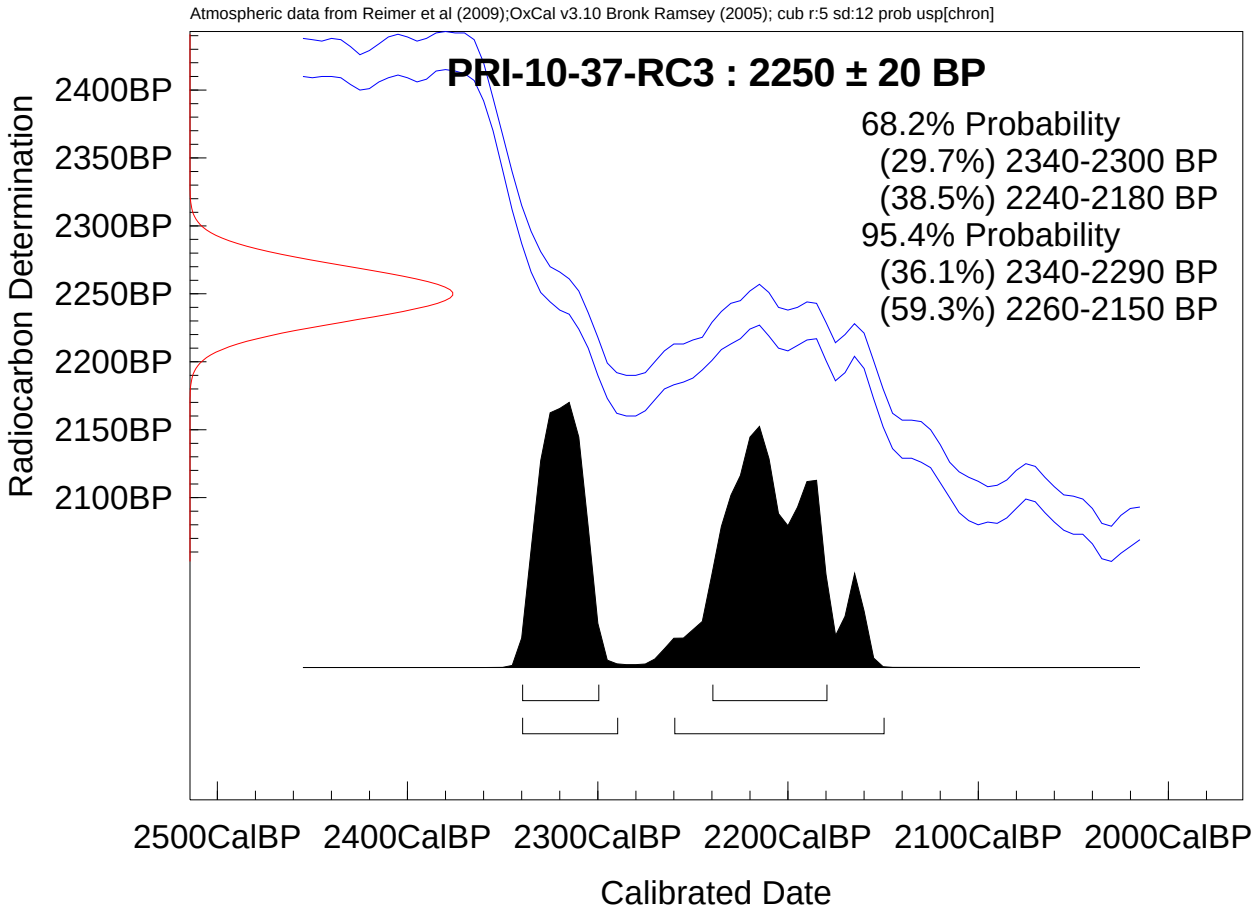

Intercept Statement. PaleoResearch Institute utilizes OxCal3.10 (Bronk Ramsey, 2005) for radiocarbon calibration, which is a probability-based method for determining conventional ages. We prefer this method over the intercept-based alternative because it provides our clients with a calibrated date that reflects the probability of its occurrence within a given distribution (reflected by the amplitude (height) of the curve), as opposed to individual point estimates (Telford, et al. 2004). As a result, the probability-based method offers more stability to the calibrated values than those derived from intercept-based methods that are subject to adjustments in the calibration curve (Telford, et al. 2004).

References

Telford, R. J., E. Heegaard, and H. J. B. Birks, 2004, *The Holocene* 14(2), pp. 296-298.

FIGURE 3. PRI RADIOCARBON AGE CALIBRATION

Laboratory Number: PRI-10-37-RC4
Sample Identification: Peat (Fibrous organic material)
Conventional AMS ^{14}C Date: 2615 ± 15 RCYBP
1-sigma Calibrated Date (68.2%): 2755-2740 CAL yr. BP
2-sigma Calibrated Date (95.4%): 2765-2735 CAL yr. BP
$\delta^{13}C$ ($^{o}/_{oo}$): -27.1 (Measured for ^{14}C calculation, not valid for dietary or paleoenvironmental interpretations)

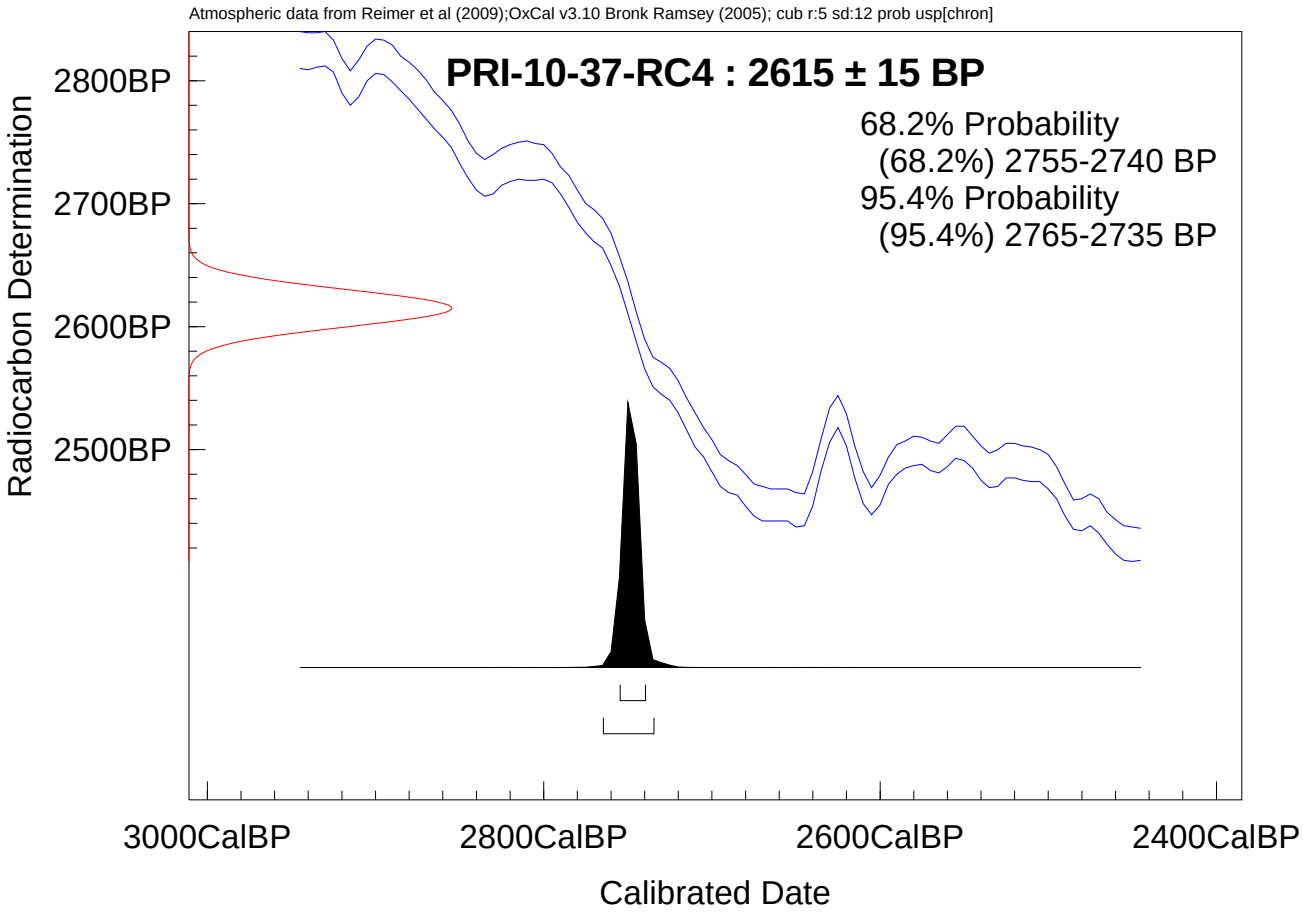

Intercept Statement. PaleoResearch Institute utilizes OxCal3.10 (Bronk Ramsey, 2005) for radiocarbon calibration, which is a probability-based method for determining conventional ages. We prefer this method over the intercept-based alternative because it provides our clients with a calibrated date that reflects the probability of its occurrence within a given distribution (reflected by the amplitude (height) of the curve), as opposed to individual point estimates (Telford, et al. 2004). As a result, the probability-based method offers more stability to the calibrated values than those derived from intercept-based methods that are subject to adjustments in the calibration curve (Telford, et al. 2004).

References

Telford, R. J., E. Heegaard, and H. J. B. Birks, 2004, *The Holocene* 14(2), pp. 296-298.

REFERENCES CITED

Telford, R. J., E. Heegaard and H. J. B. Birks
2004 The Intercept is a Poor Estimate of a Calibrated Radiocarbon Age. *The Holocene* 14(2):296-298.

BETA ANALYTIC INC.
DR. M.A. TAMERS and MR. D.G. HOOD
4985 S.W. 74 COURT
MIAMI, FLORIDA, USA 33155
PH: 305-667-5167 FAX:305-663-0964
beta@radiocarbon.com

REPORT OF RADIOCARBON DATING ANALYSES

Mr. Robert Givler

Report Date: 6/18/2010

Fugro William Lettis & Associates

Material Received: 5/7/2010

Sample Data	Measured Radiocarbon Age	13C/12C Ratio	Conventional Radiocarbon Age(*)
Beta - 279299	2200 +/- 40 BP	-20.3 o/oo	2280 +/- 40 BP

SAMPLE : VC2 RC-8
ANALYSIS : AMS-Standard delivery
MATERIAL/PRETREATMENT : (organic sediment): acid washes
2 SIGMA CALIBRATION : Cal BC 400 to 350 (Cal BP 2350 to 2300) AND Cal BC 300 to 210 (Cal BP 2260 to 2160)

Dates are reported as RCYBP (radiocarbon years before present, "present" = AD 1950). By international convention, the modern reference standard was 95% the 14C activity of the National Institute of Standards and Technology (NIST) Oxalic Acid (SRM 4990C) and calculated using the Libby 14C half-life (5568 years). Quoted errors represent 1 relative standard deviation statistics (68% probability) counting errors based on the combined measurements of the sample, background, and modern reference standards. Measured 13C/12C ratios (delta 13C) were calculated relative to the PDB-1 standard.

The Conventional Radiocarbon Age represents the Measured Radiocarbon Age corrected for isotopic fractionation, calculated using the delta 13C. On rare occasion where the Conventional Radiocarbon Age was calculated using an assumed delta 13C, the ratio and the Conventional Radiocarbon Age will be followed by "*". The Conventional Radiocarbon Age is not calendar calibrated. When available, the Calendar Calibrated result is calculated from the Conventional Radiocarbon Age and is listed as the "Two Sigma Calibrated Result" for each sample.

CALIBRATION OF RADIOCARBON AGE TO CALENDAR YEARS

(Variables: C13/C12=-20.3:lab. mult=1)

Laboratory number:	**Beta-279299**
Conventional radiocarbon age:	**2280±40 BP**
2 Sigma calibrated results: (95% probability)	**Cal BC 400 to 350 (Cal BP 2350 to 2300) and Cal BC 300 to 210 (Cal BP 2260 to 2160)**

Intercept data

Intercept of radiocarbon age with calibration curve:	Cal BC 380 (Cal BP 2330)
1 Sigma calibrated result: (68% probability)	Cal BC 390 to 360 (Cal BP 2340 to 2310)

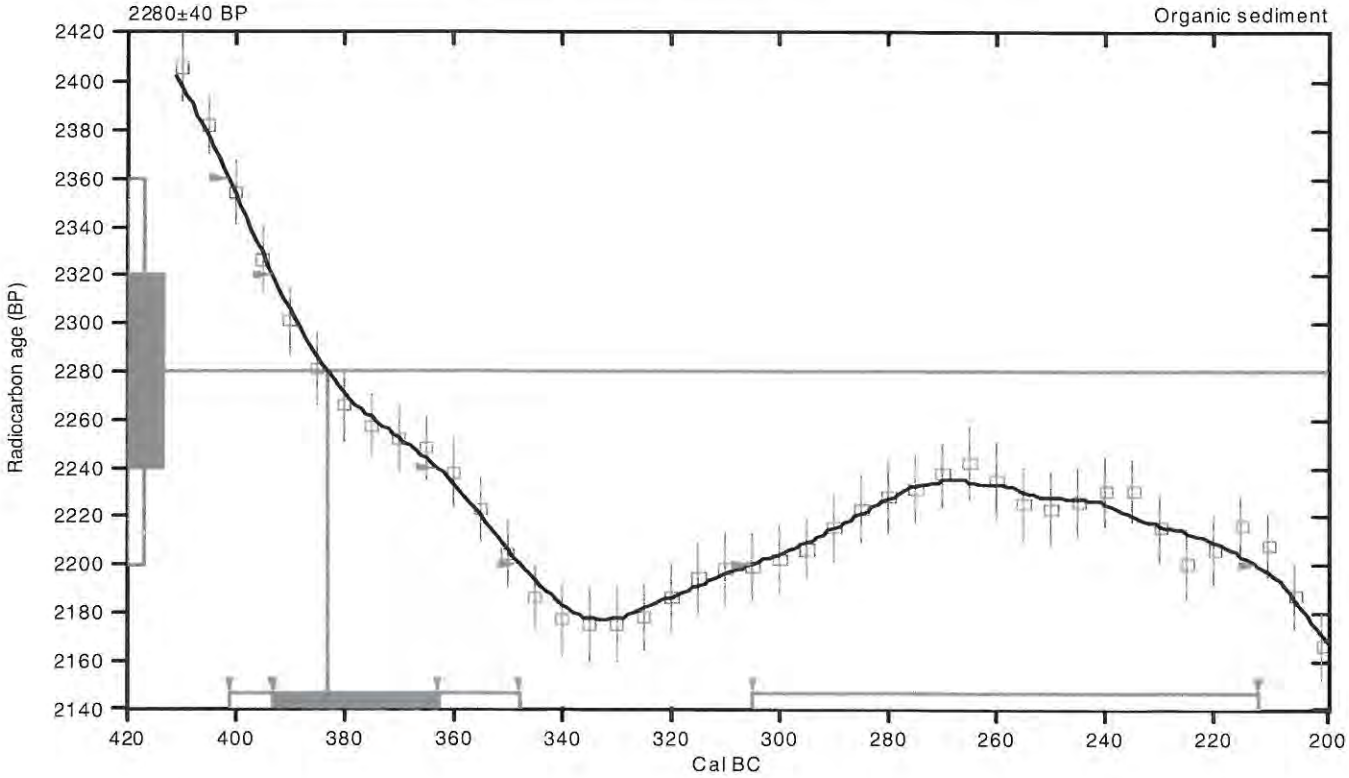

References:

Database used

INTCAL04

Calibration Database

INTCAL04 Radiocarbon Age Calibration

IntCal04: Calibration Issue of Radiocarbon (Volume 46, nr 3, 2004).

Mathematics

A Simplified Approach to Calibrating C14 Dates

Talma, A. S., Vogel, J. C., 1993, Radiocarbon 35(2), p317-322

Beta Analytic Radiocarbon Dating Laboratory

4985 S.W. 74th Court, Miami, Florida 33155 • Tel: (305)667-5167 • Fax: (305)663-0964 • E-Mail: beta@radiocarbon.com

Beta Analytic Inc
4985 SW 74 Court
Miami, Florida 33155
Tel: 305-667-5167
Fax: 305-663-0964
beta@radiocarbon.com
www.radiocarbon.com

Consistent Accuracy
Delivered On Time

Mr. Darden Hood
President

Mr. Ronald Hatfield
Mr. Christopher Patrick
Deputy Directors

The Radiocarbon Laboratory Accredited to ISO-17025 Testing Standards (PJLA Accreditation #59423)

Final Report

The final report package includes the final date report, a statement outlining our analytical procedures, a glossary of pretreatment terms, calendar calibration information, billing documents (containing balance/credit information and the number of samples submitted within the yearly discount period), and peripheral items to use with future submittals. The final report includes the individual analysis method, the delivery basis, the material type and the individual pretreatments applied. The final report has been sent by mail and e-mail (where available).

Pretreatment

Pretreatment methods are reported along with each result. All necessary chemical and mechanical pretreatments of the submitted material were applied at the laboratory to isolate the carbon, which may best represent the time event of interest. When interpreting the results, it is important to consider the pretreatments. Some samples cannot be fully pretreated, making their ^{14}C ages more subjective than samples, which can be fully pretreated. Some materials receive no pretreatments. Please look at the pretreatment indicated for each sample and read the pretreatment glossary to understand the implications.

Analysis

Materials measured by the radiometric technique were analyzed by synthesizing sample carbon to benzene (92% C), measuring for ^{14}C content in one of 53 scintillation spectrometers, and then calculating for radiocarbon age. If the Extended Counting Service was used, the ^{14}C content was measured for a greatly extended period of time. AMS results were derived from reduction of sample carbon to graphite (100 %C), along with standards and backgrounds. The graphite was then detected for ^{14}C content in one of 9 accelerator-mass-spectrometers (AMS).

The Radiocarbon Age and Calendar Calibration

The "Conventional ^{14}C Age (*)" is the result after applying $^{13}C/^{12}C$ corrections to the measured age and is the most appropriate radiocarbon age. If an "*" is attached to this date, it means the $^{13}C/^{12}C$ was estimated rather than measured (The ratio is an option for radiometric analysis, but included on all AMS analyses.) Ages are reported with the units "BP" (Before Present). "Present" is defined as AD 1950 for the purposes of radiocarbon dating.

Results for samples containing more ^{14}C than the modern reference standard are reported as "percent modern carbon" (pMC). These results indicate the material was respiring carbon after the advent of thermo-nuclear weapons testing and is less than ~ 50 years old.

Applicable calendar calibrations are included for materials between about 100 and 19,000 BP. If calibrations are not included with a report, those results were too young, too old, or inappropriate for calibration. Please read the enclosed page discussing calibration.

PRETREATMENT GLOSSARY
Standard Pretreatment Protocols at Beta Analytic

Unless otherwise requested by a submitter or discussed in a final date report, the following procedures apply to pretreatment of samples submitted for analysis. This glossary defines the pretreatment methods applied to each result listed on the date report form (e.g. you will see the designation "acid/alkali/acid" listed along with the result for a charcoal sample receiving such pretreatment).

Pretreatment of submitted materials is required to eliminate secondary carbon components. These components, if not eliminated, could result in a radiocarbon date, which is too young or too old. Pretreatment does not ensure that the radiocarbon date will represent the time event of interest. This is determined by the sample integrity. Effects such as the old wood effect, burned intrusive roots, bioturbation, secondary deposition, secondary biogenic activity incorporating recent carbon (bacteria) and the analysis of multiple components of differing age are just some examples of potential problems. The pretreatment philosophy is to reduce the sample to a single component, where possible, to minimize the added subjectivity associated with these types of problems. If you suspect your sample requires special pretreatment considerations be sure to tell the laboratory prior to analysis.

"acid/alkali/acid"

The sample was first gently crushed/dispersed in deionized water. It was then given hot HCI acid washes to eliminate carbonates and alkali washes (NaOH) to remove secondary organic acids. The alkali washes were followed by a final acid rinse to neutralize the solution prior to drying. Chemical concentrations, temperatures, exposure times, and number of repetitions, were applied accordingly with the uniqueness of the sample. Each chemical solution was neutralized prior to application of the next. During these serial rinses, mechanical contaminants such as associated sediments and rootlets were eliminated. This type of pretreatment is considered a "full pretreatment". On occasion the report will list the pretreatment as "acid/alkali/acid - insolubles" to specify which fraction of the sample was analyzed. This is done on occasion with sediments (See "acid/alkali/acid - solubles"

Typically applied to: charcoal, wood, some peats, some sediments, and textiles "acid/alkali/acid - solubles"

On occasion the alkali soluble fraction will be analyzed. This is a special case where soil conditions imply that the soluble fraction will provide a more accurate date. It is also used on some occasions to verify the present/absence or degree of contamination present from secondary organic acids. The sample was first pretreated with acid to remove any carbonates and to weaken organic bonds. After the alkali washes (as discussed above) are used, the solution containing the alkali soluble fraction is isolated/filtered and combined with acid. The soluble fraction, which precipitates, is rinsed and dried prior to combustion.

"acid/alkali/acid/cellulose extraction"

Following full acid/alkali/acid pretreatments, the sample is bathed in (sodium chlorite) $NaClO_2$ under very controlled conditions (Ph = 3, temperature = 70 degrees C). This eliminates all components except wood cellulose. It is useful for woods that are either very old or highly contaminated.

Applied to: wood

"acid washes"

Surface area was increased as much a possible. Solid chunks were crushed, fibrous materials were shredded, and sediments were dispersed. Acid (HCl) was applied repeatedly to ensure the absence of carbonates. Chemical concentrations, temperatures, exposure times, and number of repetitions, were applied accordingly with the uniqueness of each sample. The sample was not be subjected to alkali washes to ensure the absence of secondary organic acids for intentional reasons. The most common reason is that the primary carbon is soluble in the alkali. Dating results reflect the total organic content of the analyzed material. Their accuracy depends on the researcher's ability to subjectively eliminate potential contaminants based on contextual facts.

Typically applied to: organic sediments, some peats, small wood or charcoal, special cases

Beta Analytic Inc
4985 SW 74 Court
Miami, Florida 33155
Tel: 305-667-5167
Fax: 305-663-0964
beta@radiocarbon.com
www.radiocarbon.com

Consistent Accuracy
Delivered On Time

Mr. Darden Hood
President

Mr. Ronald Hatfield
Mr. Christopher Patrick
Deputy Directors

The Radiocarbon Laboratory Accredited to ISO-17025 Testing Standards (PJLA Accreditation #59423)

Calendar Calibration at Beta Analytic

Calibrations of radiocarbon age determinations are applied to convert BP results to calendar years. The short-term difference between the two is caused by fluctuations in the heliomagnetic modulation of the galactic cosmic radiation and, recently, large scale burning of fossil fuels and nuclear devices testing. Geomagnetic variations are the probable cause of longer-term differences.

The parameters used for the corrections have been obtained through precise analyses of hundreds of samples taken from known-age tree rings of oak, sequoia, and fir up to about 10,000 BP. Calibration using tree-rings to about 12,000 BP is still being researched and provides somewhat less precise correlation. Beyond that, up to about 20,000 BP, correlation using a modeled curve determined from U/Th measurements on corals is used. This data is still highly subjective. Calibrations are provided up to about 19,000 years BP using the most recent calibration data available.

The Pretoria Calibration Procedure (Radiocarbon, Vol 35, No.1, 1993, pg 317) program has been chosen for these calendar calibrations. It uses splines through the tree-ring data as calibration curves, which eliminates a large part of the statistical scatter of the actual data points. The spline calibration allows adjustment of the average curve by a quantified closeness-of-fit parameter to the measured data points. A single spline is used for the precise correlation data available back to 9900 BP for terrestrial samples and about 6900 BP for marine samples. Beyond that, splines are taken on the error limits of the correlation curve to account for the lack of precision in the data points.

In describing our calibration curves, the solid bars represent one sigma statistics (68% probability) and the hollow bars represent two sigma statistics (95% probability). Marine carbonate samples that have been corrected for $^{13}C/^{12}C$, have also been corrected for both global and local geographic reservoir effects (as published in Radiocarbon, Volume 35, Number 1, 1993) prior to the calibration. Marine carbonates that have not been corrected for $^{13}C/^{12}C$ are adjusted by an assumed value of 0 %0 in addition to the reservoir corrections. Reservoir corrections for fresh water carbonates are usually unknown and are generally not accounted for in those calibrations. In the absence of measured $^{13}C/^{12}C$ ratios, a typical value of -5 %0 is assumed for freshwater carbonates.

(Caveat: the correlation curve for organic materials assume that the material dated was living for exactly ten years (e.g. a collection of 10 individual tree rings taken from the outer portion of a tree that was cut down to produce the sample in the feature dated). For other materials, the maximum and minimum calibrated age ranges given by the computer program are uncertain. The possibility of an "old wood effect" must also be considered, as well as the potential inclusion of younger or older material in matrix samples. Since these factors are in determinant error in most cases, these calendar calibration results should be used only for illustrative purposes. In the case of carbonates, reservoir correction is theoretical and the local variations are real, highly variable and dependent on provenience. Since imprecision in the correlation data beyond 10,000 years is high, calibrations in this range are likely to change in the future with refinement in the correlation curve. The age ranges and especially the intercept ages generated by the program must be considered as approximations.)

BETA ANALYTIC INC.
DR. M.A. TAMERS and MR. D.G. HOOD
4985 S.W. 74 COURT
MIAMI, FLORIDA, USA 33155
PH: 305-667-5167 FAX:305-663-0964
beta@radiocarbon.com

REPORT OF RADIOCARBON DATING ANALYSES

Mr. Robert Givler — Report Date: 6/14/2010

Fugro William Lettis & Associates — Material Received: 5/7/2010

Sample Data	Measured Radiocarbon Age	13C/12C Ratio	Conventional Radiocarbon Age(*)
Beta - 279300	NA	NA	2040 +/- 40 BP

SAMPLE : VC2 RC-9
ANALYSIS : AMS-Standard delivery
MATERIAL/PRETREATMENT : (plant material): acid/alkali/acid
2 SIGMA CALIBRATION : Cal BC 170 to Cal AD 50 (Cal BP 2120 to 1900)
COMMENT: The original sample was too small to provide a 13C/12C ratio on the original material. However, a ratio including both natural and laboratory effects was measured during the 14C detection to calculate the true Conventional Radiocarbon Age.

Beta - 279301	1950 +/- 40 BP	-14.5 o/oo	2120 +/- 40 BP

SAMPLE : VC2 RC-10
ANALYSIS : AMS-Standard delivery
MATERIAL/PRETREATMENT : (plant material): acid/alkali/acid
2 SIGMA CALIBRATION : Cal BC 350 to 300 (Cal BP 2300 to 2260) AND Cal BC 210 to 40 (Cal BP 2160 to 1990)

Beta - 279302	NA	NA	2260 +/- 40 BP

SAMPLE : VC2 RC-11
ANALYSIS : AMS-Standard delivery
MATERIAL/PRETREATMENT : (charred material): acid/alkali/acid
2 SIGMA CALIBRATION : Cal BC 400 to 340 (Cal BP 2350 to 2290) AND Cal BC 330 to 200 (Cal BP 2280 to 2150)
COMMENT: The original sample was too small to provide a 13C/12C ratio on the original material. However, a ratio including both natural and laboratory effects was measured during the 14C detection to calculate the true Conventional Radiocarbon Age.

Dates are reported as RCYBP (radiocarbon years before present, "present" = AD 1950). By international convention, the modern reference standard was 95% the 14C activity of the National Institute of Standards and Technology (NIST) Oxalic Acid (SRM 4990C) and calculated using the Libby 14C half-life (5568 years). Quoted errors represent 1 relative standard deviation statistics (68% probability) counting errors based on the combined measurements of the sample, background, and modern reference standards. Measured 13C/12C ratios (delta 13C) were calculated relative to the PDB-1 standard.

The Conventional Radiocarbon Age represents the Measured Radiocarbon Age corrected for isotopic fractionation, calculated using the delta 13C. On rare occasion where the Conventional Radiocarbon Age was calculated using an assumed delta 13C, the ratio and the Conventional Radiocarbon Age will be followed by "*". The Conventional Radiocarbon Age is not calendar calibrated. When available, the Calendar Calibrated result is calculated from the Conventional Radiocarbon Age and is listed as the "Two Sigma Calibrated Result" for each sample.

CALIBRATION OF RADIOCARBON AGE TO CALENDAR YEARS

(Variables: C13/C12=N/A:lab. mult=1)

Laboratory number:	**Beta-279300**
Conventional radiocarbon age:	**2040±40 BP**
2 Sigma calibrated result: (95% probability)	**Cal BC 170 to Cal AD 50 (Cal BP 2120 to 1900)**

Intercept data

Intercept of radiocarbon age with calibration curve:	Cal BC 40 (Cal BP 1990)
1 Sigma calibrated result: (68% probability)	Cal BC 90 to Cal AD 10 (Cal BP 2040 to 1940)

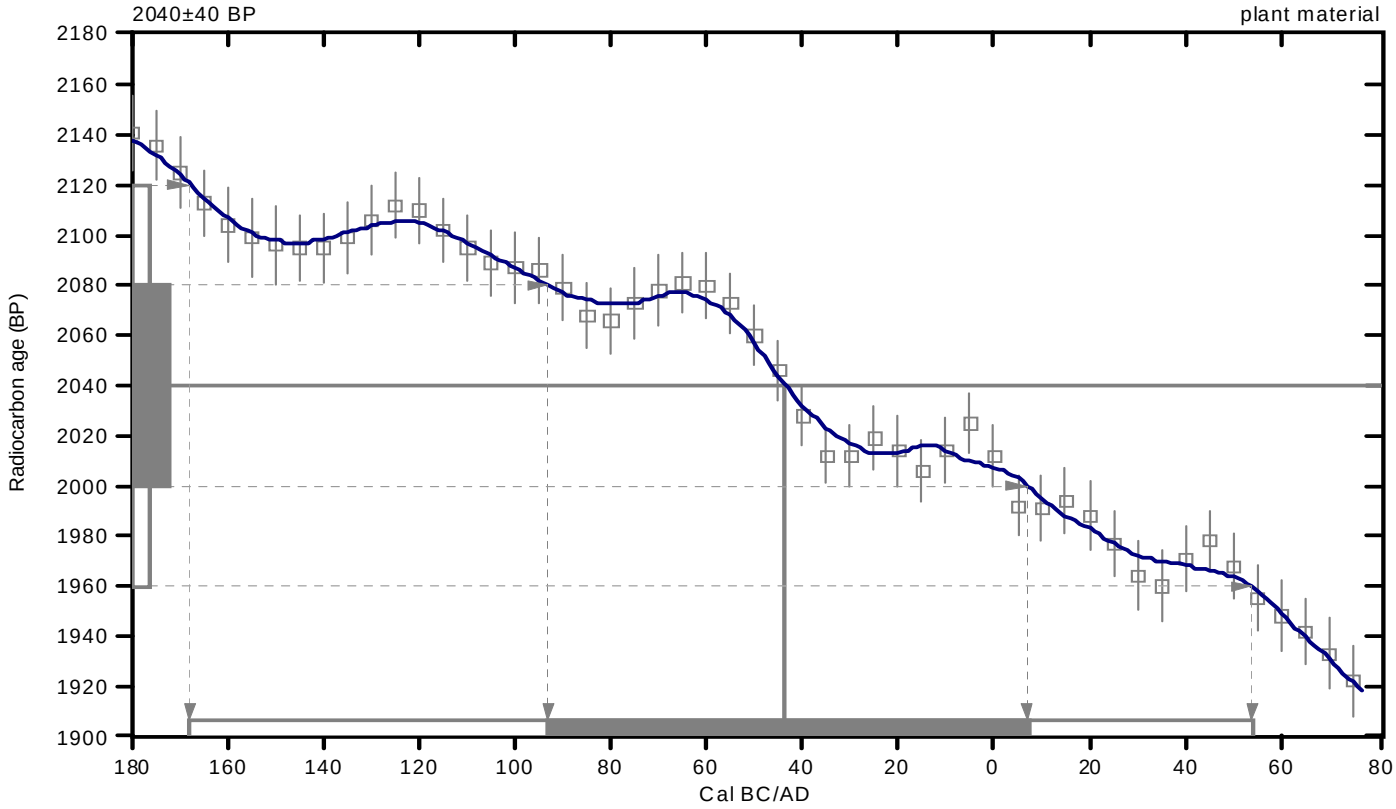

References:

Database used

INTCAL04

Calibration Database

INTCAL04 Radiocarbon Age Calibration

IntCal04: Calibration Issue of Radiocarbon (Volume 46, nr 3, 2004).

Mathematics

A Simplified Approach to Calibrating C14 Dates

Talma, A. S., Vogel, J. C., 1993, Radiocarbon 35(2), p317-322

Beta Analytic Radiocarbon Dating Laboratory

4985 S.W. 74th Court, Miami, Florida 33155 • Tel: (305)667-5167 • Fax: (305)663-0964 • E-Mail: beta@radiocarbon.com

CALIBRATION OF RADIOCARBON AGE TO CALENDAR YEARS

(Variables: C13/C12=-14.5:lab. mult=1)

Laboratory number:	**Beta-279301**
Conventional radiocarbon age:	**2120±40 BP**
2 Sigma calibrated results: (95% probability)	**Cal BC 350 to 300 (Cal BP 2300 to 2260) and Cal BC 210 to 40 (Cal BP 2160 to 1990)**

Intercept data

Intercept of radiocarbon age with calibration curve:	Cal BC 170 (Cal BP 2120)
1 Sigma calibrated result: (68% probability)	Cal BC 200 to 90 (Cal BP 2150 to 2040)

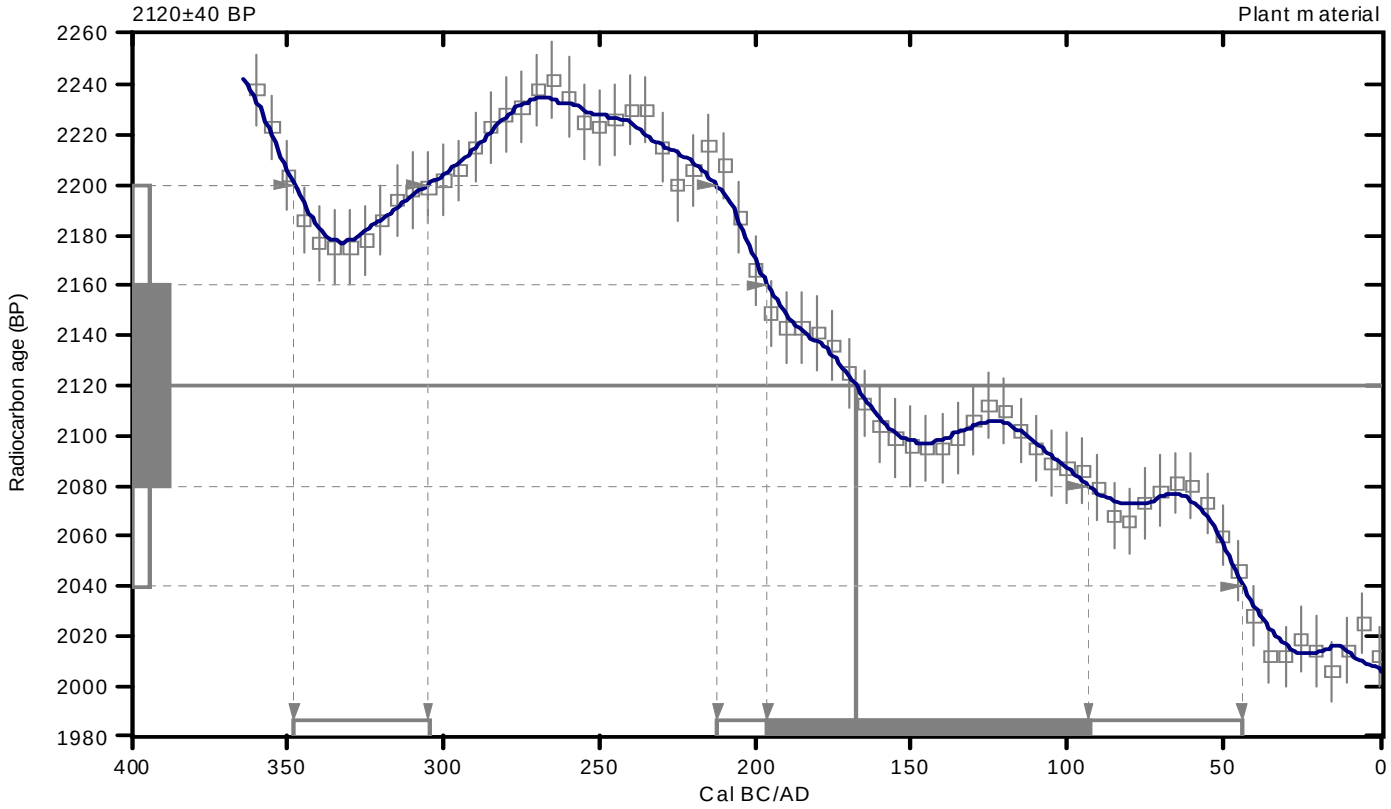

References:

Database used

INTCAL04

Calibration Database

INTCAL04 Radiocarbon Age Calibration

IntCal04: Calibration Issue of Radiocarbon (Volume 46, nr 3, 2004).

Mathematics

A Simplified Approach to Calibrating C14 Dates

Talma, A. S., Vogel, J. C., 1993, Radiocarbon 35(2), p317-322

Beta Analytic Radiocarbon Dating Laboratory

4985 S.W. 74th Court, Miami, Florida 33155 • Tel: (305)667-5167 • Fax: (305)663-0964 • E-Mail: beta@radiocarbon.com

CALIBRATION OF RADIOCARBON AGE TO CALENDAR YEARS

(Variables: C13/C12=N/A:lab. mult=1)

Laboratory number:	**Beta-279302**
Conventional radiocarbon age:	**2260±40 BP**
2 Sigma calibrated results: (95% probability)	**Cal BC 400 to 340 (Cal BP 2350 to 2290) and Cal BC 330 to 200 (Cal BP 2280 to 2150)**

Intercept data

Intercept of radiocarbon age with calibration curve:	Cal BC 370 (Cal BP 2320)
1 Sigma calibrated results: (68% probability)	Cal BC 390 to 360 (Cal BP 2340 to 2300) and Cal BC 290 to 240 (Cal BP 2240 to 2180)

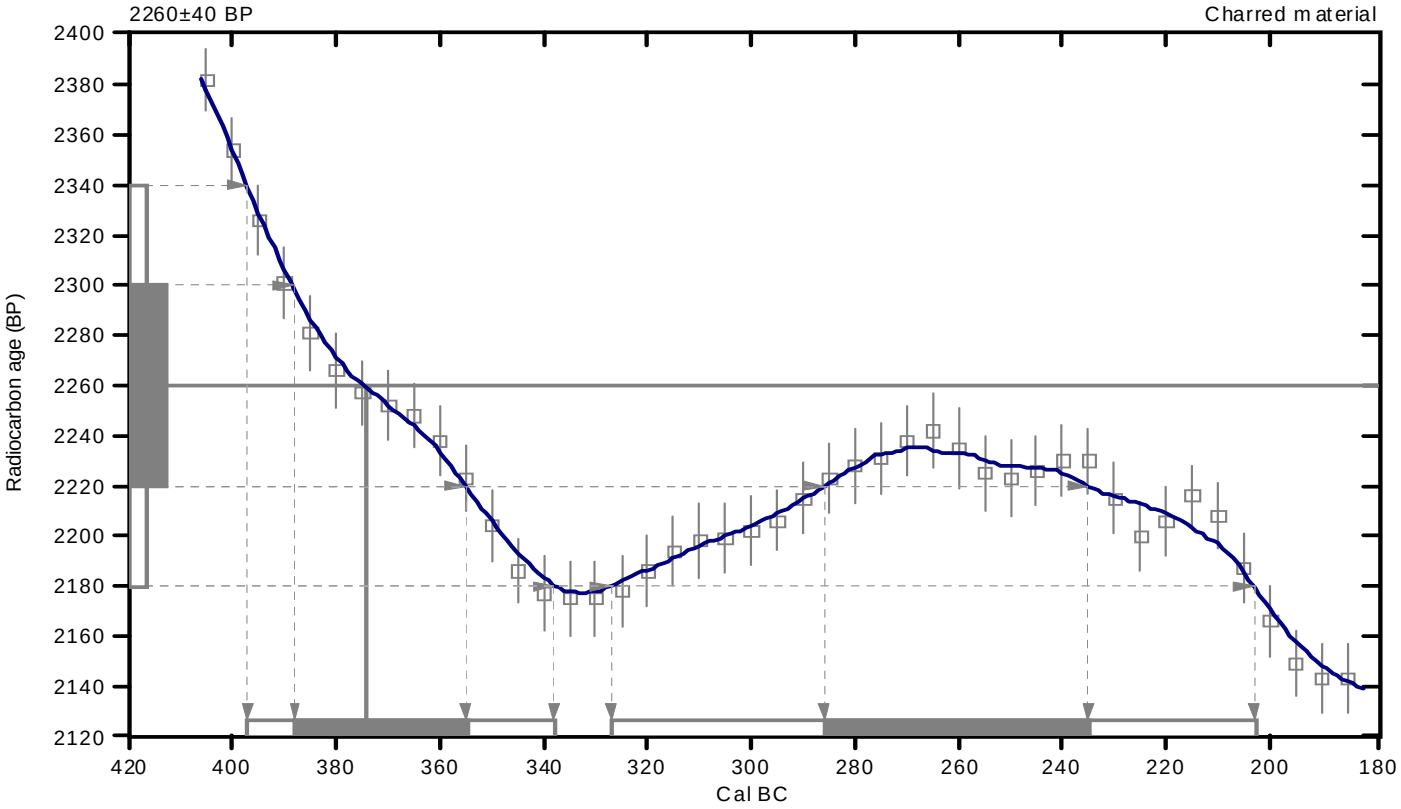

References:

Database used

INTCAL04

Calibration Database

INTCAL04 Radiocarbon Age Calibration

IntCal04: Calibration Issue of Radiocarbon (Volume 46, nr 3, 2004).

Mathematics

A Simplified Approach to Calibrating C14 Dates

Talma, A. S., Vogel, J. C., 1993, Radiocarbon 35(2), p317-322

Beta Analytic Radiocarbon Dating Laboratory

4985 S.W. 74th Court, Miami, Florida 33155 • Tel: (305)667-5167 • Fax: (305)663-0964 • E-Mail: beta@radiocarbon.com